

**COMPUTER SIMULATIONS OF MELATONIN IN
AQUEOUS SOLUTION AND ITS INTERACTIONS WITH
NIOSOME BILAYERS**



Aksornnarong Ritwiset

**A Thesis Submitted in Partial Fulfillment of the Requirement for the
Degree of Doctor of Philosophy in Physics
Suranaree University of Technology
Academic Year 2020**

การจำลองเชิงคอมพิวเตอร์ของเมลาโทนินในสารละลายน้ำและอันตรกิริยากับ
ผนังสองชั้นของนีโอโซม



นายอัษฎรณรงค์ ฤทธิวิเศษ

วิทยานิพนธ์นี้เป็นส่วนหนึ่งของการศึกษาตามหลักสูตรปริญญาวิทยาศาสตรดุษฎีบัณฑิต
สาขาวิชาฟิสิกส์
มหาวิทยาลัยเทคโนโลยีสุรนารี
ปีการศึกษา 2563

**COMPUTER SIMULATIONS OF MELATONIN IN AQUEOUS
SOLUTION AND ITS INTERACTIONS WITH NIOSOME
BILAYERS**

Suranaree University of Technology has approved this thesis submitted in partial fulfillment of the requirement for the Degree of Doctor of Philosophy.

Thesis Examining Committee



(Assoc. Prof. Dr. Panomsak Meemon)

Chairperson



(Prof. Dr. Santi Maensiri)

Member (Thesis Advisor)



(Assoc. Prof. Dr. Sriprajak Kongsuk)

Member (Thesis Co-advisor)



(Assoc. Prof. Dr. Pairot Moontragoon)

Member



(Asst. Prof. Dr. Michael F. Smith)

Member



(Prof. Dr. Santi Maensiri)



(Assoc. Prof. Dr. Chatchai Jothityangkoon)

Vice Rector for Academic Affairs

and Quality Assurance

Dean of Institute of Science

อักษรณรงค์ ฤทธิวิเศษ : การจำลองเชิงคอมพิวเตอร์ของเมลาโทนินในสารละลายน้ำและอันตรกิริยากับผนังสองชั้นของนีโอโซม (COMPUTER SIMULATIONS OF MELATONIN IN AQUEOUS SOLUTION AND ITS INTERACTIONS WITH NIOSOME BILAYERS). อาจารย์ที่ปรึกษา : ศาสตราจารย์ ดร.สันติ แม่นศิริ, 98 หน้า.

เมลาโทนิน / ความเสถียร / การรวมเป็นกลุ่มก้อน / ผนังชั้นเดียว / สารละลายที่เป็นน้ำ / พันธะไฮโดรเจน / ระบบนำส่งยา / การห่อหุ้ม / ผนังสองชั้นนีโอโซม / การจำลองพลวัตเชิงโมเลกุล

เมลาโทนินเป็นฮอร์โมนธรรมชาติที่มีบทบาทในการควบคุมวงจรการนอนหลับและมีศักยภาพในการใช้ในการรักษาโรคต่าง ๆ เช่น โรคนอนไม่หลับ โรคหลอดเลือดหัวใจ โรคอัลไซเมอร์ และมะเร็งบางชนิดเนื่องจากมีคุณสมบัติที่โดดเด่นในการต่อต้านสารอนุมูลอิสระ เมื่อเร็ว ๆ นี้ได้มีการนำอนุภาคนีโอโซมมาใช้กันอย่างแพร่หลายในการห่อหุ้มเมลาทินเพื่อเพิ่มประสิทธิภาพในการนำส่งยา ในการศึกษานี้ได้ทำการวิเคราะห์หาสมบัติเชิงโครงสร้างและเชิงพลวัตของเมลาโทนินในสารละลายน้ำและที่รอยต่อระหว่างน้ำกับอากาศ ในแง่ของการพัฒนาการนำส่งยาคุณสมบัติทางกายภาพและความเสถียรของเมลาโทนินในตัวกลางน้ำจึงมีความน่าสนใจสำหรับการศึกษา เพราะข้อมูลเหล่านี้มีความจำเป็นสำหรับการเตรียมตำรับยาเมลาโทนิน สำหรับการศึกษาของระบบเมลาโทนินในสารละลายน้ำและที่รอยต่อระหว่างน้ำและอากาศ เราพบว่าโมเลกุลของเมลาโทนินส่วนใหญ่จะรวมตัวเป็นกลุ่มก้อนที่มีอันตรกิริยาที่แข็งแรงระหว่างเมลาโทนินกับเมลาโทนินและก่อตัวเป็นผนังฟิล์มชั้นเดียวที่มีโครงสร้างเป็นระเบียบมากกว่าโดยลำดับ ความแข็งแรงของส่วนที่ขอบน้ำสำหรับเมลาโทนินนั้นจะขึ้นอยู่กับหมู่ฟังก์ชันซึ่งเรียงลำดับได้ดังนี้: carbonyl O > indole NH > amide NH > methoxy OA ตามลำดับ การสร้างพันธะไฮโดรเจนระหว่างหมู่ carbonyl O และกลุ่ม indole NH กับน้ำแสดงให้เห็นอย่างชัดเจน ซึ่งส่งผลต่อการเอียงของกลุ่มหัวเมลาโทนินสองรูปแบบที่เป็นไปได้ที่รอยต่อระหว่างน้ำและอากาศ การเกิดพันธะไฮโดรเจนของเมลาโทนินกับเมลาโทนินในระบบสารละลายน้ำมีระยะเวลาที่ยาวนานกว่าการเกิดพันธะไฮโดรเจนของเมลาโทนินกับเมลาโทนินในระบบรอยต่อระหว่างน้ำและอากาศ ซึ่งข้อมูลนี้แสดงให้เห็นว่าการรวมตัวของเมลาโทนินในสารละลายน้ำมีความเสถียรมากและส่งผลทำให้เมลาโทนินละลายในน้ำได้น้อย นอกจากนี้ยังได้ศึกษาเมลาโทนินที่แทรกเข้าไปในผนังสองชั้นนีโอโซมที่มีและปราศจากองค์ประกอบของคอเรสเตอรอลและทำการจำลองที่อุณหภูมิ 298 เคลวินและความดัน 1 บาร์ ผนังสองชั้นนีโอโซมทั้งสองแบบพบว่าอยู่ในสถานะของเหลวที่มีโครงสร้างความเป็นระเบียบน้อยลง (liquid phase) สำหรับ

ระบบผนังสองชั้น Span60 โดยเมลาโทนินส่วนใหญ่จะอยู่ในบริเวณระหว่างกลุ่มหัวและกลุ่มหางของ Span60 อย่างไรก็ตาม การเติมเมลาโทนินลงในผนังสองชั้น Span60/Chol นั้นส่งผลอย่างมีนัยสำคัญต่อสมบัติเชิงโครงสร้างและสมบัติเชิงพลวัต เมลาโทนินส่วนใหญ่จะอยู่ในบริเวณรอยต่อระหว่าง Span60 กับน้ำ มีการแพร่ที่เพิ่มขึ้นทั้งในทิศทางในระนาบและแนวขวาง นอกจากนี้ การศึกษาของเราชี้ให้เห็นว่าการเติมคอเลสเตอรอลในผนังสองชั้น Span60 สามารถเพิ่มเสถียรภาพของนีโอโซม ซึ่งจะช่วยให้ประสิทธิภาพของการห่อหุ้มเมลาโทนินเมื่อเทียบกับผนังสองชั้น Span60 บริสุทธิ์ ข้อมูลดังกล่าวเป็นสิ่งที่จำเป็นสำหรับการเตรียมการอนุภาคนีโอโซมที่ใช้ในการนำส่งยา



สาขาวิชาฟิสิกส์
ปีการศึกษา 2563

ลายมือชื่อนักศึกษา อัครพงศ์
ลายมือชื่ออาจารย์ที่ปรึกษา พี.พี.อ.
ลายมือชื่ออาจารย์ที่ปรึกษาร่วม อ.วิมล นนท

AKSORNNARONG RITWISSET : COMPUTER SIMULATIONS OF
MELATONIN IN AQUEOUS SOLUTION AND ITS INTERACTIONS
WITH NIOSOME BILAYERS. THESIS ADVISOR : PROF. SANTI
MAENSIRI, D.Phil. 98 PP.

MELATONIN / STABILITY / AGGREGATION / MONOLAYER / AQUEOUS
SOLUTION / HYDROGEN BOND / DRUG DELIVERY / ENCAPSULATION /
NIOSOME BILAYER / MOLECULAR DYNAMICS SIMULATIONS

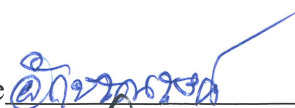
Melatonin is a natural hormone that regulates the sleep-wake cycle. It is also used for treatment in some diseases such as insomnia, cardiovascular, Alzheimer, and the certain types of cancers due to its remarkable antioxidant properties. Recently, niosomes have been widely used for encapsulating melatonin to improve the efficiency of drug delivery systems. In this study, we have investigated the structural and dynamical properties of melatonin in an aqueous solution and at the water-air interface using molecular dynamics simulations. In terms of drug delivery development, the solubility and stability of melatonin in the presence of aqueous media are of interest for investigation because this information is necessary for the melatonin formulation. We found that most melatonin molecules are self-aggregated with the stronger melatonin-melatonin interaction and formed a monolayer film with a more ordered structure, respectively. The hydrophilic interaction strength was sequenced as follows: carbonyl O > indole NH > amide NH > methoxy OA, respectively. The competition of hydrogen bonds between the carbonyl O and the indole NH groups with water molecules were clearly demonstrated, leading to two

possible tilts of the melatonin head groups for the water-air interface system. The hydrogen bond formation between melatonin themselves for the bulk water system showed a longer lifetime than that for the water-air interface system. This suggests that the formation of melatonin aggregation in an aqueous solution is more stable and subsequently melatonin is less soluble in water. Next, we have investigated melatonin inserted into the niosome bilayers with and without cholesterol incorporation and simulated at the temperature of 298 K and the pressure of 1 bar. Both bilayers formed in the liquid phase with a less ordered structure. For the Span60 bilayer, most melatonin molecules are preferentially located in the region between the head and tail groups of Span60. However, the addition of melatonin in the Span60/Chol bilayer results in the structural and dynamical properties significantly. Most melatonin molecules have locally stayed at the water-Span60 interface with higher diffusion in both lateral and transverse directions. Furthermore, our study suggests that the addition of cholesterol in the Span60 bilayers can increase the stability and rigidity of niosomes which can improve the efficacy of melatonin encapsulation, compared with the pure Span60 bilayer. Such information is necessary for the preparation of niosomes for the drug delivery system.

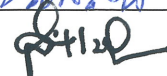
School of Physics

Academic Year 2020

Student's Signature



Advisor's Signature



Co-advisor's Signature



ACKNOWLEDGEMENT

First, I would like to express my sincere to myself for learning a lot about how to work as a good theorist and I have gained so many skills working with myself. I also would like to thank my advisor Prof. Dr. Santi Maensiri for inspiring my research career since I was a first-year student and for financial support throughout this study. Without the kindness of co-advisor Assoc. Prof. Dr. Sripajak Kongsuk principal senior research at Khon Kaen University, this work and my Doctor of Philosophy could not be done. Working and living at Suranaree University of Technology was the turning point in my life and it was the most rewarding moment of my life. I was appreciated with general support from my advisor Prof. Dr. Santi Maensiri, and the computer simulation skills from Assoc. Prof. Dr. Sripajak Kongsuk

This project aims to fundamental understanding on bilayer structure and dynamics properties of drug carrier, named niosomes, which were employed to melatonin encapsulation. Computer simulation techniques such as molecular dynamics play a major role in this investigation. Experimental studies using X-ray scattering and NMR, for example, are needed to test the theoretical models presented in this work. The preliminary works of Dr. Sripajak Kongsuk and Dr. Jeffrey Roy Johns gave a priceless guiding way for solving the problem of my thesis work.

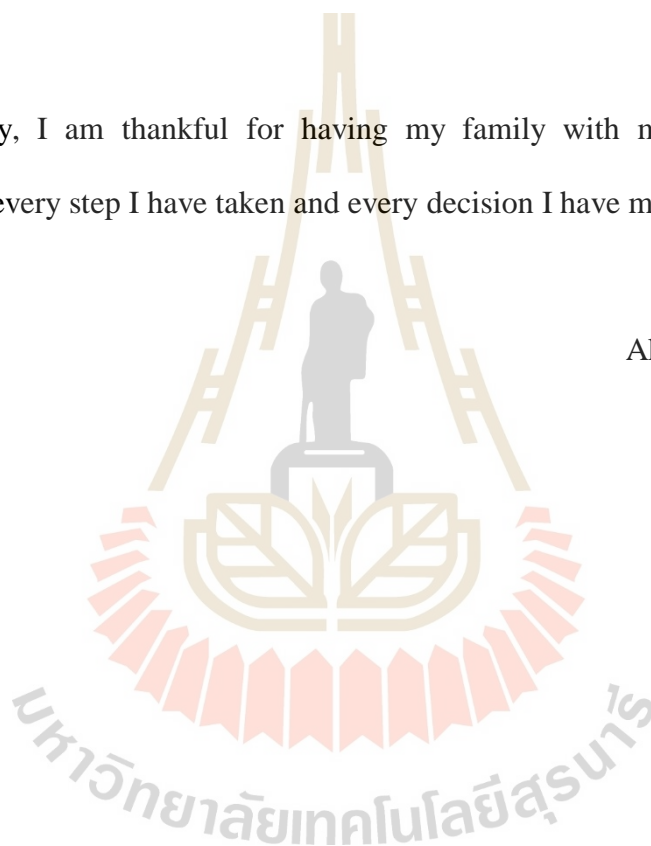
There are many people behind the success of my thesis. The support from Advanced Materials Physics laboratory (AMP) members is indispensable and I am grateful to be a part of AMP group. I am confident that the study environment is a key

factor that shapes my perspective and performance. I would like to mention my friends at the School of Physics who have helped me with every problem. I have met and my teachers teach me valuable lessons and encourage me to do what I want.

I would like to thank the SUT Center of Excellence on Advanced Functional Materials (SUT-AFM), Suranaree University of Technology, Nakhon Ratchasima, Thailand. For funding my entire study since the beginning of my Doctor's degree until now.

Finally, I am thankful for having my family with me and always small supports me every step I have taken and every decision I have made.

Aksornnarong Ritwiset



CONTENTS

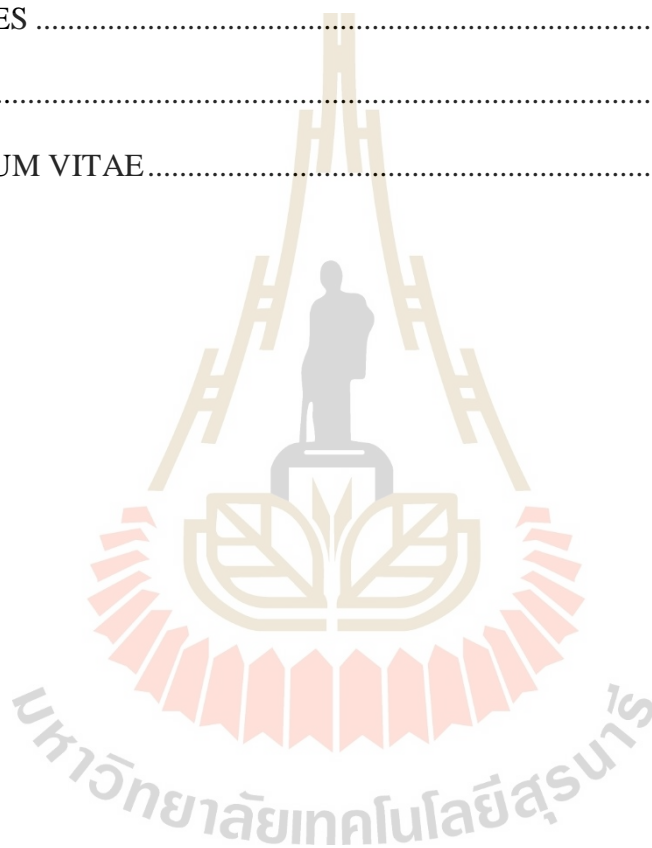
	Page
ABSTRACT IN THAI.....	I
ABSTRACT IN ENGLISH	III
ACKNOWLEDGEMENT	V
CONTENTS.....	VII
LIST OF TEBLES	X
LIST OF FIGURES	XII
LIST OF ABBREVIATIONS.....	XXII
CHAPTER	
I INTRODUCTION.....	1
1.1 Significant and rational of the research	1
1.2 Research objectives	5
1.3 Scope of the study	5
1.4 Location of the research	6
1.5 Outline of thesis.....	6
II LITERATURE REVIEWS	8
2.1 Introduction	8
2.2 Melatonin in aqueous solution.....	10
2.3 Melatonin encapsulated niosomes	12
2.4 Effect of melatonin and cholesterol on the lipid bilayer membranes	14

CONTENS (Continued)

		Page
III	COMPUTATIONAL METHODOLOGY	23
	3.1 Basic of the molecular dynamic method	23
	3.2 General system setting and simulation details.....	26
	3.2.1 Melatonin in aqueous solution and at the water-air interface.....	26
	3.2.2 Melatonin inserted into niosome bilayers	30
IV	RESULTS AND DISCUSSION	35
	4.1 Melatonin in aqueous solution and at the water-air interface.....	35
	4.1.1 Energetic and density profiles	35
	4.1.2 Hydrogen bond analysis	38
	4.1.3 Molecular orientation	41
	4.1.4 Dynamical properties of melatonin	44
	4.1.5 Hydrogen bond dynamics.....	48
	4.2 Melatonin in the niosome bilayers	51
	4.2.1 Bilayer structures.....	51
	4.2.2 Molecular orientation	59
	4.2.3 Order parameters	63
	4.2.4 Hydrogen bond and energetic interaction analysis.....	65
	4.2.5 Lateral and transversal diffusion	69
V	CONCLUSIONS & FUTURE DIRECTION OF WORK.....	73
	5.1 Melatonin in aqueous solution and at the water-air interface.....	73

CONTENS (Continued)

	Page
5.2 Melatonin in the niosome bilayers	74
5.3 Future direction of work	75
REFERENCES	77
APPENDIX.....	95
CURRICULUM VITAE.....	98



LIST OF TEBLES

Table	Page
2.1 Bilayer properties of Span60 bilayers containing flavones, chrysin, and luteolin respectively, at different concentrations (Myung <i>et al.</i> , 2016).....	22
3.1 Definitions of atom types of melatonin molecule, atomic partial charges using the B3LYP/6–31G(d,p) calculation and generated from the CHELPG technique, as well as corresponding atomic mass.....	29
4.1 The average number of hydrogen bonds per melatonin molecule, $\langle n_{\text{HB}} \rangle$, for the melatonin–water and the melatonin–melatonin interactions based on considering all pairs of donors and acceptors.....	44
4.2 The self–diffusion coefficients (D_s) of melatonin and water molecules obtained from three different systems.....	47
4.3 Average hydrogen bond lifetime, ($\langle \tau_{\text{HB}} \rangle$), for the melatonin–water and the melatonin–melatonin interactions considered the pair of donor and acceptor atoms on both melatonin and water molecules.....	50
4.4 Comparison of some physical properties of the pure Span60 and the Span60/Chol bilayers which were added with melatonin, flavone, chrysin, and luteolin molecules, respectively.....	56

LIST OF TEBLES (Continued)

Table	Page
4.5 The calculated average hydrogen bond number per molecule ($\langle n_{HB} \rangle$) for the Span60, the Span60/Mel, the Sapn60/Chol, and the Span60/Chol/Mel bilayers, respectively. The pair of hydrogen bond formation was represented as the Span60/water (SW), the Span60/Span60 (SS), the Span60/cholesterol (SC), the Span60/melatonin (SM), the cholesterol/water (CW), the cholesterol/melatonin (CM), the melatonin/water (MW), and the melatonin/melatonin (MM), respectively.....	66
4.6 The calculated average van der Waals interaction ($\langle E_{vdW} \rangle$) for the Span60, the Span60/Mel, the Sapn60/Chol, and the Span60/Chol/Mel bilayers, respectively. The van der Waals interactions were represented by the pair of the Span60/Span60(SS), the Span60/cholesterol (SC), the cholesterol/cholesterol (CC), the Span60/melatonin (SM), the cholesterol/melatonin (CM), and the melatonin/melatonin (MM), respectively.....	68
4.7 The diffusion coefficients of Span60, cholesterol, and melatonin molecules, obtained from MD simulations of the Span60 bilayers with and without cholesterol and melatonin inclusion.....	71

LIST OF FIGURES

Figure	Page
2.1 Molecular structure of (a) sorbitan monostearate (Span60); formula $C_{24}H_{46}O_6$; molecular weight $430.62 \text{ g.mol}^{-1}$; melting point $54\text{--}57 \text{ }^\circ\text{C}$, (b) cholesterol; formula $C_{27}H_{46}O$; molecular weight $386.65 \text{ g.mol}^{-1}$; melting point $148\text{--}150 \text{ }^\circ\text{C}$ and (c) melatonin; formula $C_{13}H_{16}N_2O_2$; molecular weight $232.283 \text{ g.mol}^{-1}$; melting point $117 \text{ }^\circ\text{C}$ (From: https://en.wikipedia.org/wiki/Main_Page).....	9
2.2 Structure of niosome vesicle that can encapsulate both hydrophobic drugs and hydrophilic drugs into its bilayer shell and inner core (Sajid <i>et al.</i> , 2014).....	12
2.3 (a) Morphology and particle size distribution of melatonin niosomes revealed by scanning electron microscope $20,000\times$ (Priprem <i>et al.</i> , 2014), and (b) TEM image of Span60 formulation prepared 1 : 1 ratio with cholesterol $40,000\times$ (Shilakari Asthana <i>et al.</i> , 2016).....	13

LIST OF FIGURES (Continued)

Figure	Page
<p>2.4 MD simulations of DPPC and DOPC bilayers presence and absence melatonin. DPPC (upper) and DOPC (lower) bilayers. Left: absence melatonin: (a) DPPC, (c) DOPC. Right: presence melatonin: (b) DPPC–melatonin, (d) DOPC–melatonin. Orange is shown in melatonin molecules. Snapshots of MD simulation were taken after 400 ns at $T = 300$ K. Simulation time of the total in each system was 500 ns. Note the pure DPPC system (for DPPC, $T_m = 314$ K) in gel phase on the left–hand side. To enhance and maintain local fluidity appears by melatonin. A visible in the DPPC membrane with melatonin (upper right) this is Q2. Since is above its main phase transition ($T_m = 253$ K) of the DOPC system, the melatonin effects are more subtle (Drolle <i>et al.</i>, 2013).....</p>	15
<p>2.5 Thicknesses of DOPC (upper) and DPPC (lower) bilayers when the cholesterol (left) and melatonin (right) were added into the systems. Changes to the D_{HH} thickness obtained from SAND represent by blue circles, while changes in the D_s thickness obtained from SANS correspond to green squares. Fits to the data are black lines (Drolle <i>et al.</i>, 2013).....</p>	16
<p>2.6 Schematics represent locations of (a) cholesterol and (b) melatonin in the lipid membrane (Drolle <i>et al.</i>, 2013).....</p>	16

LIST OF FIGURES (Continued)

Figure	Page
2.7 Electron density profile shown as a function of the position of melatonin molecules along the anionic lipid membranes (z-axis) (Dies <i>et al.</i> , 2014).....	16
2.8 Z-axis position of melatonin as a function of simulation times. Inside DMPC bilayer were penetrated by melatonin (red symbols stand for the phosphorus atoms position in each layer while green symbols specify the position of the center of mass of melatonin) at cholesterol concentrations of 0%, 30%, and 50%, respectively (Lu and Martí, 2019).....	18
2.9 Representative bound states of snapshots for melatonin at the membrane interface. Melatonin colors, DMPC, and cholesterol: cyan (carbon), dark blue (nitrogen), red (oxygen), white (hydrogen). Green solid lines indicated hydrogen bonds. (a): a case at cholesterol concentration of 0%, with two DMPC molecules bound to melatonin; (b): a case at cholesterol concentration of 30%, with one DMPC and one cholesterol molecule bound to melatonin (Lu and Marti, 2020).....	19
2.10 Electron density normalized black (Span60), green (cholesterol), and orange (unsubstituted flavone) for (a) 3 mol%, (b) 25 mol%, and (c) 50 mol% unsubstituted flavone were contained in a Span60 bilayer (Myung <i>et al.</i> , 2016).....	21

LIST OF FIGURES (Continued)

Figure	Page
2.11 Left: Electron density normalized black (Span60), green (cholesterol), and orange (chrysin) for (a) 3 mol%, (b) 25 mol%, and (c) 50 mol% chrysin were contained in a Span60 bilayer. Right: Electron density normalized black (Span60), green (cholesterol), and orange (luteolin) for (a) 3 mol%, (b) 25 mol%, and (c) 50 mol% luteolin were contained in a Span60 bilayer (Myung <i>et al.</i> , 2016).....	21
3.1 The intramolecular interactions of (a) the bond stretching, (b) the angle bending, and (c) the dihedral rotation, respectively. Additional details see in gromacs user manual (ftp://ftp.gromacs.org/pub/manual).....	24
3.2 The intermolecular interactions of (a) the van der Waals and (b) the electrostatic interactions. Additional details see in Gromacs user manual (ftp://ftp.gromacs.org/pub/manual).....	25
3.3 (a) The structure of melatonin with atom type names as defined in Table 3.1, (b) a system model of melatonin molecules in aqueous solution, and (c) a system model of melatonin molecules at the water-air interface. Coloring in Figure 3.3a: the carbon atom and hydrocarbon group (e.g., C, CR51, CR61, CH2, and CH3), cyan; O, red; N, blue; H, gray. The two yellow arrows shown in Figure 3.3a were defined as the two vectors for the calculation of tilt angle distributions of head and tails.....	30

LIST OF FIGURES (Continued)

Figure	Page
<p>3.4 The molecular structures of (a) Span60 (b) cholesterol and (c) melatonin, respectively. With defined the head and tail group and included number index of atomic types for clarifying discussion. Coloring scheme in Figure 3.4: the carbon atom and hydrocarbon group (e.g., C, CH1, CH2, CH3 or others) include green, gray, cyan; O, red; N, blue; H, white. The two yellow arrows shown in Figures 3.4a and c were defined as the two vectors for the calculation of tilt angle distributions.....</p>	31
<p>3.5 Schematic representations of (a) the Span60/Mel, and (b) the Span60/Chol/Mel bilayers, respectively.....</p>	33
<p>4.1 Time evaluation of total potential energy (U) of the system of melatonin in the bulk water (green) and that of melatonin at the water-air interfaces (blue). The inset figure shows the time variation of the simulation box size in the three directions for the bulk water system.....</p>	36
<p>4.2 Density distributions of water and melatonin molecules for the bulk water system as a function of (a) x-, (b) y- and (c) z-coordinates, respectively. The head and tail groups of melatonin were separately plotted for clarifying discussion.....</p>	37

LIST OF FIGURES (Continued)

Figure	Page
4.3 Density distributions of water and some molecular sites of melatonin as a function of z-coordinate for the system of melatonin at the water-air interface. The functional groups of melatonin including the head, the tail, carbonyl (C=O), amide (N-H), indole (N-H), and methoxy (-OCH ₃) were separately plotted for clarifying discussion.....	39
4.4 Two configurations of melatonin at the initial time (0 ns) and at the final time (260 ns) of the simulation of (a) the system of melatonin in aqueous solution and (b) the system of melatonin at the water-air interface. Coloring scheme: carbon atom and hydrocarbon group are cyan; oxygen is red; nitrogen is blue, and hydrogen is gray.....	39
4.5 The hydrogen bond distribution as a function of the DA distance for the melatonin-water interaction (a) in the aqueous solution and (b) at the water-air interface as well as that for the melatonin-melatonin interaction (c) in the aqueous solution and (d) at the water-air interface. Coloring schemes for the melatonin-water hydrogen bonding are defined as follows: carbonyl O-HW, black; indole NH-OW, blue; amide NH-OW, red; methoxy OA-HW, dark cyan; and that for the melatonin-melatonin hydrogen bonding is defined as follows: indole NH-carbonyl O, black; amide NH-carbonyl O, blue; indole NH-methoxy OA, red; amide NH-methoxy OA, dark cyan.....	43

LIST OF FIGURES (Continued)

Figure	Page
4.6 Tilt angle distributions of the head and tail groups of melatonin (a) for the bulk water and (b) for the water-air interface systems.....	44
4.7 Average displacement of the center of mass of melatonin molecules in x -(black), y -(red), and z -(blue) directions: (a) for the bulk water and (b) for the water-air interface systems.....	45
4.8 (a) Mean squared displacement (MSD) plots of the water molecule for the bulk water with (red) and without (black) melatonin inclusion, and for the water-air interface (blue) systems, (b) The MSD plots of melatonin for the bulk water (red) and the water-air interface (blue) systems.....	47
4.9 Intermittent hydrogen bond time correlation function, $C(t)$, of the melatonin-water interactions for (a) the bulk water and (b) the water -air interface systems. The $C(t)$ plots of the melatonin-melatonin interactions for (c) the bulk water and (d) the water-air interface systems.....	51

LIST OF FIGURES (Continued)

Figure	Page
<p>4.10 Mass density distributions of the Span60 head and tail groups, cholesterol, melatonin, and water molecules versus to z-direction for (a) the Span60 bilayer with melatonin (solid line) and without melatonin (short dash-dot line) addition and (b) the Span60/Chol bilayer with melatonin (solid line) and without melatonin (short dash-dot line) addition. Coloring schemes are defined as follows: water, blue; Span60 head, dark cyan; Span60 tail, green; cholesterol, cyan; melatonin, magenta.....</p>	53
<p>4.11 Two dimensional–radial distribution functions (2D–rdfs), calculated only on the <i>xy</i>–plane for the Span60/cholesterol (SC) and Span60/melatonin (SM) bilayer systems. The 2D–rdfs were calculated from the Span60 head group to cholesterol (green line) and melatonin (blue line) for (a) the Span60/Chol and the Span60/Mel bilayers, and (b) the Span60/Chol/Mel bilayer. The centers of mass of the Span60 head group, cholesterol, and melatonin were used throughout these calculations.....</p>	58
<p>4.12 Molecular configurations of (a) the Span60, (b) the Span60/Mel, (c) the Span60/Chol, and (d) the Span60/Chol/Mel bilayers, respectively which were taken from the MD simulation. Color scheme: cholesterol, green; Span60 tails, cyan; melatonin, gray; oxygen, red; nitrogen, blue; hydrogen, gray.....</p>	60

LIST OF FIGURES (Continued)

Figure	Page
4.13 (a) The tilt–angle distribution of the Span60 tail for the pure Span60 (green short dashed line), Span60/mel (green solid line), the Span60/chol (blue short dashed line), and the Span60/chol/mel bilayers (blue solid line), respectively. (b) the tilt–angle distribution of melatonin for the Span60/mel (green solid line) and the Span60/Chol/Mel bilayers (blue solid line), respectively.....	61
4.14 Molecular configuration of melatonin molecules (Span60 and cholesterol were not shown) distributed in the Span60 bilayer (a) without cholesterol and (b) with cholesterol inclusion, respectively. Melatonin molecule color scheme: the carbon atom and hydrocarbon group, cyan; oxygen, red; nitrogen, blue; hydrogen, gray.....	62
4.15 Order parameter, S_{CD} , on hydrocarbon chains of the Span60 molecules, as depend on carbon sites position for the pure Span60, the Span60/Mel, the Span60/Chol, and the Span60/Chol/Mel bilayers, respectively.....	64
4.16 Mean squared displacement (MSD) of lateral diffusion (a) for Span60 and (b) for the cholesterol molecules obtained from the simulations of the pure Span60, the Span60/Mel, the Span60/Chol, and the Span60/Chol/Mel bilayers, respectively.....	70

LIST OF FIGURES (Continued)

Figure	Page
4.17 Mean squared displacement (MSD) of the lateral and the transversal diffusions of melatonin molecule obtained from the simulations of the Span60/Mel and the Span60/Chol/Mel bilayers, respectively.....	71



LIST OF ABBREVIATIONS

MD	=	Molecular dynamics
NTP	=	Particles number (N), temperature(T), and pressure (P) constant
NVT	=	Particles number (N), volume (V), and temperature (T) constant
U	=	Total potential energy
HW	=	Hydrogen water
OW	=	Oxygen water
COM	=	Center of mass
n_{HB}	=	Hydrogen bond number per molecule
MSD	=	Mean squared displacement
D_s	=	Self-diffusion coefficient
$\langle \dots \rangle$	=	Average overall
$C(t)$	=	Intermittent hydrogen bond time correlation function
τ_{HB}	=	Hydrogen bond lifetime
mel	=	Melatonin molecule
Span60	=	Sorbitan monostearate molecule
chol	=	Cholesterol molecule
A_0	=	Area per one lipid leaflet
D_{HH}	=	Bilayer thickness
$g(r)$	=	Radial distribution functions
L_α	=	Gel phase

LIST OF ABBREVIATIONS (Continued)

L_o	=	Liquid-ordered phase
L_E	=	Liquid-expanded phase
L_C	=	Liquid-condensed phase
S_{CD}	=	deuterium order parameters
E_{vdW}	=	van der Waals interactions
D_{xy}	=	the lateral diffusion coefficients
D_z	=	the transversal diffusion coefficients

CHAPTER I

INTRODUCTION

1.1 Significant and rational of the research

Nanotechnology applications in the nanomedicine field for diagnosis and therapy have made rapid progress, especially in drug delivery systems (Moghassemi and Hadjizadeh, 2014). In recent years, much more attention has been paid to vesicular drug delivery systems including liposomes, ethosomes, and niosomes due to has special characteristics, e.g. high entrapment and release rate, low toxicity, and biodegradability (Moghassemi and Hadjizadeh, 2014; Heneweer *et al.*, 2012). As a result, synthesis and characterization of these carriers for drug delivery to specific targets through nanoencapsulation have been widely studied by theoretical and experimental methods (Yeom *et al.*, 2014; Ritwiset *et al.*, 2014; Han, 2013; Pirvu *et al.*, 2010). These studies provide necessary information on mechanisms of vesicular formation, stability, molecular transport through the cell– membrane, and molecular interaction between drug/lipid membranes. However, liposomes and ethosomes suffer from the problem that they are composed of very reactive naturally occurring phospholipids that are not stable in air and rapidly undergo oxidation and hydrolysis, leading to effects on long-term stability and making formulation very costly (Giddi *et al.*, 2007). Furthermore, natural sources of phospholipids are not also pure and the synthesis sources prohibitively expensive for production drug manufacture. Niosomes have similar structural like liposomes and ethosomes but are composed of synthesis

non-ionic surfactants, e.g. sorbitans (Spans) or polysorbates (Tweens), usually employed in combination with cholesterol (Giddi *et al.*, 2007). This makes them more durable to oxidation and hydrolysis, doing formulation compares to liposomes much cheaper and simpler, as well as giving good long-term stability (Nasr *et al.*, 2008). The surfactants of Span and Tween are also biocompatible, have very low toxicity, and are cheaply available that high purity (Moghassemi and Hadjizadeh, 2014). Due to their prominent properties, they are popularly used in the food and drug industry (Sankhyan and Pawar, 2012). Spans are often used as absorption enhancers (Bhattacharjee *et al.*, 2010; Yamamoto *et al.*, 1996) due to their properties of surfactant. It is well-known that the mechanism of niosome formation has related to the self-assembly of non-ionic surfactants on water surfaces, making to the formation of monolayer/bilayer structures (Uchegbu and Vyas, 1998).

In the past decades, many MD simulations have extensively studied liposomes and ethosomes because of a lot of available experimental data to contribute to the models (Xiang and Anderson, 2006; Poger and Mark, 2010; Siwko *et al.*, 2009). A few MD studies of Span60 bilayer in the presence of 50 mol% cholesterol were used in drug delivery include flavonoids have also reported (Myung *et al.*, 2016). However, there are needed of experimental data to test the theoretical models. These previous reports provide insight into the bilayer structure and dynamics properties, including the thickness, surface area per molecule, order parameters, diffusion coefficient, and the interactions of the drug with a niosome bilayer. The study of Nasserri (Nasserri, 2005) found that Span60 prepared with ~50 mol% cholesterol exhibits layers of most stable and elasticity at both room and body temperatures. According to Ritwiset *et al.* (Ritwiset *et al.*, 2016) absence of cholesterol, the bilayer less fluidity and was in the

gel-phase. The closely packed Span60 molecules and their tail groups were tilted along the bilayer normal direction. The presence of 50 mol% cholesterol, more loosely packed of Span60 molecules with a less ordered structure, and bilayer in a liquid-order phase. To the best of our knowledge, the MD simulation of the melatonin's effects in the bilayers of pure Span60 and Span60 with 50 mol% cholesterol in an aqueous solution has never been studied before. Thus, the investigation of melatonin influence on the structure and phase formation of the niosome bilayers is interesting.

N-acetyl-5-methoxytryptamine of melatonin, is a natural hormone produced by the pineal gland in humans and animals, has been extensively studied for its therapeutic potential in sleep disorders (Chen *et al.*, 2011; Bubenik *et al.*, 1999). It also plays an important role in preventing some diseases including cardiovascular disease (Tengattini *et al.*, 2008), Alzheimer's disease (Rosales-Corral *et al.*, 2012), and certain types of cancers (Vijayalaxmi *et al.*, 2002). In addition also shown protective effects in bacterial and viral infections of melatonin likely due to its anti-inflammatory and anti-oxidative effects (García *et al.*, 2020). Recently, a further benefit of melatonin can reduce the severity of influenza and the COVID-19 pandemic (Shneider *et al.*, 2020). As above information, a treatment to overcome a COVID-19 infection use of supplemental melatonin is justified (Reiter *et al.*, 2020). Previously, there have been many efforts of the preparation and characterization of melatonin loaded vesicular nanocarriers such as liposomes, ethosomes, and niosomes for decreased side effects and enhanced specificity of drug uptakes to the target cells (Priprem *et al.*, 2018; Dubey *et al.*, 2007; Khan and Irchhaiya, 2016). Generally, respiratory system has containing of secretions as an important component. Therefore,

the solubility of melatonin in aqueous solution is a basic key factor that leads to solve a something puzzles in systems are more complex. It is well-known that melatonin is less soluble in aqueous buffers compared with organic solvents. However, the solubility of melatonin in aqueous solution can be improved and stable over a wide range of the temperature (4 °C – 37 °C) based on using the appropriate preparation method (Shida *et al.*, 1994; Daya *et al.*, 2001; Cavallo and Hassan, 1995). It remains the question of how melatonin interacting with the aqueous compartment of the cell as well as how the formation of melatonin in the presence of aqueous media. To the best of our knowledge, detailed information at the molecular level of structural and dynamical properties of melatonin in the aqueous solution and at the water-air interface is not available. Therefore, in-depth study of the molecular properties is necessary such as the formation structure, interactions, and dynamic properties of melatonin, which can affect the macromolecular behaviors of fluidity and stability of melatonin in the aqueous solution. Such information is necessary for drug delivery development.

In the first part, we have addressed the investigation of molecular structure and dynamical behaviors of melatonin in the aqueous solution and at the water-air interface, systems based on using MD simulation techniques. The simulation results not only provide a clear molecular picture of the structure and dynamic behavior of melatonin in the aqueous solution and at the water-air interface but also give good agreement with the previous experimental studies (García *et al.*, 1997; Milani and Sparavigna, 2018; Severcan *et al.*, 2005).

In the second part, the bilayer structure and dynamical properties of the melatonin's effects on the pure Span60, and Span60 with 50 mol% cholesterol

composition were focused based on using the MD simulation technique. Structural and dynamical properties such as area per molecule, bilayer thickness, molecular orientation, order parameters, diffusion coefficient, van der Waals interactions, and hydrogen bond analysis from the simulations were calculated and compared to previous studies (Ritwiset *et al.*, 2016; Somjid *et al.*, 2018; Myung *et al.*, 2016). These simulations not only provide structural and dynamical properties, but our results also give a clear picture of the dynamics of the bilayer formation with and without melatonin inclusion at the molecular level.

1.2 Research objectives

The main objectives of this Ph.D. thesis are

1.2.1 To study the melatonin behaviors at the molecular structure and dynamical in the aqueous solution and at the water-air interface systems.

1.2.2 To study the melatonin formation and stability in an aqueous solution and at the water-air interface.

1.2.3 To study the bilayer structure and dynamics properties of the pure Span60, and the Span60 with 50 mol% cholesterol inclusion when the presence 30 mol% of melatonin into those bilayers and compared structural and dynamical properties with bilayer systems without melatonin inclusion.

1.2.4 To study the influence of melatonin on the phase transition of the Span60-based niosome bilayers.

1.3 Scope of the study

In this research, we employ the MD technique to investigate structural and dynamical properties of melatonin in aqueous solution and at the water-air interface,

as well as the niosome bilayers with and without cholesterol inclusion when the melatonin was added into those bilayers. The model of niosome bilayers is generated from the mixture of Span60 and cholesterol (Chol) molecules at the two different compositions (Span60:Chol=1:0 and Span60:Chol=1:1) in the aqueous solution. The MD simulations of the niosome bilayers with and without melatonin inclusion are performed at the temperatures of 298 K under the pressure of 1 bar, respectively. All simulations are carried out using Gromacs program. The influence of melatonin on the structure and phase transition of the niosome bilayers is investigated.

1.4 Location of the research

This study was carried out at Advanced Materials Physics (AMP) Laboratory, School of Physics, Institute of Science, Suranaree University of Technology, Nakhon Ratchasima, Thailand, and Department of Physics, Faculty of Science, Khon Kaen, Thailand.

1.5 Outline of thesis

The thesis is organized as follows:

1.5.1 Chapter I introduces the background and the research motivation.

1.5.2 Chapter II provides the literature review of information concerning the synthesis method, investigation technique, molecular interactions, structure and dynamics properties of Span60-based niosome bilayers, melatonin in aqueous solution, and the effect of melatonin on the lipid bilayer membranes.

1.5.3 Chapter III describes the methodology procedures, system model, and simulation details of melatonin in the aqueous solution and at the water-air interface systems as well as the niosome-based materials.

1.5.4 Chapter IV presents the simulation results and discussion.

1.5.5 Chapter V contains the conclusions and recommendations of this thesis.



CHAPTER II

LITERATURE REVIEWS

2.1 Introduction

Ester of sorbitan (a sorbitol derivative) and stearic acid (see Figure 2.1a) is sorbitan monostearate (Span60) and is sometimes called synthetic wax. To keep water and oils mixed and are used in the manufacture of food and healthcare products the Span60 is primarily used as an emulsifier and is a non-ionic surfactant with emulsifying, dispersing, and wetting properties. To create synthetic fibers, metal machining fluid, and brighteners in the leather industry, and as an emulsifier in coatings, pesticides, Span60 were employed as well as various applications in the plastics, food and cosmetics industries. It is also approved by the European Union for use as a food additive (emulsifier) by Span60 (Agency, 2011). Nowadays Span60 is widely accepted and used to prepare vesicular drug carriers for drug delivery systems. The mixture of Span60 and cholesterol with a proper composition ratio in aqueous media resulted in a vesicular nanoparticle which is called niosome. Cholesterol (Figure 2.1b) was added into the niosome to make its stability and fluidity. However, these properties of niosome particles strongly depended on the preparation method and cholesterol concentration. Also, the efficiency of drug entrapment of niosomes was closely related to these properties. A hormone primarily released by the pineal gland is melatonin (Figure 2.1c),

that regulates the sleep-wake cycle (Auld *et al.*, 2017; Faraone, 2014). It is often used for the short-term treatment of insomnia since is a dietary supplement, such as from jet lag or shift work. Important roles in many regulatory processes of melatonin such as protection against inflammation, intestinal reflexes, reproduction, and metabolism.

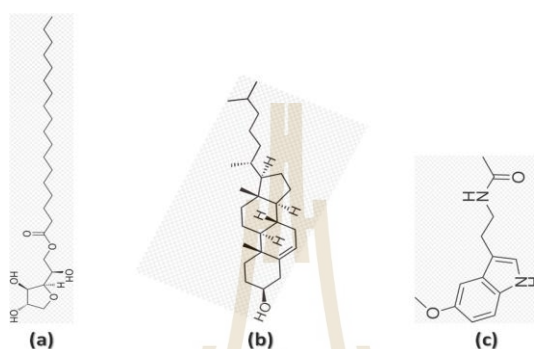


Figure 2.1 Molecular structure of (a) sorbitan monostearate (Span60); formula $C_{24}H_{46}O_6$; molecular weight $430.62 \text{ g.mol}^{-1}$; melting point $54\text{--}57 \text{ }^\circ\text{C}$, (b) cholesterol; formula $C_{27}H_{46}O$; molecular weight $386.65 \text{ g.mol}^{-1}$; melting point $148\text{--}150 \text{ }^\circ\text{C}$ and (c) melatonin; formula $C_{13}H_{16}N_2O_2$; molecular weight $232.283 \text{ g.mol}^{-1}$; melting point $117 \text{ }^\circ\text{C}$ (From: https://en.wikipedia.org/wiki/Main_Page).

Additionally, several studies indicated that melatonin has protective effects in many diseases including Alzheimer's disease, cardiovascular disease, and antioxidant effects as well as certain types of cancers (Beyer *et al.*, 1998). However, although the synthesis of melatonin has been achieved and widely used for medical and cosmetic purposes, the underlying mechanisms of melatonin delivery through cell membranes have yet to be adequately explained. Therefore, many efforts have been addressed on the influence of melatonin in lipid membrane structure and its dynamical properties (Bubenik *et al.*, 1999; Tengattini *et al.*, 2008; Rosales-Corral *et al.*, 2012; Vijayalaxmi *et al.*, 2002; Reiter *et al.*, 1998; Reiter *et al.*, 1999). Understanding interactions of

melatonin with lipid membranes and water molecules surrounding the membranes are necessary information for therapeutic applications. It is well known that water is of major importance to all living things and most of the water in the human body is contained in our cells. This leads all the cells and organs to function efficiently. One of the main water functions is that water act as a medium in metabolic and biochemical reactions, absorption of various nutrients in the digestive system, and transport of chemicals to or from the cell. As mentioned above, melatonin can interact at the membrane surface with protein receptors to transfer it into the blood. However, it has been reported that there are many sites of melatonin interaction with the cell membrane where a protein receptor is not necessary (Pshenichnyuk *et al.*, 2017). It indicates that this molecule can penetrate the lipid bilayer and bath of the cell in every part.

2.2 Melatonin in aqueous solution

Melatonin molecules in aqueous solution have been investigated in both experimental and theoretical studies for the understanding of their hydration structure and interaction with lipid membranes (Filadelfi and Castrucci, 1994). According to the quantum calculations combined with magnetic circular dichroism (MCD) study of melatonin in an aqueous solution (Shillady *et al.*, 2003), a preferable hydration structure of melatonin is the water bridged structure in which a water molecule interacts with the amide–keto oxygen and indole N–H atoms. This similar result has been confirmed by the ultraviolet and infrared spectroscopy studies of melatonin–water clusters (García *et al.*, 1997). These studies imply that water plays a crucial role in the conformational change of melatonin because it processes several hydrogen

bonding sites for the attachment of water, especially the water molecules in the first hydration. Such interactions result significantly in the stability of melatonin in aqueous solution (Daya *et al.*, 2001; Cavallo and Hassan, 1995), dynamic properties of blood (Milani and Sparavigna, 2018), and transportation through cell membranes (Filadelfi and Castrucci, 1994; García *et al.*, 1997; Akkas *et al.*, 2007).

As reviewed above, we found that the behavior of melatonin–aggregation in aqueous solution has been widely studied in experiments. Thus, it is interesting for us to investigate the formation structure, dynamical behaviors, and interactions of melatonin molecules in the aqueous solution and at the water-air interface systems based on using MD simulation techniques. This study not only shows a clear picture of molecular structure and dynamical properties of melatonin in the presence of different water phases for using the information supported in experimental results but also provides demonstrated the interactions of melatonin aggregation–water in both aqueous solution and at the water-air interface systems which are according to the previous theoretical and experimental studies (Shillady *et al.*, 2003; Florio and Zwier, 2003; Milani and Sparavigna, 2018).

Considering the nature of melatonin structure having a high hydrophobic property, it remains the question of how melatonin interacts with the aqueous compartment of the cell as well as how the formation of melatonin in the presence of aqueous media. To the best of our knowledge, detailed information at the molecular level of structural and dynamical properties of melatonin in the aqueous solution and the water-air interface is not available. Therefore, in-depth study of the molecular properties is necessary such as the formation structure, interactions, and dynamic properties of melatonin, which can affect the macromolecular behaviors of fluidity and

stability of melatonin in the aqueous solution. Such information is necessary for drug delivery development. In the present study, we have addressed the investigation of molecular structure and dynamical behaviors of melatonin in the aqueous solution and at the water-air interface based on using MD simulation techniques. The simulation results not only provide a clear molecular picture of the structure and dynamic behavior of melatonin in the aqueous solution and at the water-air interface but also give good agreement with the previous experimental studies (García *et al.*, 1997; Milani and Sparavigna, 2018; Severcan *et al.*, 2005).

2.3 Melatonin encapsulated niosomes

The sizes of niosome vesicles are microscopic from micro to nano-size depending on the preparation method as shown in Figure 2.2.

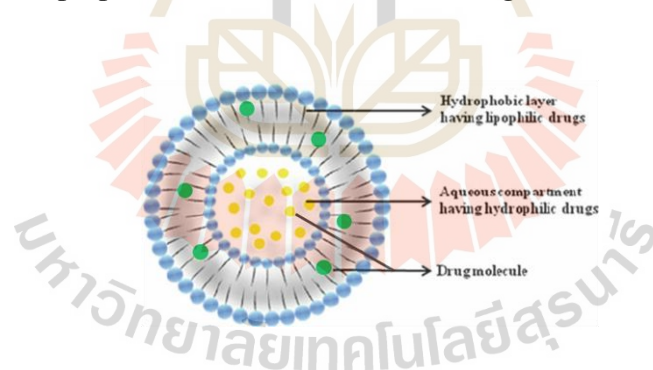


Figure 2.2 Structure of niosome vesicle that can encapsulate both hydrophobic drugs and hydrophilic drugs into its bilayer shell and inner core (Sajid *et al.*, 2014).

Niosome-based Span60 has a high phase transition temperature due to the long saturated alkyl chain (C16) resulting in high entrapment efficiency (El-Mahdy *et al.*, 2020). The additives cholesterol were used as its molecular size fits into the bilayer structure of the niosomes, thus able to decrease the hydrodynamic diameter or stabilize

through hydrogen bonding and enhance entrapment efficiency (Ritwiset *et al.*, 2016; Mahale *et al.*, 2012). This can be developed melatonin encapsulated by niosome vesicles to reduce adverse side effects, avoid the first-pass metabolism, decrease dosing frequency, improve efficacy, promote skin permeation, and delay rapid elimination of drugs (Manosroi *et al.*, 2010; Muzzalupo *et al.*, 2011). The average size of niosome vesicle (Span60-based niosomes) encapsulated melatonin is about 197 nm, zeta potential -78.8 mV, and entrapment efficiency 92.7% (Figure 2.3a).

This nanocarrier was prepared by the sonication method (Priprem *et al.*, 2014). Monitoring zeta potential provides information on the surface properties and an indication of the stability of the vesicles, which could prevent particle aggregation for negatively charged interface and therefore high stability. According to the negatively zeta potential in the case of Span60 prepared by thin-film hydration technique (Shilakari Asthana *et al.*, 2016), niosomal formulation containing Span60 (surfactant to cholesterol ratio 1:1) presented the highest entrapment efficiency and TEM analyses found that spherical in the shape of niosomal (see Figure 2.3b). This formulation has a stable storage condition at the end of the study.

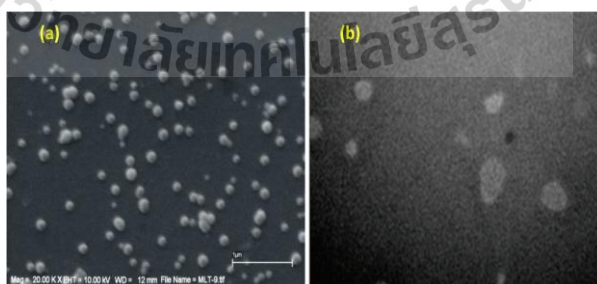


Figure 2.3 (a) Morphology and particle size distribution of melatonin niosomes revealed by scanning electron microscope 20,000 \times (Priprem *et al.*, 2014), and (b) TEM image of Span60 formulation prepared 1 : 1 ratio with cholesterol 40,000 \times (Shilakari Asthana *et al.*, 2016).

2.4 Effect of melatonin and cholesterol on the lipid bilayer membranes

Melatonin's ability to non-specifically bind has previous studies as well as interact with the lipid membrane, and alter its biophysical properties (Benloucif *et al.*, 2008; De Lima *et al.*, 2007; De Lima *et al.*, 2010). Melatonin can interact with lipids of the biological membrane at the subcellular level (Akkas *et al.*, 2007), and preferentially forms H-bonds between polar groups of surfactants and the N-H group of the melatonin (Bongiorno *et al.*, 2004). The studies of Akkas and co-workers (Akkas *et al.*, 2007) reported that melatonin is to disorder the phospholipids at CH₂ asymmetric stretching as well as preferentially located at hydrophilic/hydrophobic interfaces and strong hydrogen bonding with carbonyl stretching and PO²⁻ group. According to the study of Drolle and co-workers (Drolle *et al.*, 2013), the interaction between melatonin with the bilayers made of DPPC and DOPC, used computer modeling in combination with small-angle scattering and neutron diffraction. Melatonin molecules were determined at the concentrations of ~10 mol% in experiment and simulation as well as ~30 mol% in experiments. Melatonin prefers to stay in the head group region of the bilayers (see Figure 2.4), leading to a decrease in bilayer thickness and increase in the head group area while the cholesterol has the exact opposite effect (see Figure 2.5 and Figure 2.6). These bilayers show more fluid and disordered structure in the presence of melatonin while they show condense and ordered structure in the presence of cholesterol. This result is in agreement with Dies and co-workers (Dies *et al.*, 2014), the difference in electron densities were determined from the positions of the melatonin molecules to study the anionic lipid with including 30 mol% melatonin membranes reported that melatonin is

preferentially located at between the hydrophilic head group region and the hydrophobic hydrocarbon chain core interface (see Figure 2.7) as well as at the membrane–water interface. Melatonin contributions based on the area of 26% are found at the hydrophobic membrane core interface, 74% at the water interface. When melatonin molecules are incorporated the electron density reduces, they indicated that the smaller melatonin molecules replaced electron-rich phospholipid molecules.

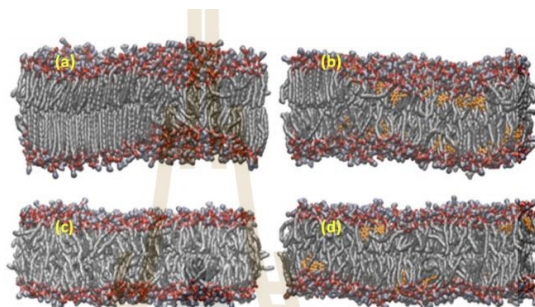


Figure 2.4 MD simulations of DPPC and DOPC bilayers presence and absence melatonin. DPPC (upper) and DOPC (lower) bilayers. Left: absence melatonin: (a) DPPC, (c) DOPC. Right: presence melatonin: (b) DPPC–melatonin, (d) DOPC–melatonin. Orange is shown in melatonin molecules. Snapshots of MD simulation were taken after 400 ns at $T = 300$ K. Simulation time of the total in each system was 500 ns. Note the pure DPPC system (for DPPC, $T_m = 314$ K) in gel phase on the left–hand side. To enhance and maintain local fluidity appears by melatonin. A visible in the DPPC membrane with melatonin (upper right) this is Q2. Since is above its main phase transition ($T_m = 253$ K) of the DOPC system, the melatonin effects are more subtle (Drolle *et al.*, 2013).

Furthermore, the study of Severcan *et al.* (Severcan *et al.*, 2005), revealed that the physical properties of the DPPC bilayers changes by melatonin which decreasing the system ordering in the gel phase, abolishing the pretransition,

transition temperature of the main phase, and increasing dynamics of both systems in the gel and liquid phases at melatonin concentrations of high (24 and 30 mol%), which indicates phase separation in DPPC membranes by inducing of melatonin.

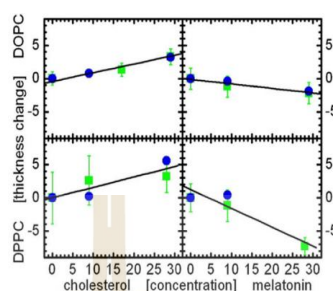


Figure 2.5 Thicknesses of DOPC (upper) and DPPC (lower) bilayers when the cholesterol (left) and melatonin (right) were added into the systems. Changes to the D_{HH} thickness obtained from SAND represent by blue circles, while changes in the D_S thickness obtained from SANS correspond to green squares. Fits to the data are black lines (Drolle *et al.*, 2013).

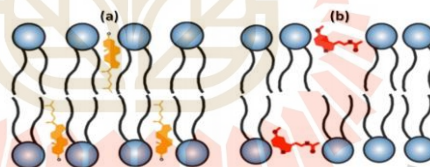


Figure 2.6 Schematics represent locations of (a) cholesterol and (b) melatonin in the lipid membrane (Drolle *et al.*, 2013).

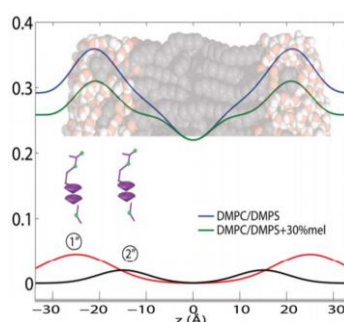


Figure 2.7 Electron density profile shown as a function of the position of melatonin molecules along the anionic lipid membranes (z -axis) (Dies *et al.*, 2014).

Cholesterol is a steroid molecule with a hydrophobic tail and a hydrophilic head, it is well-known to insert itself into lipid bilayers (Rheinstädter and Mouritsen, 2013; Armstrong *et al.*, 2013; Pabst *et al.*, 2010; Vance and Van den Bosch, 2000; Mouritsen, 2010; Armstrong *et al.*, 2012). The cholesterol molecules align parallel to the lipid acyl chains in saturated lipid bilayers, an arrangement that is well-known as the umbrella-model (Huang and Feigenson, 1999; Dai *et al.*, 2010). In fully hydrated lipid membranes when the addition of cholesterol often leads to a significant increase in bilayer thickness and a decrease in the area per lipid molecule. The suppression of the ordering and fluctuations of a lipid's hydrocarbon chains is the result of cholesterol's condensation effect (de Meyer and Smit, 2009; de Meyer *et al.*, 2010). Additionally, the liquid-ordered, L_o , phase is not uniform in lipid membranes, but also consists of lipid domains that are saturated with cholesterol in a disordered fluid membrane in equilibrium (Rheinstädter and Mouritsen, 2013; Meinhardt *et al.*, 2013; Armstrong *et al.*, 2013; Armstrong *et al.*, 2012; Sodt *et al.*, 2014; Armstrong *et al.*, 2014). A decrease in fluidity since the cholesterol effects, some hydrophilic amino acid derivative hormone is well-known as the melatonin, which to reside in the head group region (De Lima *et al.*, 2010) causing a corresponding increase in head group area and increasing membrane fluidity as well as a decrease in bilayer thickness (De Lima *et al.*, 2010; Drolle *et al.*, 2013; Saija *et al.*, 2002).

Recently, the studies of Lu and Martí (Lu and Martí, 2019) present MD simulations of all-atom on bilayer membrane made up from the DMPC zwitterionic phospholipid at three different cholesterol concentrations (0%, 30%, and 50%) with a single melatonin molecule inclusion. They reported that melatonin also in the internal region of DMPC bilayers most of the time at cholesterol systems of 0% and 30%, with

occasional visits to the membrane interface, i.e. environment of the P atoms; however, as more cholesterol was added into the system (i.e. at 50%), melatonin can be diffused into water bulk and become fully solvated by the head groups of DMPC or water (see Figure 2.8) without changing too much of system size, indicating between lipids and water the competition to solvate melatonin. In the case of 50% cholesterol, it is shown that melatonin, either stay for long periods in the water bulk but also has the ability of either being absorbed by the DMPC head groups, it is not difficult for a small molecule like melatonin as them expected to cross between the two states of the free energy barrier (solvated by the DMPC head groups or solvated by water) and also with the fact that, as cholesterol concentration increases melatonin can move outside the membrane more easily.

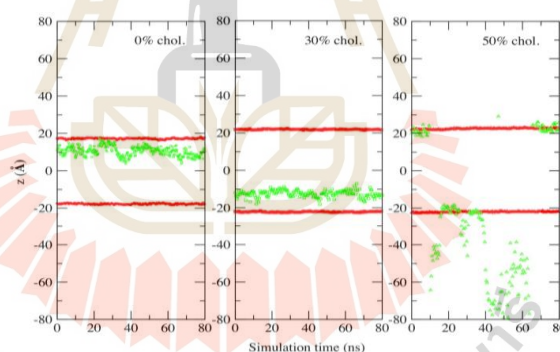


Figure 2.8 Z-axis position of melatonin as a function of simulation times. Inside DMPC bilayer were penetrated by melatonin (red symbols stand for the phosphorus atoms position in each layer while green symbols specify the position of the center of mass of melatonin) at cholesterol concentrations of 0%, 30%, and 50%, respectively (Lu and Martí, 2019).

They are in good agreement with these results (Lu and Marti, 2020) performed the binding states with Gibbs free energy calculations of melatonin at

surfaces of phospholipid membrane made by DMPC lipids and cholesterol. The molecular configurations characteristic of melatonin when located at the membrane interface, two snapshots characteristic at cholesterol concentrations of 0 and 30% are given in Figure 2.9. They have included only melatonin in the figure and lipids that are closest solvating, viz two DMPC at 0% and one cholesterol and one DMPC at 30%.

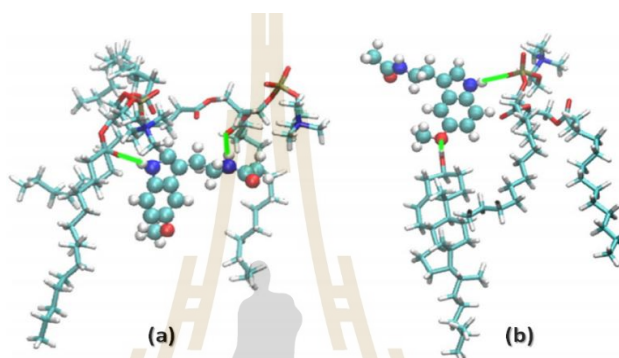


Figure 2.9 Representative bound states of snapshots for melatonin at the membrane interface. Melatonin colors, DMPC, and cholesterol: cyan (carbon), dark blue (nitrogen), red (oxygen), white (hydrogen). Green solid lines indicated hydrogen bonds. (a): a case at cholesterol concentration of 0%, with two DMPC molecules bound to melatonin; (b): a case at cholesterol concentration of 30%, with one DMPC and one cholesterol molecule bound to melatonin (Lu and Marti, 2020).

The melatonin can be simultaneously bound to both cholesterol and DMPC chains which can be observed through the hydrogen-bonds. Also, melatonin moved from the interface to the water-solvated region diminishes when increases the cholesterol concentration. This means that melatonin moves outside the membrane with cholesterol influence and at last stays in the interface outer regions. Interestingly, the binding behavior of melatonin in such transition at cholesterol $\approx 30\%$ mol on

DMPC–cholesterol membranes might be correlated with the phase transition point, from a liquid–disordered phase to a liquid-ordered phase in membranes change.

Recently, sorbitan monostearate (Span60) bilayers were studied using MD simulations in the presence of three representative flavones complex, e.g. unsubstituted flavone, chrysin, and luteolin (Myung *et al.*, 2016) were done. Niosome bilayers models were generated by the equal ratio of Span60 and cholesterol composition (1:1) with the 3%, 25%, and 50% flavone concentrations. Phytochemicals group derived from benzo–g–pyrone is well–known as the flavonoids. Have attracted much attention from them due to their biological activity against inflammation, cancer, and oxidative stress (Romano *et al.*, 2013). Flavones, a subclass of flavonoids, have a backbone structure with aromatic rings consisting of hydroxylation that generates naturally occurring flavones such as 6–hydroxy flavone, baicalein, apigenin, chrysin, and luteolin. Their study provides information about the local orientation of flavones in the bilayer membrane and their physical properties.

The electron density showed that penetrates deep of flavone into the hydrophobic core of the bilayer as concentration increases due to the most hydrophobic member (Figure 2.10), while chrysin and luteolin can be moved from head group hydrophilic region and the hydrophobic chain into solvated by the head groups of lipids or water (Figure 2.11). In addition, the bilayer thickness and surface area per lipid fluctuated as the concentration of flavone increased, while the bilayer thickness decreases and surface area per lipid increase as the concentration of chrysin and luteolin (see Table 2.1).

The previous simulation study of the DMPC lipid-containing with 30 mol% melatonin has a significant impact on the bilayer structure, phase transition, and

dynamical properties of the lipid bilayer membranes. Therefore, we have expected that the similar characteristics of niosome bilayer containing 30 mol% melatonin will significantly affect the dynamical properties and bilayer structure.

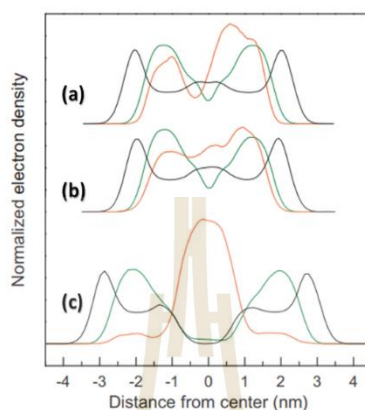


Figure 2.10 Electron density normalized black (Span60), green (cholesterol), and orange (unsubstituted flavone) for (a) 3 mol%, (b) 25 mol%, and (c) 50 mol% unsubstituted flavone were contained in a Span60 bilayer (Myung *et al.*, 2016).

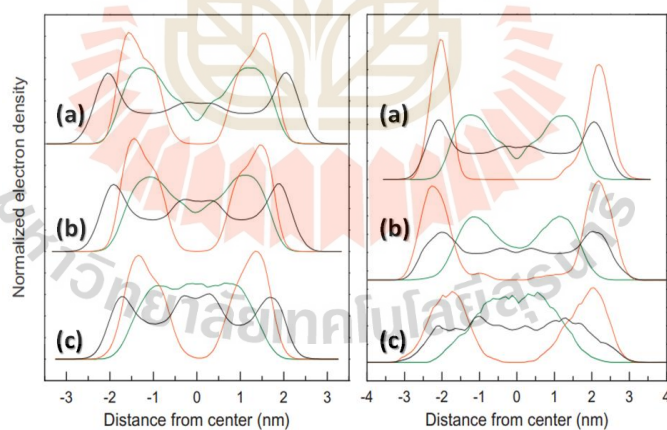


Figure 2.11 Left: Electron density normalized black (Span60), green (cholesterol), and orange (chrysin) for (a) 3 mol%, (b) 25 mol%, and (c) 50 mol% chrysin were contained in a Span60 bilayer. Right: Electron density normalized black (Span60), green (cholesterol), and orange (luteolin) for (a) 3 mol%, (b) 25 mol%, and (c) 50 mol% luteolin were contained in a Span60 bilayer (Myung *et al.*, 2016).

Table 2.1 Bilayer properties of Span60 bilayers containing flavones, chrysin, and luteolin respectively, at different concentrations (Myung *et al.*, 2016).

Flavonoid	Mol% ^a	Thickness (nm) ^b	Surface area per lipid (nm ²) ^c
None	–	3.74	0.299
Flavone (unsubstituted)	3.3	3.73	0.304
	25	3.61	0.358
	50	5.25	0.318
Chrysin	3.3	3.73	0.305
	25	3.29	0.376
	50	2.89	0.525
Luteolin	3.3	3.80	0.298
	25	3.79	0.310
	50	n.d. ^d	0.413

^a Refers to a flavone ratio per total lipid, which being Span60/cholesterol (1:1).

^b Defined as a distance between leaflets seized from C1 of Span60.

^c At equilibrium of simulation box area was divided by total lipids number (Span 60 and cholesterol) in one leaflet of the bilayer.

^d Not determined.

CHAPTER III

COMPUTATIONAL METHODOLOGY

In this chapter, we describe an overview of basic molecular dynamics and computational methodology. The molecular dynamics (MD) method is a powerful tool for investigating biological systems such as biomolecules, lipid membranes, or protein membranes. Preparation of model systems and the simulation details are presented as well as how to analyze some structural and dynamical properties.

3.1 Basic of the molecular dynamic method

It is well-known that quantum mechanics (QM) simulation is not a suitable technique for applying on large molecular systems such as lipid membrane, protein folding, etc., due to its required time consuming for the calculations. Therefore, a molecular mechanics (MM) simulation is an alternative method for solving this problem. To study the physical movements of atoms and molecules a computer simulation method is well-known as molecular dynamics (MD) was used to study based on classical laws of mechanics. Information at the microscopic level including velocities and atomic positions has generated this technique. This microscopic data conversion to macroscopic observables such as temperature, heat capacities, pressure, etc., must use statistical mechanics. However, it is well-known that the potential interactions between atoms in the molecular system are used to derive the force acting on any atom.

Therefore, the quality of the potential model influences directly to reliability and accuracy of simulation results. Generally, the potential energy function, or so-called force fields consist of intramolecular and intermolecular interaction terms which can be written as the following equation,

$$\begin{aligned}
 V(r) = & \frac{1}{2} \sum_{\text{bonds}} K_b (b - b_0)^2 + \frac{1}{2} \sum_{\text{angle}} K_\theta (\theta - \theta_0)^2 + \\
 & \frac{1}{2} \sum_{\text{dihedral}} K_\chi [1 + \cos(n\chi - \delta)] + \frac{1}{2} \sum_{\text{impropers}} K_{\text{imp}} (\phi - \phi_0)^2 + \\
 & \sum_{\text{nonbonded}} \epsilon_{ij} \left[\left(\frac{\sigma_{ij}}{r_{ij}} \right)^{12} - \left(\frac{\sigma_{ij}}{r_{ij}} \right)^6 \right] + \frac{q_i q_j}{4\pi\epsilon_0 r_{ij}}
 \end{aligned} \quad (3.1)$$

The first four terms in Equation (3.1) represents intramolecular interactions which are defined as follows:

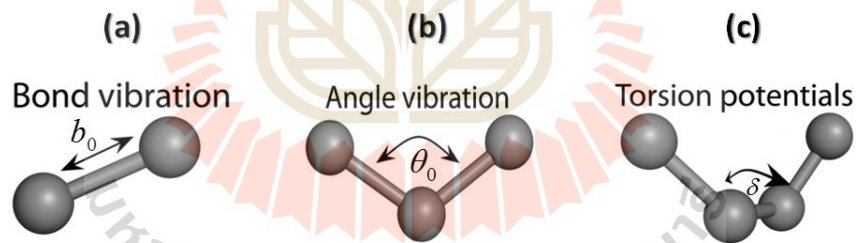


Figure 3.1 The intramolecular interactions of (a) the bond stretching, (b) the angle bending, and (c) the dihedral rotation, respectively. Additional details see in gromacs user manual (<ftp://ftp.gromacs.org/pub/manual>).

- i) The bond stretching between two atoms of a covalent bond was represented by a harmonic potential.
- ii) The vibration between triplet atoms of bond angle was displayed by a harmonic potential.

- iii) The proper dihedral angles of four atoms were described by surrounding bond rotations between the first and the last atom among the potential barrier and represented by a periodic potential based on expansion in powers of $\cos \chi$.
- iv) The improper dihedral angles between four atoms were represented by a harmonic potential used to prevent molecules from flipping over to their mirror images or to keep planar groups (e.g. aromatic rings).

The last term in Equation (3.1) represent intermolecular interactions which are defined as follows:



Figure 3.2 The intermolecular interactions of (a) the van der Waals and (b) the electrostatic interactions. Additional details see in Gromacs user manual (<ftp://ftp.gromacs.org/pub/manual>).

- v) The Lennard–Jones interactions are short–length interactions and depend on pairs of atom types which consist of repulsion and attraction terms.
- vi) The Coulomb interaction between charged particles is long–length interaction that consists of repulsion and attraction on particle pairs.

MD technique generates the trajectory of all atoms in the phase space based on Newton's laws of motion. Thus, a force that acts on a particle i from other particles can be defined as the second Newton's law of motion,

$$\vec{F}_i = m_i \vec{a}_i = m_i \frac{d\vec{v}_i}{dt} = m_i \frac{d^2\vec{r}_i}{dt^2} \quad (3.2)$$

However, the resultant force that acts on particle i can be obtained from the negative gradient of the potential function as given in Equation (3.3).

$$\vec{F}_i = \sum_{\substack{j=1 \\ j \neq i}} \vec{F}_{ij} = - \sum_{\substack{j=1 \\ j \neq i}} \frac{\partial V(r_{ij})}{\partial r_{ij}} \hat{e}_r \quad (3.3)$$

Based on using Equation (3.2) and (3.3), we can solve the equation of motion of any atom to generate their trajectory using the finite different methods (e.g., verlet, leapfrog, Euler's algorithm). At every time step on the movement of particles, several properties of the system such as the total energy, temperature, and pressure are calculated. The simulation process will be continuing until the system reaches equilibrium. After the equilibration, the trajectory (position and velocity) of all atoms were collected for the subsequent analysis.

3.2 General system setting and simulation details

3.2.1 Melatonin in aqueous solution and at the water-air interface

Firstly, the geometry optimization of the melatonin molecule was carried out using the B3LYP/6-31G(d,p) calculations via Gaussian 09 program (Frisch *et al.*, 2009). Then, the optimized structure of melatonin (Figure 3.3a) was used to generate the initial configuration of melatonin molecules in an aqueous solution. To do this, 100 melatonin molecules were randomly distributed in a cubic box with a side length of 4.62 nm containing 2300 water molecules as displayed in Figure 3.3b. To prepare the initial configuration of melatonin molecules at the water-air interface, a water slab containing 2300 water molecules in a cubic box with the

side length of 4.20 nm was firstly generated and then equilibrated at a pressure of 1 bar and a temperature of 298 K using molecular dynamic simulation. This simulation was carried out using Gromacs program version 5.0.4 (Berendsen *et al.*, 1995; Van Der Spoel *et al.*, 2005). Next, 50 melatonin molecules were randomly distributed in a rectangular box of 4.09 nm × 4.09 nm × 2.02 nm in $-x$, $-y$, and $-z$ directions, respectively. Afterward, this melatonin layer was duplicated and inverted to make symmetric two layers i.e., one layer capped at the bottom and the other capped at the top of the equilibrated water slab, resulting the two symmetric melatonin layers covered on the water surface. Finally, this system was controlled at the middle of a box with the sizes of 4.09 nm x 4.09 nm x 15.00 nm in the $-x$, $-y$, and $-z$ directions, respectively. A schematic representation of the initial configuration of melatonin at the water-air interface was revealed in Figure 3.3c. The molecular topology of melatonin was created using PRODRG server program (Schüttelkopf and Van Aalten, 2004). In this procedure, all bonded and non-bonded parameters describing the interaction of melatonin were taken from the GROMOS96 force field (Gunsteren and Berendsen, 1987), except atomic partial charges using the B3LYP/6-31G(d,p) calculation and received from the CHELPG process (Breneman and Wiberg, 1990). Description of a united atom was used with hydrocarbon sites, such as CH₁, CH₂, and CH₃. Atom types definitions and their partial charges were given in Table 3.1. SPC/E water model (Berendsen *et al.*, 1987) was employed for this study because it is proper to describe the interface behavior of the lipid monolayer system (Ritwiset *et al.*, 2014).

The steepest descent method for energy minimization (EM) was applied to reduce undesired overlap between neighboring atoms of the bulk water and

the water-air interface systems. Then, the first system was simulated at a pressure of 1 bar and a temperature of 298 K (*NTP* ensemble), while the second system was simulated at a temperature of 298 K and a constant volume (*NVT* ensemble). To control a constant pressure, Berendsen barostat (Berendsen *et al.*, 1984) and isotropic coupling with a time constant (τ_p) of 1.0 ps and compressibility of $4.5 \times 10^{-5} \text{ bar}^{-1}$ were employed for the bulk water system. The *v*-rescale thermostat (Bussi *et al.*, 2007) was used to maintain a constant temperature for both systems with a coupling time constant (τ_T) of 0.1 ps.

This applies in all three directions for periodic boundary conditions. The dispersion correction method (Shirts *et al.*, 2007) was employed to handle the long-range Van der Waals interactions for the energy and pressure terms due to their cut-off distance. The LINCS algorithm (Hess *et al.*, 1997) was used constraining all bond lengths of melatonin with fourth-order expansion, while the SETTLE algorithm (Miyamoto and Kollman, 1992) kept as a rigid particle were used constraining water bond lengths. The leap-frog algorithm was used to solve equations of motion with a time step (Δt) of 2 fs. The Particle Mesh Ewald (PME) method (Petersen, 1995) use calculated the electrostatic interactions with a fourth-order (cubic) interpolation, the grid spacing of 0.15 nm, and a cutoff distance of 0.9 nm.

A cutoff of 0.9 nm was used for van der Waals interactions and was treated with a switching algorithm that started at 0.8 nm. Every 10-time steps use updated for a neighbor list with a verlet cutoff scheme (Páll and Hess, 2013). The simulation in each system of 260 ns including 100 ns for the equilibrium run and 160 ns for the production run. The molecular structure and configuration of the two systems were analyzed using the VMD program (Humphrey *et al.*, 1996).

Table 3.1 Definitions of atom types of melatonin molecule, atomic partial charges using the B3LYP/6–31G(d,p) calculation and generated from the CHELPG technique, as well as corresponding atomic mass.

Atom Number	Atom Type	Charge (e)	Mass (u)
1	CH3	-0.089	15.0350
2	C	0.690	12.0110
3	O	-0.541	15.9994
4	N	-0.653	14.0067
5	H	0.331	1.0080
6	CH2	0.250	14.0270
7	CH2	0.083	14.0270
8	C	-0.157	12.0110
9	C	0.136	12.0110
10	CR61	-0.207	13.0190
11	C	0.366	12.0110
12	OA	-0.392	15.9994
13	CH3	0.220	15.0350
14	CR61	-0.115	13.0190
15	CR61	-0.070	13.0190
16	C	0.141	12.011
17	NR5*	-0.395	14.0067
18	H	0.342	1.0080
19	CR51	0.061	13.0190

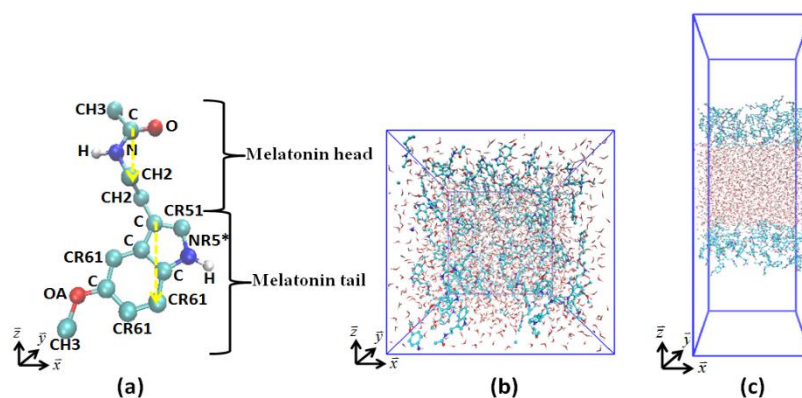


Figure 3.3 (a) The structure of melatonin with atom type names as defined in Table 3.1, (b) a system model of melatonin molecules in aqueous solution, and (c) a system model of melatonin molecules at the water-air interface. Coloring in Figure 3.3a: the carbon atom and hydrocarbon group (e.g., C, CR51, CR61, CH2, and CH3), cyan; O, red; N, blue; H, gray. The two yellow arrows shown in Figure 3.3a were defined as the two vectors for the calculation of tilt angle distributions of head and tails.

3.2.2 Melatonin inserted into niosome bilayers

Firstly, the geometrically optimized of the Span60, cholesterol (Chol), and melatonin (Mel) molecular structures by using B3LYP/6–31G (d,p) calculations. Then the structures (in Figure 3.4) obtained from these optimizations were generated to insert melatonin into the pure Span60, and Span60/Chol bilayers by using the CELL microcosmos 2.2 software (Sommer *et al.*, 2011). To generate these niosome bilayers formed with different compositions: Span60, Chol, and Mel molecules were placed on a box area of 7.20 nm × 7.20 nm randomly. The head groups of Span60 in each layer point away from each other while the tail groups of Span60 face each other. The Span60/Chol/Mel system consisted of 64 Span60, 64 cholesterol, and 55 melatonin molecules in each monolayer, leading to 128 Span60, 128 cholesterol, and 110 melatonin molecules in the total bilayer. For comparison as generated in the same

manner of the niosome bilayer consisting of the Span60 and melatonin molecules (Span60/Mel bilayer). The Span60/Mel system contained 128 Span60 and 55 melatonin molecules in each monolayer, leading to 256 Span60 and 110 melatonin molecules in the total bilayer. The niosomes composed of the Span60 and cholesterol mixture with equal ratio from the experimental study revealed that have more stability than the other compositions (Nasseri, 2005). As a result, this model was selected from our for the simulation study.

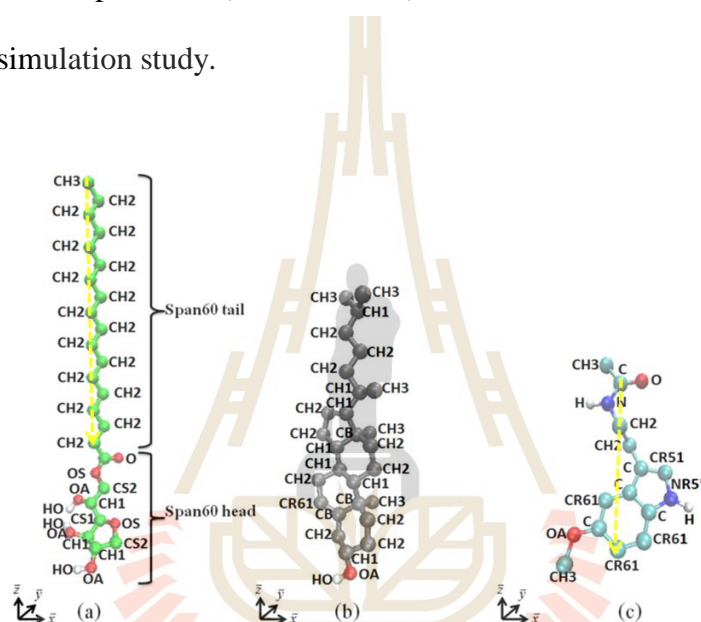


Figure 3.4 The molecular structures of (a) Span60 (b) cholesterol and (c) melatonin, respectively. With defined the head and tail group and included number index of atomic types for clarifying discussion. Coloring scheme in Figure 3.4: the carbon atom and hydrocarbon group (e.g., C, CH₁, CH₂, CH₃ or others) include green, gray, cyan; O, red; N, blue; H, white. The two yellow arrows shown in Figures 3.4a and c were defined as the two vectors for the calculation of tilt angle distributions.

To set up the systems of melatonin inserted into the pure Span60, and the Span60/Chol bilayers in aqueous solution: a water slab in a rectangular box of 7.20 nm × 7.20 nm × 2.30 nm in x, y, and z directions, respectively consisting of 3840

water molecules were prepared using the Gromacs v. 2016 program tools (Abraham *et al.*, 2015). To make a bilayer the water slab was duplicated and inverted: i.e. one capped at the bottom of the Span60 layer and the other capped at the top of the Span60 layer, leading to form the niosome bilayers in an aqueous solution with the melatonin inclusion in bilayer membranes. Next, set up the simulation box of 7.20 nm \times 7.20 nm \times 10.90 nm within containing each bilayer system which full hydrated by 7680 total water molecules as displayed in Figure 3.5a and b, respectively. In these bilayer structures, the hydrocarbon tails point toward the center of the bilayers while the hydrophilic head groups are exposed to the water bulk phase. The initial surface area per molecule of the Span60/Mel, and Span60/Chol/Mel bilayer systems was 40.50 \AA^2 equally.

The cholesterol and Span60 force field parameters were obtained from the MD study of Holtje *et al.* (Höltje *et al.*, 2001) and our previous work (Ritwiset *et al.*, 2014), respectively. Base on the Gromos87 force field (Gunsteren and Berendsen, 1987) for these all bonded and non-bonded parameters. Description of a united atom was used with hydrocarbon sites, such as CH₁, CH₂, CH₃, and others. Ryckaert-Bellemans potential model was employed for describing dihedral interactions of all hydrocarbon chains because it can be reproduced experimentally measurement in hydrocarbon chains of phospholipids displayed by trans/gauche ratios (Ryckaert and Bellemans, 1978). To describe water molecules in bilayer membrane systems the SPC/E model was employed in this study.

The steepest descent method base on energy minimization (EM) was applied to reduce undesired overlap between neighboring atoms for all systems. After that, to remove any undesired interaction between neighboring molecules the resultant

configurations on each system were used to perform molecular dynamics (*NVT*-ensemble) for 10 ns at a temperature of 410 K. The pressure and temperature were kept to be constant via the coupling algorithms using Berendsen barostat (Berendsen *et al.*, 1984) and stochastic velocity rescaling thermostat (Bussi *et al.*, 2007), respectively.

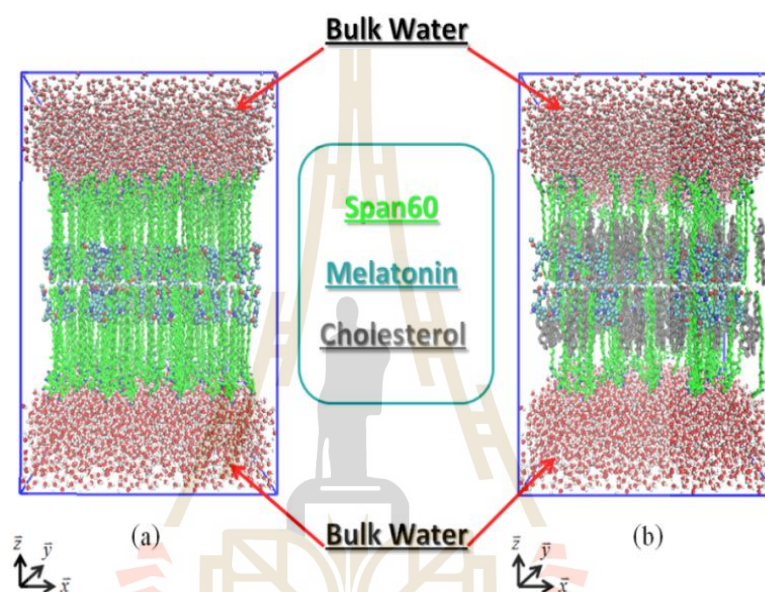


Figure 3.5 Schematic representations of (a) the Span60/Mel, and (b) the Span60/Chol/Mel bilayers, respectively.

Finally, the two systems were equilibrated with molecular dynamics (*NPT*-ensemble) at a constant pressure of 1 bar and temperature of 298 K with the simulation time of 200 ns. To keep constant pressure, a Parrinello–Rahman barostat (Parrinello and Rahman, 1981) with semi-isotropic coupling in the normal direction (in the *z*-direction) and the lateral direction (in the *xy*-plane) were used with the compressibility of $4.5 \times 10^{-5} \text{ bar}^{-1}$ and a time constant (τ_P) of 0.5, respectively. To keep a constant temperature in the system, the *v*-rescale thermostat (Bussi *et al.*, 2007) was coupled separately to the Span60, cholesterol, melatonin, and water with a

coupling constant $\tau_T = 0.1$ ps. This applies in all three directions for periodic boundary conditions. The LINCS algorithm (Hess *et al.*, 1997) was used constraining all bond lengths between atoms of, the Span60, cholesterol, and melatonin molecules with fourth-order expansion; while the SETTLE algorithm (Miyamoto and Kollman, 1992) kept as a rigid particle were used constraining water bond lengths. The leap-frog algorithm was used to solve equations of motion with a time step (Δt) of 2 fs. The Fast Particle Mesh Ewald (PME) method (Petersen, 1995) use calculated the electrostatic interactions with a fourth-order (cubic) interpolation and a grid spacing of 0.15 nm. A cutoff at 1.5 nm was used for van der Waals and Coulomb interactions. Every 10-time steps use updated for a neighbor list with a verlet cutoff scheme (Páll and Hess, 2013). After that, we have removed the melatonin molecules from systems to make a comparison of the simulation results obtained to the niosome bilayer systems without melatonin composition. The resultant configurations for two systems were used to the same parameter and MD algorithm series, without performing short molecular dynamics simulations for *NPT*-ensemble. All simulations were carried out by using Gromacs v. 2016 package (Abraham *et al.*, 2015). Configurations and molecular structures of four systems were visualized by using the VMD program (Humphrey *et al.*, 1996).

CHAPTER IV

RESULTS AND DISCUSSION

In this chapter, we were taken statistical mechanics equations for applied in the found calculation of the various quantities *e.g.* mean square displacements (MSD), intermittent hydrogen bond time correlation function $C(t)$, hydrogen bond lifetime (τ_{HB}), area per one lipid leaflet (A_0), radial distribution functions $g(r)$, and deuterium order parameters (S_{CD}), *etc.* These data are then interpreted both qualitatively and quantitatively to lead to a better understanding of the dynamic and structural properties of melatonin in aqueous solution and at the water-air interface, as well as the niosome bilayers with and without cholesterol inclusion when the melatonin was added into those bilayers.

4.1 Melatonin in aqueous solution and at the water-air interface

4.1.1 Energetic and density profiles

Figure 4.1 shows the time evolutions of total potential energy (U) for the two systems. At the beginning of the simulation time (0–10 ns), the total potential energy of each system decreased rapidly, and afterward, it remained constant with small variation. The standard deviation of total potential energy for each system is less than 1% when compared with its average value. Additionally, the time variation of the simulation box size in all directions for the bulk water system remained constant as shown in the inset figure of Figure 4.1.

This suggests that the equilibration process can be achieved in a course of simulation time for both systems.

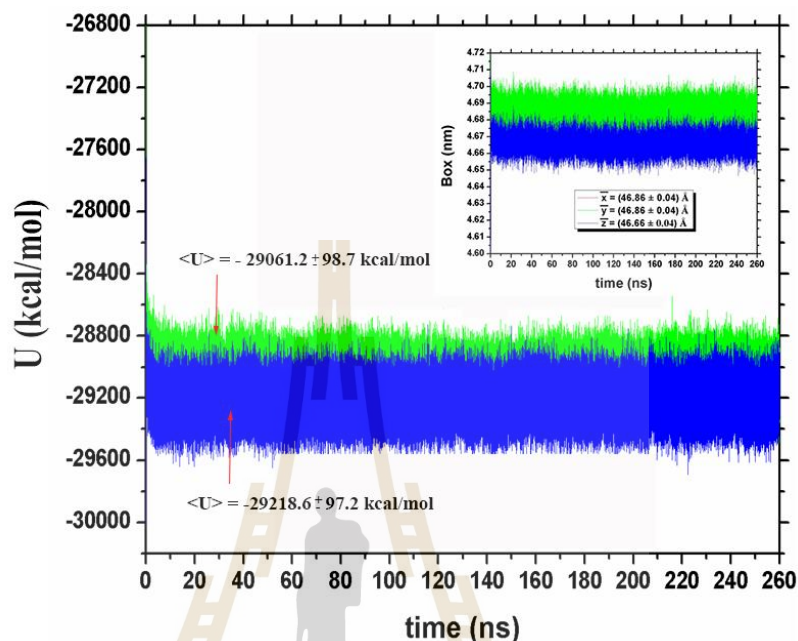


Figure 4.1 Time evaluation of total potential energy (U) of the system of melatonin in the bulk water (green) and that of melatonin at the water-air interfaces (blue). The inset figure shows the time variation of the simulation box size in the three directions for the bulk water system.

Figure 4.2 shows density distributions of water, the head, and the tail group (defined as in Figure 3.3a) for the system of melatonin in bulk water. These density profiles were separately plotted as a function of x -, y -, and z -coordinates and given in Figure 4.2(a-c), respectively. The density profiles of head and tail groups showed a pronounced peak located at the center of the box length ($z \sim 2.6$ nm) in the z -direction, but they exhibited broad distribution in the x - and y -directions. Also, the water density in each direction was varied according to the change of density profiles of melatonin. Most melatonin molecules were distributed along the x - and y -axis but

stayed locally in the z-axis. This result suggests that most melatonin molecules were self-aggregated in an aqueous solution, due to more hydrocarbon sites than hydrophilic groups that were contacted with water molecules. The existence of melatonin aggregation indicates that the solubility of melatonin in an aqueous solution is too low as the previous reports (Shida *et al.*, 1994; Mark and Nilsson, 2002; Lee *et al.*, 1997).

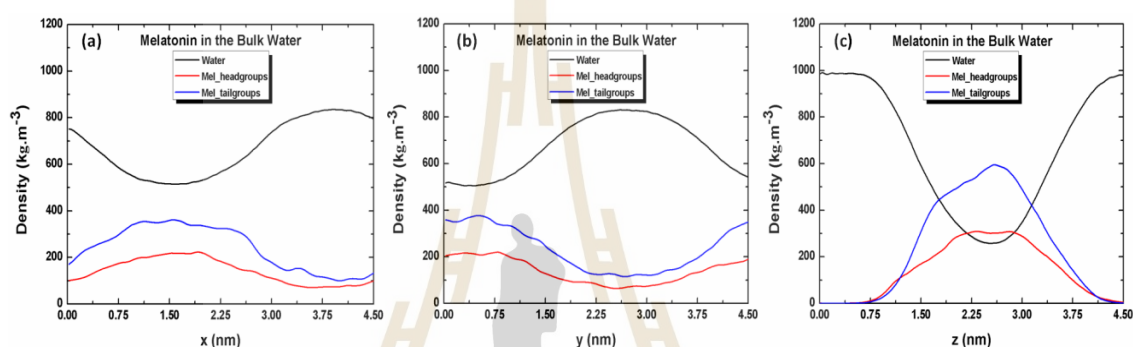


Figure 4.2 Density distributions of water and melatonin molecules for the bulk water system as a function of (a) *x*-, (b) *y*- and (c) *z*-coordinates, respectively. The head and tail groups of melatonin were separately plotted for clarifying discussion.

Figure 4.3 shows the density distributions of water and some molecular sites of melatonin including the head, the tail, carbonyl (C=O), amide (N-H), indole (N-H), and methoxy (-OCH₃) for the system of melatonin at the water-air interface. It can be seen from Figure 4.3 that all density distributions of the two monolayers are symmetrical, which confirmed that the system is well-equilibrium. Clearly, the density profiles of the head and tail groups showed a narrow sharp peak located at the interface, indicating that all melatonin molecules were absorbed on the water surface due to a hydrophilic group that was induced with a water molecule. The density peaks of the head group were located closer to the bulk water phase than that of the tail

group. This means that the melatonin head groups are favorably interacting with the water molecules at the interface region. Furthermore, the density profiles of the four hydrophilic parts including the carbonyl (C=O), the amide (N-H), the indole (N-H), and the methoxy (-OCH₃) were examined to identify which functional group of melatonin is more contribution to the hydrophilic interactions. Clearly, the density profile of the carbonyl (C=O) group showed more overlap with the water density, indicating that the carbonyl group is the stronger hydrophilic interaction. While the density profiles of amide, indole and methoxy groups exhibited a reduced overlap with the water density distribution, respectively. This result suggests that these functional groups of melatonin play a major role to interact with the water molecules located in the interface region. However, the carbonyl group showed the most hydrophilic interactions. Furthermore, the indole group exhibits more interaction with water rather than the methoxy group which is in good agreement with previous studies (Choi *et al.*, 2014; Pala *et al.*, 2013; Vöhringer-Martinez and Toro-Labbé, 2010). A clear picture of melatonin aggregation in aqueous solution and at the water-air interface was displayed in Figures 4.4a and 4.4b, respectively. These snapshots were taken at the initial and the final simulation times for the two systems. It can be seen that most melatonin molecules were self-aggregated in the aqueous solution while they were self-assembled to form a monolayer structure at the water-air interface.

4.1.2 Hydrogen bond analysis

The hydrophilic interaction and dynamic behavior of melatonin molecules in the bulk water and at the water-air interfaces can be examined in terms of hydrogen bond analysis.

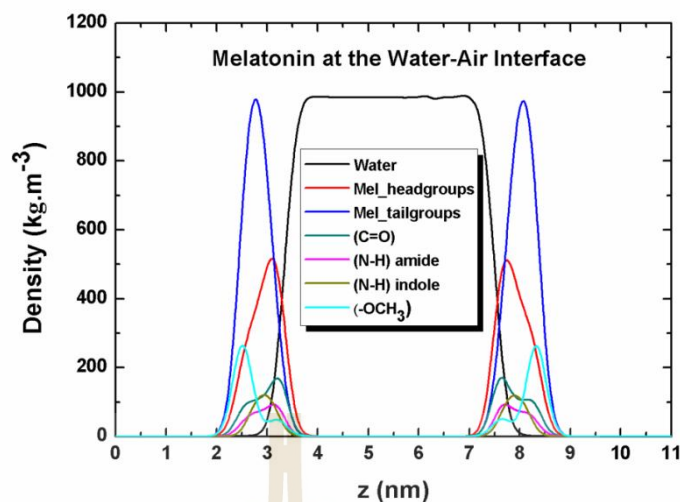


Figure 4.3 Density distributions of water and some molecular sites of melatonin as a function of z -coordinate for the system of melatonin at the water-air interface. The functional groups of melatonin including the head, the tail, carbonyl (C=O), amide (N-H), indole (N-H), and methoxy (-OCH₃) were separately plotted for clarifying discussion.

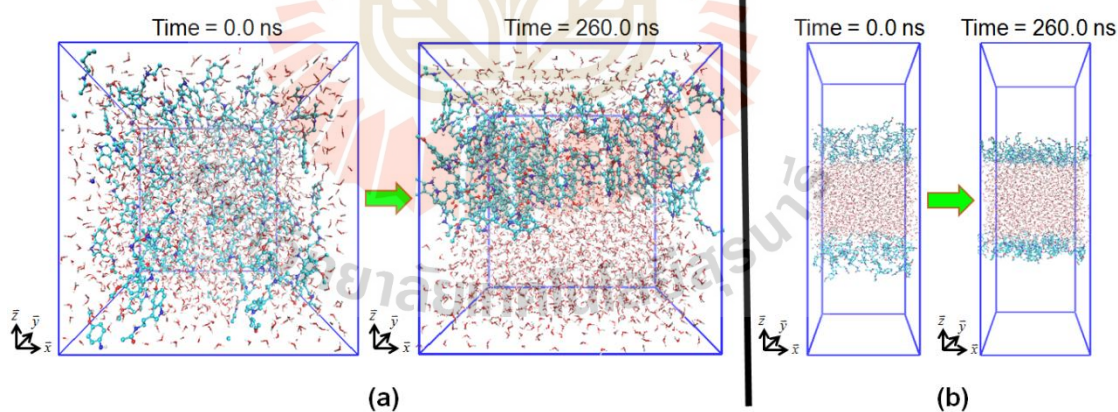


Figure 4.4 Two configurations of melatonin at the initial time (0 ns) and at the final time (260 ns) of the simulation of (a) the system of melatonin in aqueous solution and (b) the system of melatonin at the water-air interface. Coloring scheme: carbon atom and hydrocarbon group are cyan; oxygen is red; nitrogen is blue, and hydrogen is gray.

The hydrogen bonds (H-bonds) formed between all possible donors and acceptors can be defined using the geometrical criterion which the donor-acceptor (DA) distance is less than 0.35 nm, and simultaneously the donor-hydrogen-acceptor (DHA) angle is less than 30° (Luzar and Chandler, 1996). This criterion provided more reliable simulation results (Starr *et al.*, 2000). The DA distance distributions of all H-bonds for the two systems are given in Figure 4.5. The distributions of the H-bond distance between the donor (or acceptor) atoms of melatonin (*i.e.*, carbonyl O, indole NH, amide NH, and methoxy O) to the oxygen (OW) and the hydrogen (HW) atoms of water for the bulk water and that for the water-air interface were presented in Figures 4.5a and 4.5b, respectively. While the DA distance distributions of all H-bonds formed between all possible donor atoms and acceptor atoms of melatonin for both systems were given in Figures 4.5c and 4.5d, respectively. Clearly, all the DA distance distributions obtained from the melatonin-water interactions or that of the melatonin-melatonin interactions show a similar pattern for both systems. The most probable DA distance for each H-bond pair of the melatonin-water interaction can be sequenced as follows: the carbonyl O-HW < indole NH-OW < amide NH-OW < methoxy OA-HW, respectively. Likewise, the most probable DA distance for each H-bond pair of the melatonin-melatonin interaction can be sequenced as follows: indole NH-carbonyl O < amide NH-carbonyl O < indole NH-methoxy OA < amide NH-methoxy OA, respectively. An appearance of the shortest DA distance and the highest peak of the carbonyl O-HW bond distribution indicates the greatest strength of the carbonyl O-HW interaction as well as the most contribution in the formation of melatonin-water hydrogen bonds. This result is according to the C=O density distribution for the water-air interface system as given in Figure 4.3. Similar behavior

can be observed for the H-bonds between the indole NH of melatonin and the carbonyl O of another melatonin. Based on these results, we can be concluded that the strength hydrophilic interaction for each function group of melatonin molecules can be sequenced as follows: carbonyl O > indole NH > amide NH > methoxy OA, respectively. According to the IR spectroscopy and ab initio studies of Florio and Zwier (Shillady *et al.*, 2003; Florio and Zwier, 2003) indicated that the carbonyl group of melatonin is the primary point of the water binding.

Average H-bond number per molecule, $\langle n_{\text{HB}} \rangle$, were calculated for all the pairs of hydrogen bond formations for both systems and summarized in Table 4.1. It is seen that the average H-bond numbers for each pair of the melatonin–water interactions and of the melatonin–melatonin interactions obtained from the aqueous solution and the water-air interface systems were decreased with the corresponding order of DA distance as mentioned above. The average H-bonds of the carbonyl O–HW showed the highest value for both systems. This indicates that the carbonyl group plays a major role in hydrogen bonding with the water molecules. Compared with the bulk water system, the average H-bonds numbers of the carbonyl O–HW and indole NH–OW interactions of the water-air interface system were increased while the rest was reduced. This result indicates the low stability of aggregation formation of melatonin at the water-air interface.

4.1.3 Molecular orientation

To characterize the preferential orientation of melatonin molecules in the bulk water and at the water-air interface systems, the probability distributions of the tilt angle (θ) of the head and the tail groups of melatonin were calculated and,

displayed in Figure 4.6. The tilt angles of the head are defined as the angle between the vector pointing from C to CH₂ and the z-axis and that of the tail is defined as the angle between the vector pointing from C to CR61 and the z-axis, respectively (see definition of these vectors in Figure 3.3a). Figure 4.6a shows the distributions of the tilt angles of the head and tail groups of melatonin for the bulk water system. Clearly, these distributions showed a similar pattern with a broad peak which indicates a random distribution of molecular orientation. However, an appearance of the peak at around 90° for the head and tail groups suggests that most melatonin molecules favor aligning their structure perpendicular to the z-axis. Figure 4.6b shows the tilt angle distributions of the head and tail groups of melatonin for the water-air interface system. The tilt angle distribution of the head group showed two possible orientations, namely, the first one is to turn the head groups to the water surface ($\theta \sim 40^\circ - 60^\circ$) and the second one is to turn the head group away from the water surface ($\theta \sim 130^\circ$). These two peaks are corresponding the competition of the carbonyl O–HW and the indole NH–OW interactions to form hydrogen bonds as above mentioned in the previous section. While the tilt angle distribution of the tail group showed a sharp peak at 30°, indicating that the tail groups preferred to point away from the water surface.

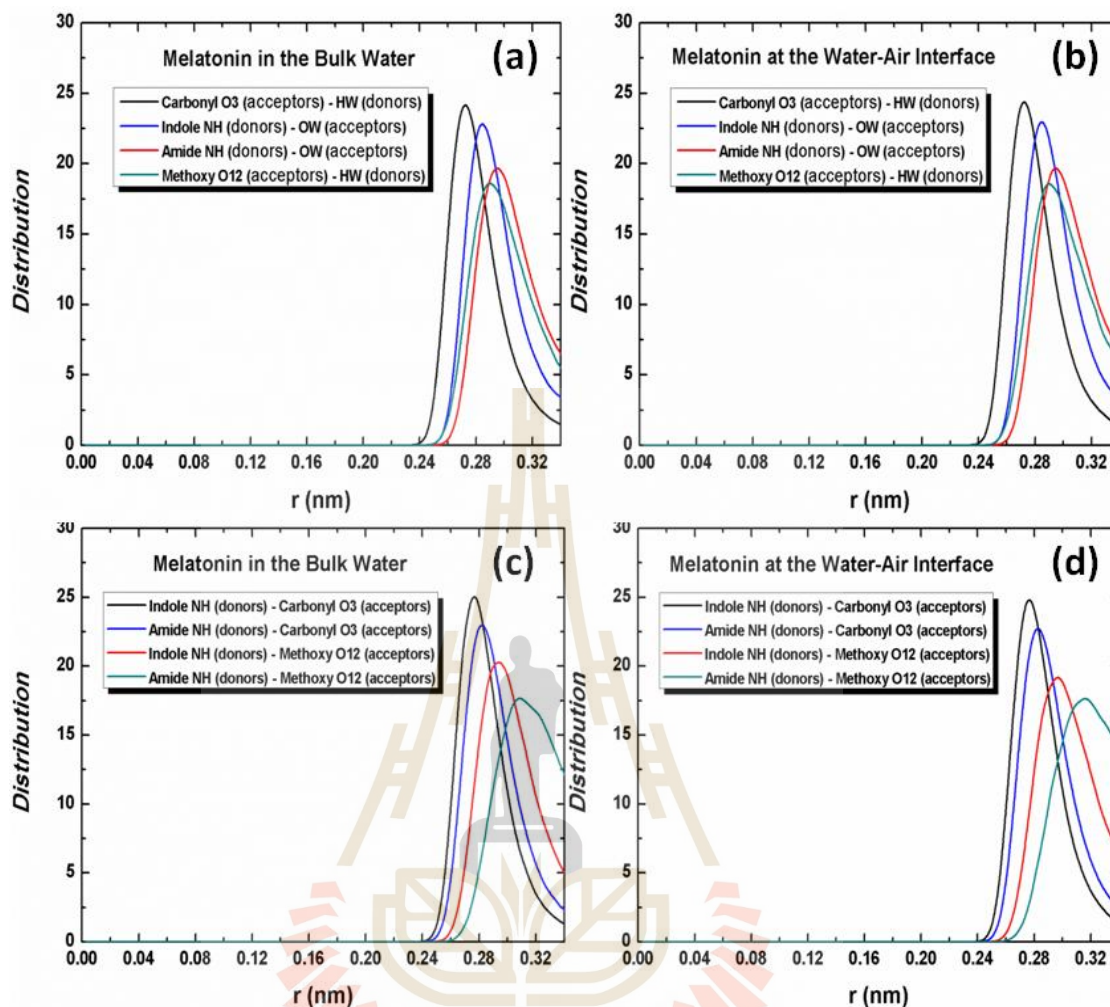


Figure 4.5 The hydrogen bond distribution as a function of the DA distance for the melatonin–water interaction (a) in the aqueous solution and (b) at the water-air interface as well as that for the melatonin–melatonin interaction (c) in the aqueous solution and (d) at the water-air interface. Coloring schemes for the melatonin–water hydrogen bonding are defined as follows: carbonyl O–HW, black; indole NH–OW, blue; amide NH–OW, red; methoxy OA–HW, dark cyan; and that for the melatonin–melatonin hydrogen bonding is defined as follows: indole NH–carbonyl O, black; amide NH–carbonyl O, blue; indole NH–methoxy OA, red; amide NH–methoxy OA, dark cyan.

Table 4.1 The average number of hydrogen bonds per melatonin molecule, $\langle n_{\text{HB}} \rangle$, for the melatonin–water and the melatonin–melatonin interactions based on considering all pairs of donors and acceptors.

$\langle n_{\text{HB}} \rangle$	Bulk water	Water-air interface
Melatonin–water interaction		
Carbonyl O – HW	0.648 ± 0.056	0.692 ± 0.055
Indole NH – OW	0.320 ± 0.049	0.326 ± 0.043
Amide NH – OW	0.234 ± 0.039	0.176 ± 0.036
Methoxy OA – HW	0.172 ± 0.035	0.045 ± 0.022
Melatonin–melatonin interaction		
Indole NH – Carbonyl O	0.344 ± 0.044	0.326 ± 0.040
Amide NH – Carbonyl O	0.332 ± 0.042	0.308 ± 0.045
Indole NH – Methoxy OA	0.131 ± 0.029	0.110 ± 0.028
Amide NH – Methoxy OA	0.070 ± 0.024	0.068 ± 0.024

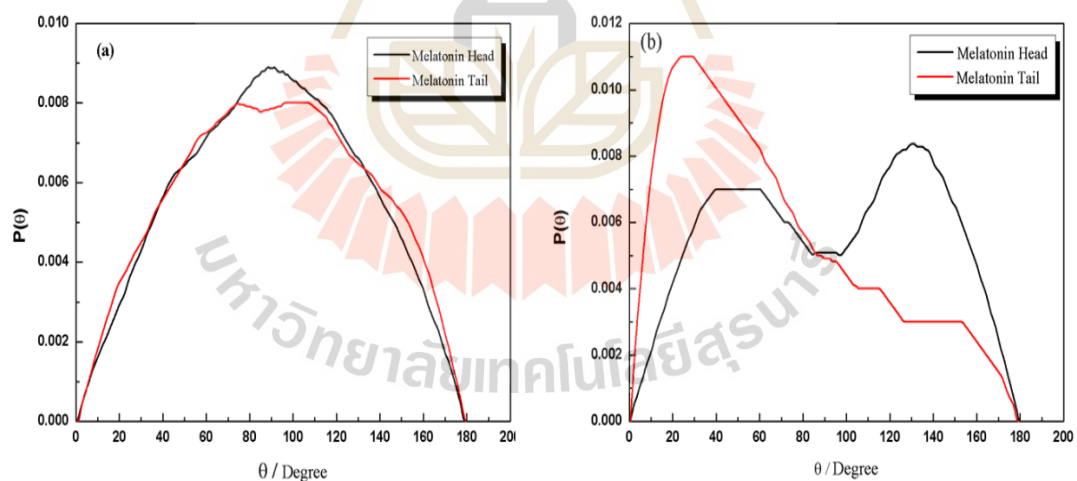


Figure 4.6 Tilt angle distributions of the head and tail groups of melatonin (a) for the bulk water and (b) for the water-air interface systems.

4.1.4 Dynamical properties of melatonin

To characterize the overall movement of melatonin molecules for the bulk water and the water-air interface systems, the average displacement of the center

of mass (COM) of all melatonin molecules in the x -, y - and z -directions for the simulation run (0–260 ns) were calculated as given in Figure 4.7. Clearly, the COM of melatonin displacement for the bulk water system (Figure 4.7a) shows more fluctuation in all three directions, while that for the water-air interface system (Figure 4.7b) exhibits more movement in the only x - and y -directions. The lateral translation of melatonin molecules in the interface plane (xy -plane) is similarly observed in lipid monolayers (Ritwiset *et al.*, 2014). These fluctuations of the COM displacements imply that melatonin molecules were not constrained in their original positions by the randomly distributed model, but were able to move, resulting in rearrangement from the original starting positions.

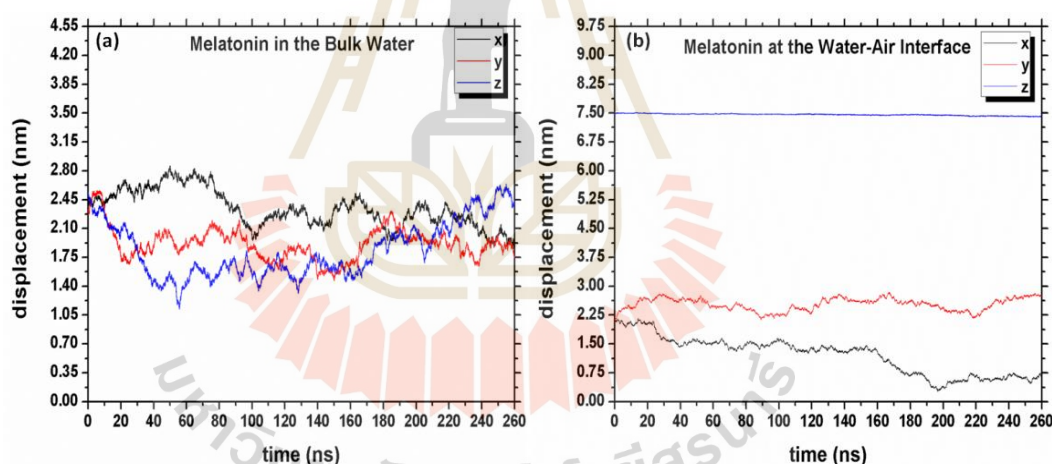


Figure 4.7 Average displacement of the center of mass of melatonin molecules in x - (black), y - (red), and z - (blue) directions: (a) for the bulk water and (b) for the water-air interface systems.

Furthermore, the translational motion of melatonin and water molecules in both systems can be examined from the mean square displacements (MSD) in terms of the self-diffusion coefficient, D_s , which was calculated using Einstein's equation (Allen and Tildesley, 2017) as follows.

$$D_s = \frac{1}{2d} \lim_{t \rightarrow \infty} \left[\frac{\langle |\vec{r}(t) - \vec{r}(0)|^2 \rangle}{t} \right] \quad (4.1)$$

Here, $\vec{r}(t)$ is the position vector of the center of mass of a molecule at the time t . d is the dimensionality of the system (i.e., $d = 1, 2, 3$ for one, or two, or three dimensions, respectively). The numerator of Equation 4.1 is the MSD. The brackets $\langle \dots \rangle$ denote an ensemble average which is an average overall molecule in the simulation and all origins. The MSD calculations of water and melatonin molecules were considered in three dimensions (3D) for the bulk water system and the two dimensions (2D) for the water-air interface. The MSD plots of water and melatonin molecules were given in Figures 4.8a and 4.8b, respectively. The self-diffusion coefficients were then derived from the slope of the linear regression fit of the time evolutions of these MSD plots and were summarized in Table 4.2. Figure 4.8a shows the MSD plots of water molecules for the bulk water with and without melatonin inclusion (pure water), and for the water-air interface systems. Among these systems, the water movement for the pure water system shows the highest mobility, while in presence of melatonin molecules the water movement is slower. This result is according to decreasing in the self-diffusion coefficient of water in Table 4.2. The self-diffusion coefficient of water for the pure water system is $2.56 \times 10^{-5} \text{ cm}^2/\text{s}$, which is in good agreement with the experimental value of $2.30 \times 10^{-5} \text{ cm}^2/\text{s}$ (Krynicky *et al.*, 1978). This indicates that the choice of SPC/E water model is suitable for investigating structural and dynamical properties of biomolecules in an aqueous solution (Mark and Nilsson, 2001).

Figure 4.8b shows the MSD plots of melatonin movement for the bulk water and the water-air interface systems. Melatonin molecules at the water-air interface diffused rapidly in the plane of the water surface leading to freely exchange

electrons with water molecules, while they diffused slowly in the aqueous solution. This is the result of the self-aggregation of melatonin molecules and the strong hydrophobic (indole-rings) interactions with the surrounding water molecules, leading to melatonin molecules can be diffusing rapidly through biological membranes and fluid or compartments within the body.

Table 4.2 The self-diffusion coefficients (D_s) of melatonin and water molecules obtained from three different systems.

Molecule	Self-diffusion coefficient ($D_s \times 10^{-6} \text{ cm}^2/\text{s}$)		
	Pure water	Melatonin in the aqueous solution	Melatonin at the water-air interface
Melatonin	–	0.06 ± 0.01 (3D)	4.00 ± 0.09 (2D) (6) ^a
Melatonin head	–	0.06 ± 0.01 (3D)	4.00 ± 0.09 (2D)
Melatonin tail	–	0.07 ± 0.01 (3D)	4.00 ± 0.09 (2D)
Water (SPC/E)	25.6 ± 0.01 (3D) (23.0) ^b	16.42 ± 0.02 (3D)	15.79 ± 0.11 (3D)

^aReference (Yu *et al.*, 2016)

^bReference (Krynicky *et al.*, 1978)

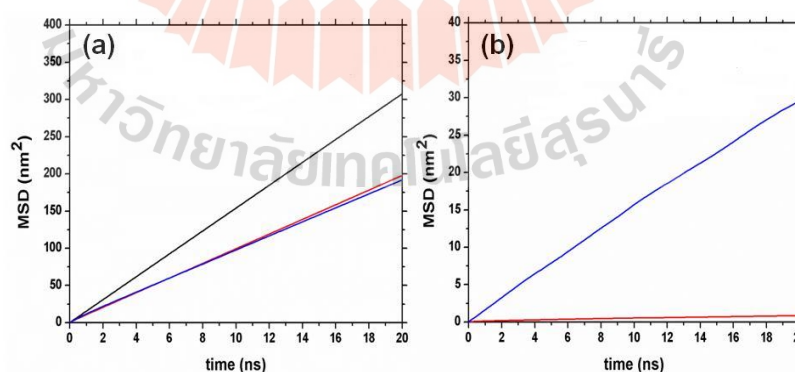


Figure 4.8 (a) Mean squared displacement (MSD) plots of the water molecule for the bulk water with (red) and without (black) melatonin inclusion, and for the water-air interface (blue) systems, (b) The MSD plots of melatonin for the bulk water (red) and the water-air interface (blue) systems.

Consequently, the molecular packing of melatonin molecules for the water-air interface is looser than that of the bulk water system due to hydrocarbon sites being disturbed with fewer water molecules. This accords to a higher self-diffusion coefficient value ($4.00 \times 10^{-6} \text{ cm}^2/\text{s}$) which is in good agreement with the experimental value of $6 \times 10^{-6} \text{ cm}^2/\text{s}$ (Yu *et al.*, 2016).

4.1.5 Hydrogen bond dynamics

Dynamics of hydrogen bonding for water and melatonin molecules and among the melatonin themselves for the aqueous solution and the water-air interface systems were analyzed in terms of the intermittent, hydrogen bond time correlation function, $C(t)$ as shown in the following equation (Luzar and Chandler, 1996; Chanda and Bandyopadhyay, 2006).

$$C(t) = \frac{\langle h(0)h(t) \rangle}{\langle h \rangle} \quad (4.2)$$

The variable $h(t)$ is unity when a pair of sites is hydrogen-bonded at time t . The $\langle h \rangle$ is the time average of h . The $C(t)$ plots of the hydrogen bonds formed by the donor (or acceptor) atoms of melatonin with the water oxygen (OW) and the water hydrogen (HW) for the aqueous solution and the water-air interface systems were given in Figures 4.9a and 4.9b, respectively. While the $C(t)$ plots of the hydrogen bonding formed between melatonin themselves for both systems were given in Figures 4.9c and 4.9d, respectively. The $C(t)$ curves of the melatonin–water hydrogen bonds showed an exponentially decrease faster than that of the melatonin–melatonin hydrogen bonds. This reveals that the interactions between melatonin and water molecules are too weak, leading to the faster hydrogen bond-forming and breaking.

This characteristic was similarly observed for the Span60 monolayer/bilayer systems (Ritwiset *et al.*, 2014; Ritwiset *et al.*, 2016). Concerning the hydrogen bond lifetime, τ_{HB} , in this work, the hydrogen bond lifetime (τ_{HB}) can be calculated from the best fit of the $C(t)$ with a sum of three exponential functions defined as follows (Starr *et al.*, 2000).

$$C(t) = \sum_{i=1}^3 a_i e^{-t/\tau_i} \quad (4.3)$$

Where τ_i are the relaxation time constants and a_i are the corresponding relative amplitudes. Then, the average hydrogen bond lifetime, $\langle\tau_{\text{HB}}\rangle$, for each pair of hydrogen bonds can be calculated as follows.

$$\langle\tau_{\text{HB}}\rangle = \sum_{i=1}^3 a_i \tau_i = a_1 \tau_1 + a_2 \tau_2 + a_3 \tau_3 \quad (4.4)$$

The $\langle\tau_{\text{HB}}\rangle$ for all the pair of hydrogen bonds were summarized in Table 4.3. The hydrogen bond lifetimes of the melatonin–melatonin interaction are longer lived than that of the melatonin–water interaction for both systems, suggesting the stronger hydrogen bond interaction between the two melatonin molecules. Additionally, the $\langle\tau_{\text{HB}}\rangle$ of the melatonin–melatonin hydrogen bonds for the bulk water system is longer than that for the water-air interface system, suggesting that the stronger interaction of melatonin aggregation. This is according to a decrease in the translational mobility of the melatonin molecules for the bulk water system. The $\langle\tau_{\text{HB}}\rangle$ of the carbonyl O–HW and the indole NH–OW hydrogen bonds are nearly the same for both systems. This suggests that water molecule interacts with both sites of melatonin simultaneously as previously reported by the infrared spectra studies (Florio and Zwier, 2003).

Table 4.3 Average hydrogen bond lifetime, ($\langle\tau_{\text{HB}}\rangle$), for the melatonin–water and the melatonin–melatonin interactions considered the pair of donor and acceptor atoms on both melatonin and water molecules.

Site-site interaction	Hydrogen bond lifetime, $\langle\tau_{\text{HB}}\rangle$ (ns)	
	Bulk Water	Water–Air interface
Melatonin–Water	Bulk Water	Water–Air interface
Carbonyl O–HW (Carbonyl O/HW)	0.038	0.035
Indole NH–OW (NR5*H/OW)	0.035	0.031
Amide NH–OW (NH/OW)	-	-
Methoxy OA–HW (OA/HW)	-	-
Melatonin–Melatonin	Bulk Water	Water–Air interface
Indole NH–Carbonyl O (NR5*H/Carbonyl O)	8.158	1.549
Amide NH–Carbonyl O (NH/Carbonyl O)	7.180	1.738
Indole NH–Methoxy OA (NR5*H/OA)	7.311	1.169
Amide NH–Methoxy OA (NH/OA)	1.678	0.515

While the $C(t)$ curves of the amide NH–OW and the methoxy OA–HW hydrogen bonds showed exponential decrease rapidly (see Figures 4.9a and 4.9b), subsequently the $\langle\tau_{\text{HB}}\rangle$ cannot be obtained from this fitting. However, it can be presumed that the lifetimes of the two hydrogen bond pairs are very small.

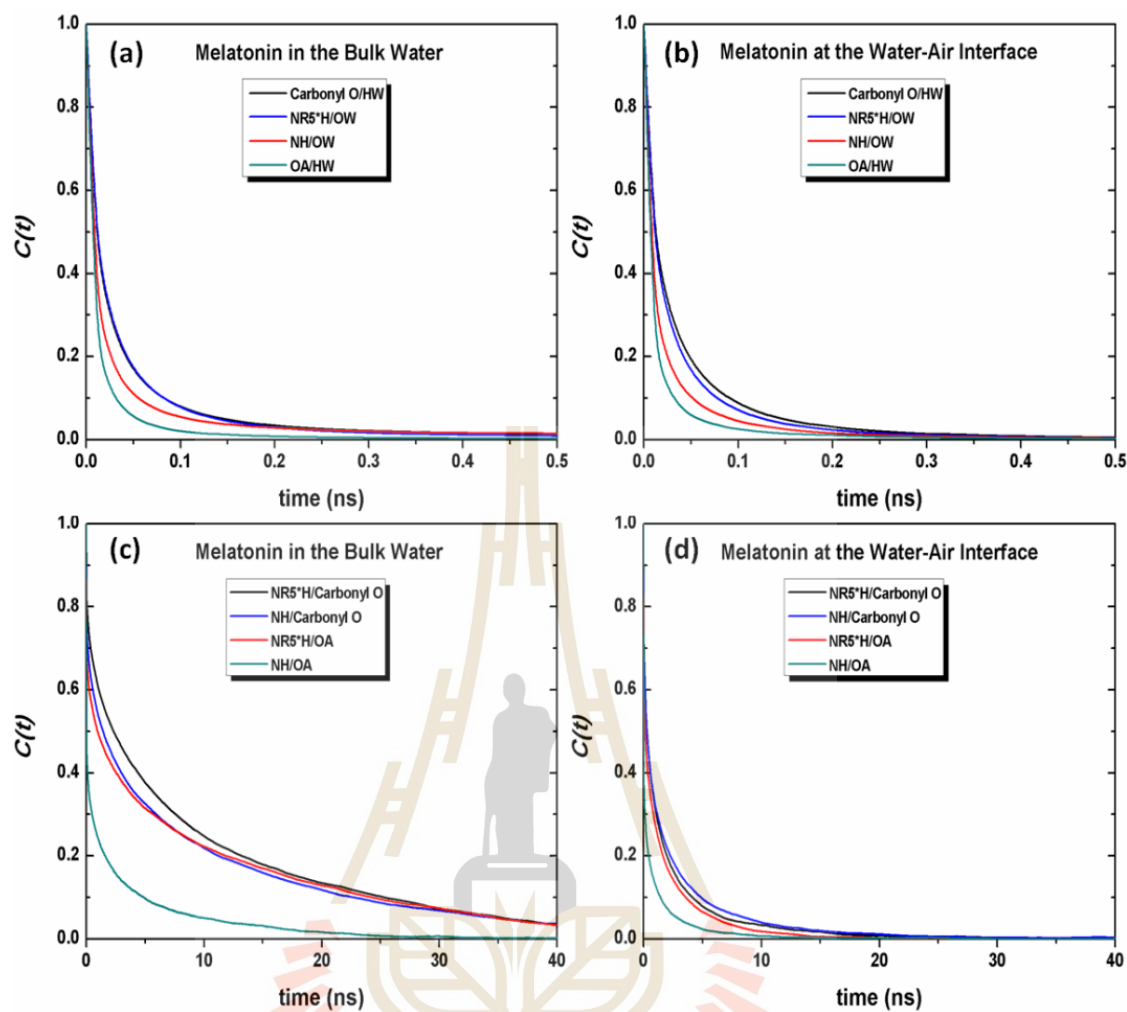


Figure 4.9 Intermittent hydrogen bond time correlation function, $C(t)$, of the melatonin–water interactions for (a) the bulk water and (b) the water-air interface systems. The $C(t)$ plots of the melatonin-melatonin interactions for (c) the bulk water and (d) the water-air interface systems.

4.2 Melatonin in the niosome bilayers

4.2.1 Bilayer structures

The overall structures of niosome bilayers with and without melatonin addition were examined in terms of mass density distribution for individual molecules and molecular sites including the head and tail groups of Span60 as shown in Figure

4.10. These density profiles were calculated as a function of the z-coordinate and were shifted their centers at $z = 0$ nm. The Span60 head and tail groups were separately plotted for clarity. Relatively symmetric of all density profiles, indicating that the four bilayer systems are well-equilibrated during the simulation run. It is seen in Figures 4.10a and 4.10b that melatonin was continuously distributed inside the bilayer along the z-axis and can be deeply penetrated the hydrophobic region for the Span60/Chol bilayer. Such a characteristic was similarly observed in the study of Han and co-workers (Myung *et al.*, 2016). In Figure 4.10 two peaks of the melatonin density were observed at ~ 1.5 and ~ -1.5 nm and they were more overlap with the density profile of the tail group than that of the head group. This suggests that melatonin is preferred to locate in the hydrophobic regions.

A similar characteristic can be seen in Figure 4.10b. However, the two peaks of the melatonin density were slightly shifted from the bilayer center at ~ 2.0 and ~ -2.0 nm and they were more overlap with the head density profile than that of the tail group. This indicates that melatonin is preferred to locate in the hydrophilic regions. Moreover, it is seen that the addition of cholesterol into the Span60 bilayer changes the density profiles of the head and tail groups of Span60 significantly as well as the melatonin density. The density profile of the Span60 head showed two pronounced peaks and located near the water bulk phase for the four bilayer systems. However, the density profile of the Span60 tail exhibited a prominent peak at the bilayer center ($z=0$) for the Span60 bilayer with cholesterol inclusion while the density profile of cholesterol lay between that of head and tail groups. Cholesterol incorporated into the Span60 bilayer it is well-known that results to disturb the alignment of the hydrocarbon chain and the hydrophilic groups which are similar to

the lipid bilayers (Ritwiset *et al.*, 2016). Additionally, the characteristics of melatonin penetration through the niosome bilayers were similarly observed to those of other lipid bilayers (Drolle *et al.*, 2013).

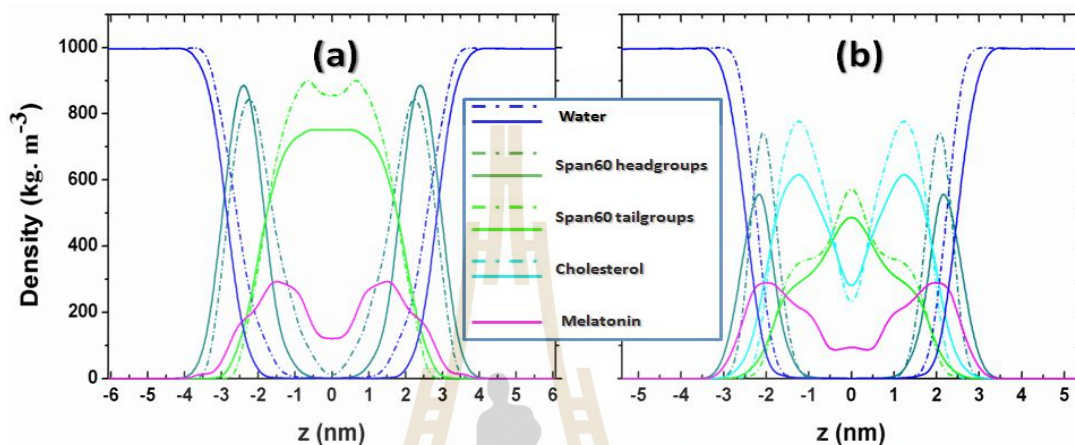


Figure 4.10 Mass density distributions of the Span60 head and tail groups, cholesterol, melatonin, and water molecules versus to z -direction for (a) the Span60 bilayer with melatonin (solid line) and without melatonin (short dash-dot line) addition and (b) the Span60/Chol bilayer with melatonin (solid line) and without melatonin (short dash-dot line) addition. Coloring schemes are defined as follows: water, blue; Span60 head, dark cyan; Span60 tail, green; cholesterol, cyan; melatonin, magenta.

Characterization of lipid bilayers the most widely used property is area per lipid which can be measured by experiments. Also, the various other properties related to the area per lipid-like membrane elasticity, lateral diffusion, etc., (Pandey and Roy, 2011). In the present work, the lengths of the box in the L_x and L_y direction was used to calculate the area per lipid by the following equation (Somjid *et al.*, 2018)

$$A_0 = \frac{A}{N} = \frac{L_x \times L_y}{N_{\text{Span60}} + N_{\text{Chol}}} \quad (4.5)$$

The product of cell size in the x - (L_x) and y - (L_y) directions is the surface area in the xy -plane of A . The sum of the Span60 number (N_{Span60}) and cholesterol number (N_{Chol}) in one layer which is the total number of the molecules of N . When the 30 mol% of melatonin was added into the pure Span60 bilayer, the area per lipid (A_0) increased from $24.6 \pm 0.1 \text{ \AA}^2$ to $30.1 \pm 0.1 \text{ \AA}^2$. This pure Span60 bilayer has a smaller area per lipid reveals that the Span60 molecules were closely packed with their orderly tilted tail groups versus to the bilayer normal direction (the z -axis) (see Figure 4.12a). Which is referred to as the gel phase or liquid-crystalline-phase (L_α). It is in good agreement with our previous studies ($23.6 \pm 0.1 \text{ \AA}^2$) for such an area per lipid (Ritwiset *et al.*, 2016). The Span60 bilayer with melatonin addition reveals more expanded area per lipid due to the melatonin insertion among the Span60 themselves, leading to more loosely-packed between the Span60 and melatonin domains. The Span60 tails are less orientational order with their tilt parallel to the bilayer normal direction (see Figure 4.12b). This characteristic of the bilayer is referred to as the liquid-expanded phase (L_E) (Drolle *et al.*, 2013; Dies *et al.*, 2015). The Span60 bilayer with melatonin addition showed a less ordered structure than the pure Span60 and the Span60/Chol bilayers. When the 50 mol % cholesterol was added to the Span60 bilayer, the area per lipid (A_0) increased from $24.6 \pm 0.1 \text{ \AA}^2$ to $27.8 \pm 0.1 \text{ \AA}^2$. The area per lipid of Span60 bilayer with cholesterol inclusion was more expanded due to the cholesterol insertion among the Span60 themselves, leading to more loosely-packed between the Span60 and cholesterol domains. Their tail groups of Span60 molecules were orderly alignment parallel to the bilayer normal direction (see

Figure 4.12c), which is referred as the liquid-ordered phase (L_O). The area per lipid of the Span60 bilayer with melatonin addition showed more expansion than that of the Span60/Chol bilayer. This result indicated that cholesterol molecules can induce the Span60 close together rather than melatonin molecules do when they are added into the Span60 bilayers. A clear picture of this behavior can be seen from the 2-dimensional radial distribution function as displayed in Figure 4.11a. Furthermore, adding melatonin to the Span60/Chol bilayer caused the area per lipid (A_0) to expand from $30.1 \pm 0.1 \text{ \AA}^2$ to $33.6 \pm 0.1 \text{ \AA}^2$. The melatonin insertion among the Span60 and cholesterol molecules resulted to phase change from the liquid-condensed phase (L_C) to the liquid-expanded phase (L_E) as displayed in Figures 4.12c and d. According to the two dimensional-radial distribution function plots for the Span60/cholesterol (SC) and the Span60/melatonin (SM) systems (see Figure 4.11b). The Span60 bilayer with both melatonin and cholesterol inclusion showed a less ordered structure when compared to the pure Span60 and the Span60 with melatonin inclusion.

The physical properties of niosome bilayers with and without cholesterol and melatonin inclusion such as an area per lipid (A_0) and bilayer thickness (D_{HH}) were summarized and compared with the other work as given in Table 4.4. The D_{HH} is defined from the center of mass of the Span60 headgroups in the upper and lower layers that were averaged overall in z-distance at the equilibrium ranges. The D_{HH} was calculated over the last 50 ns simulation run for all bilayer systems. The Span60/Chol bilayer with melatonin addition yielded the area per lipid and bilayer thickness according to that of the Span60/Chol bilayer which contained flavone, chrysin, and luteolin, respectively (Myung *et al.*, 2016). The area per lipid and bilayer thickness of our studies for the Span60 bilayer with 50 mol% cholesterol

inclusion are $27.8 \pm 0.1 \text{ \AA}^2$ and $40.0 \pm 0.2 \text{ \AA}$, respectively. Our result is in good agreement with the study of Han *et al.* (Myung *et al.*, 2016) which yielded 29.9 \AA^2 and 37.4 \AA , respectively. The area per lipid increased whereas the bilayer thickness decreased when the 30 mol% of melatonin was added to the Span60/Chol bilayer. This characteristic is similarly observed for those of the Span60/Chol bilayer with the addition of 25 mol% flavone, chrysin, and luteolin, respectively (Myung *et al.*, 2016).

Table 4.4 Comparison of some physical properties of the pure Span60 and the Span60/Chol bilayers which were added with melatonin, flavone, chrysin, and luteolin molecules, respectively.

Physical properties	Additive	Span60 bilayer	
		0 mol% Cholesterol	50 mol% Cholesterol
Area per lipid, A_0 (\AA^2)	–	24.6 ± 0.1	27.8 ± 0.1 (29.9 ^a)
	30 mol% melatonin	30.1 ± 0.1	33.6 ± 0.1
	25 mol% flavone ^a	–	35.8
	25 mol% chrysin ^a	–	37.6
	25 mol% luteolin ^a	–	31.0
Thickness, D_{HH} (\AA)	–	41.6 ± 0.2	40.0 ± 0.2 (37.4 ^a)
	30 mol% melatonin	42.6 ± 0.2	38.7 ± 0.1
	25 mol% flavone ^a	–	36.1
	25 mol% chrysin ^a	–	32.9
	25 mol% luteolin ^a	–	37.9

^aReference (Myung *et al.*, 2016)

Furthermore, the D_{HH} increased from $41.6 \pm 0.2 \text{ \AA}$ to $42.6 \pm 0.2 \text{ \AA}$ when the 30 mol% melatonin was added to the pure Span60 bilayer. Conversely, it decreased from $41.6 \pm 0.2 \text{ \AA}$ to $40.0 \pm 0.2 \text{ \AA}$ when the 50 mol% cholesterol was added to the Span60 bilayer. The bilayer thickness of this study is in good agreement with our previous works which yielded $46.3 \pm 0.2 \text{ \AA}$ and $41.3 \pm 0.1 \text{ \AA}$ for the pure Span60 and the Span60 with the 50 mol% cholesterol incorporation (Somjid *et al.*, 2018). The

lowest of D_{HH} is $38.7 \pm 0.1 \text{ \AA}$ when the 30 mol % melatonin was added to the Span60/Chol bilayer. This indicated that melatonin causes the Span60 bilayer to be the most fluidity compared with the Span60/Chol bilayer with and without melatonin incorporation.

The probability of finding two molecules at a specific distance was described in terms of the radial distribution function (rdf). In our case, the two-dimensional–radial distribution function (2D–rdf) was applied for the bilayer system. The positions of the center of mass of the Span60 head group, cholesterol, and melatonin were projected on the bilayer plane (the xy –plane). The overall rdf shape can be described as the molecular arrangement in the liquid phase while the estimation of the characteristic distances on their structure can be used for the peak position. The 2D-rdf was defined as the following equation (Spaar and Salditt, 2003; Chen *et al.*, 2015)

$$g(r) = \frac{1}{2\pi r N} \langle S(t) \cdot \frac{\delta N(r,t)}{\delta r} \rangle \quad (4.6)$$

Where the total number of molecules which are considering of N . Here, $S(t)$ is the xy cross-section area of the simulation box dependent on time t . The number of molecules with a distance to the center of mass of the molecule is located in a circular shell of radius from r to $r + \delta r$ which is $\delta N(r,t)$. The angle bracket $\langle \rangle$ denotes averaging over the total simulation time and the total number of molecules. Figure 4.11 shows the 2D–rdf plots for the pair of the Span60/cholesterol (SC) and Span60/melatonin (SM) systems. To clearly illustrate the impact of the variable melatonin or cholesterol on the bilayer structure thus were considered only lateral distributions (the xy –plane). The centers of mass of the Span60 head group,

cholesterol, and melatonin were used for these the 2D-rdf calculations. It is seen that the first sharp peak of the SC-rdf was detected at a shorter distance than that of the SM-rdf for the Span60/Chol/Mel bilayer. This means that cholesterol prefers to interact with Span60.

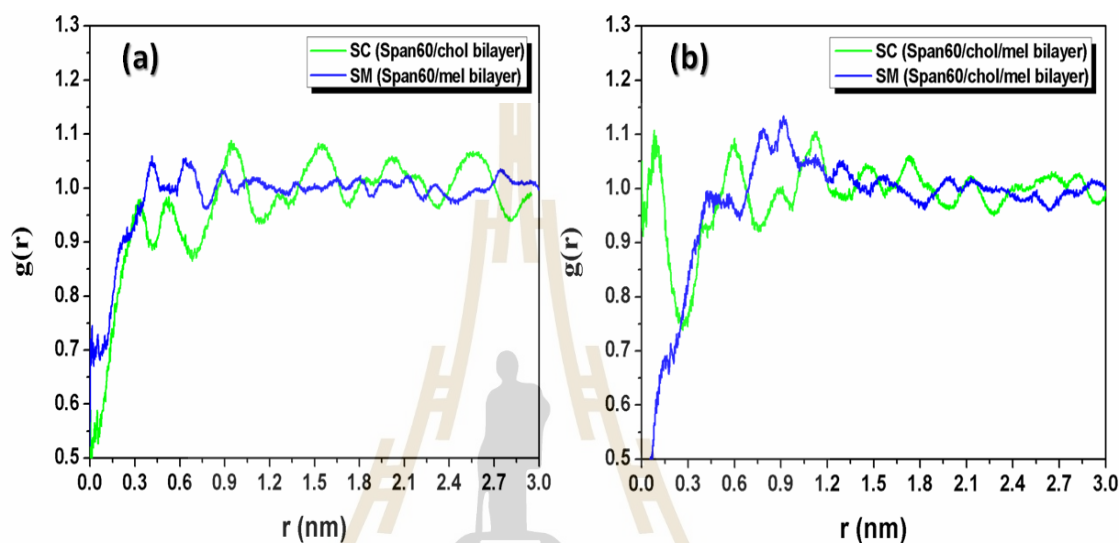


Figure 4.11 Two dimensional–radial distribution functions (2D–rdfs), calculated only on the xy –plane for the Span60/cholesterol (SC) and Span60/melatonin (SM) bilayer systems. The 2D–rdfs were calculated from the Span60 head group to cholesterol (green line) and melatonin (blue line) for (a) the Span60/Chol and the Span60/Mel bilayers, and (b) the Span60/Chol/Mel bilayer. The centers of mass of the Span60 head group, cholesterol, and melatonin were used throughout these calculations.

This result was according to the hydrogen bond strength between Span60 and cholesterol and their stronger van der Waals interaction. The SC-rdf of the Span60/Chol and the SM-rdf of the Span60/Mel bilayers showed higher a uniform distribution than those of the Span60/Chol/Mel bilayer. These characteristics are similar to cholesterol or melatonin distribution in the lipid membranes which both

systems were investigated at high concentrations using the two-dimensional X-ray diffraction technique (Dies *et al.*, 2015).

Molecular configurations of all the bilayer systems in the equilibrium can be depicted in Figure 4.12. It is seen from Figures 4.12a and 4.12c that two phases of the pure Span60 and the Span60/Chol bilayers were observed as the gel phase (L_α) and the liquid-ordered phase (L_o), respectively. This is according to our previous studies of niosome bilayer with and without cholesterol inclusion (Ritwiset *et al.*, 2016; Somjid *et al.*, 2018). Figures 4.12b and 4.12d exhibited the influence of melatonin on the orientation of the Span60 tail groups which resulted in the phase change from the liquid-expanded phase to the liquid-condensed phase for the Span60/Mel and the Span60/Chol/Mel bilayers, respectively. These characteristics are similarly observed to the saturated lipid bilayer with melatonin and cholesterol inclusion (Drolle *et al.*, 2013; Dies *et al.*, 2015).

4.2.2 Molecular orientation

It has been widely calculated in a theoretical for the tilt angle distributions to characterize the structure of the lipids bilayer and also can be compared to X-ray diffraction results (Katsaras *et al.*, 1992). The tilt angle distributions of the Span60 tail and melatonin for all bilayer systems were analyzed as given in Figure 4.13. The probability distribution of the tilt angle of the Span60 tails lying in the upper and the lower layers was obtained as displayed in Figure 4.13a. Definition of the tilt angle, θ , is a vector of acyl chains pointing from the first (CH₃) to the last hydrocarbon (CH₂) unit (see Figure 3.4a) versus to the bilayer normal vector (the z-axis).

These tilt angle distributions of the Span60 hydrocarbon chains for the pure Span60 and the Span60/Mel bilayers exhibited the highest probability of the first peak of the upper layer at $\sim 14.2^\circ$ and $\sim 11.6^\circ$ and that of the lower layer at $\sim 154.4^\circ$ and $\sim 162.9^\circ$, respectively. It also showed the different patterns of the tilt angle distribution of the Span60 tails obtained from the two systems.

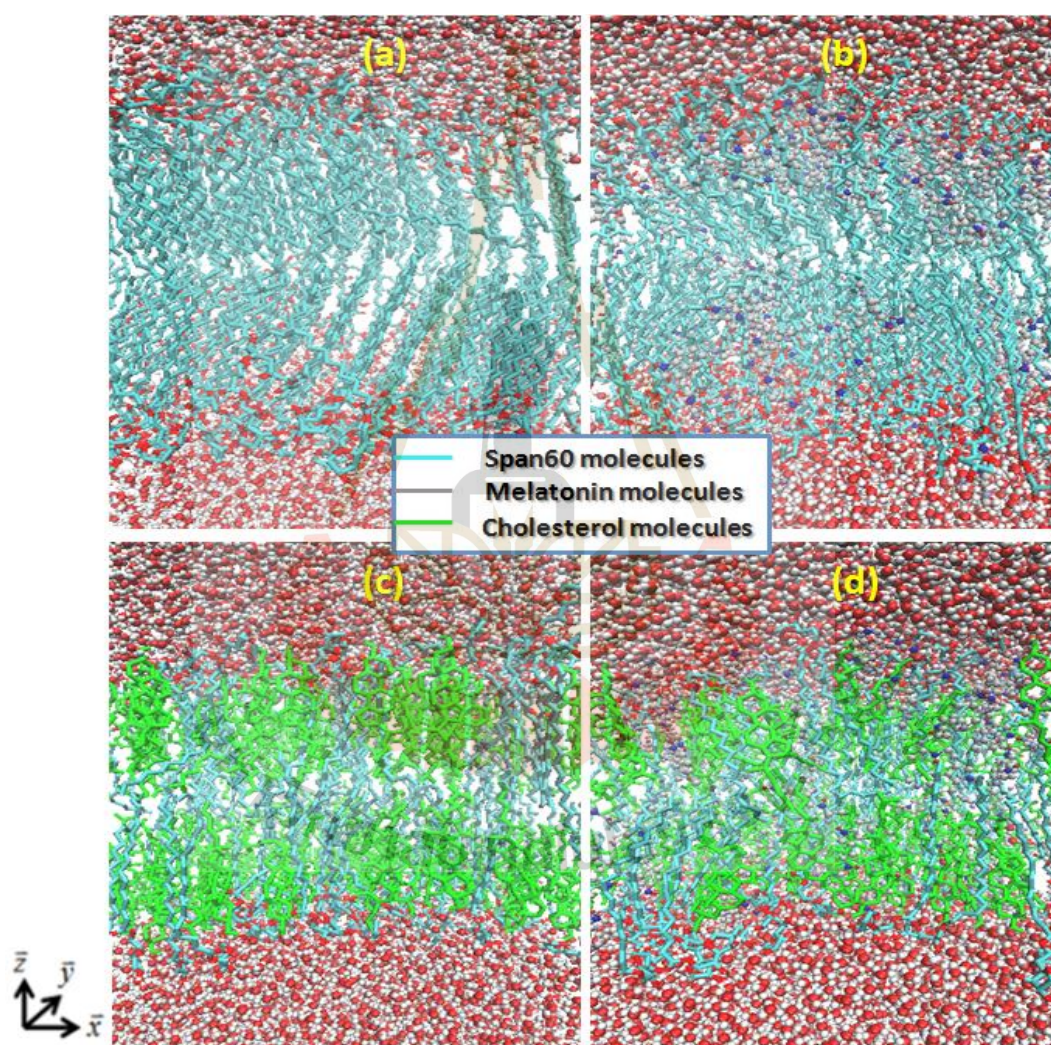


Figure 4.12 Molecular configurations of (a) the Span60, (b) the Span60/Mel, (c) the Span60/Chol, and (d) the Span60/Chol/Mel bilayers, respectively which were taken from the MD simulation. Color scheme: cholesterol, green; Span60 tails, cyan; melatonin, gray; oxygen, red; nitrogen, blue; hydrogen, gray.

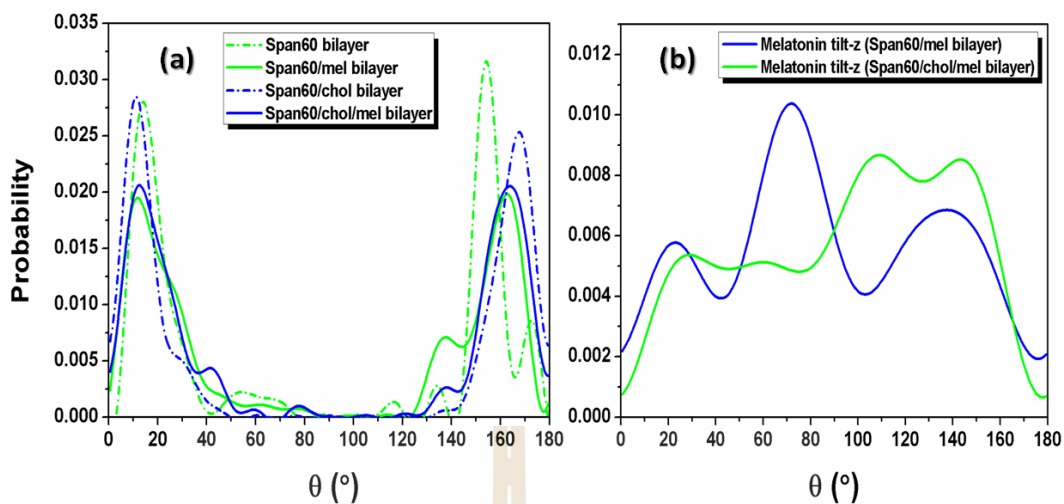


Figure 4.13 (a) The tilt–angle distribution of the Span60 tail for the pure Span60 (green short dashed line), Span60/mel (green solid line), the Span60/chol (blue short dashed line), and the Span60/chol/mel bilayers (blue solid line), respectively. (b) the tilt–angle distribution of melatonin for the Span60/mel (green solid line) and the Span60/Chol/Mel bilayers (blue solid line), respectively.

These results indicated that the Span60 tails of the pure Span60 bilayer exhibit more tilt than that of the Span60 bilayer with 30% melatonin addition. This suggested that the pure Span60 bilayer was in the gel phase and the Span60 with melatonin inclusion was in the liquid–expanded phase. This is according to the previous work (Somjid *et al.*, 2018) which reported the average tilt angle of $19.36 \pm 1.02^{\circ}$ for the pure Span60 bilayer. However, the tilt angle distributions of the Span60 hydrocarbon chains for the Span60/Chol and the Span60/Chol/Mel bilayers exhibited the highest probability of the first peak at $\sim 11.2^{\circ}$ and $\sim 12.5^{\circ}$ for the upper layer and the first peak at $\sim 167.7^{\circ}$ and $\sim 163.8^{\circ}$ for the lower layer, respectively. It also showed a similar pattern of the tilt angle distribution of the Span60 tails obtained from the two systems. The Span60 chains including both cholesterol and melatonin exhibit more tilt

than the Span60 chains with cholesterol inclusion. This is because the melatonin induced the increase of local disorder in the Span60 tail groups. The tilt angle of $15.43 \pm 0.59^\circ$ for the Span60 bilayer with 50% cholesterol inclusion was reported in previous works (Somjid *et al.*, 2018).

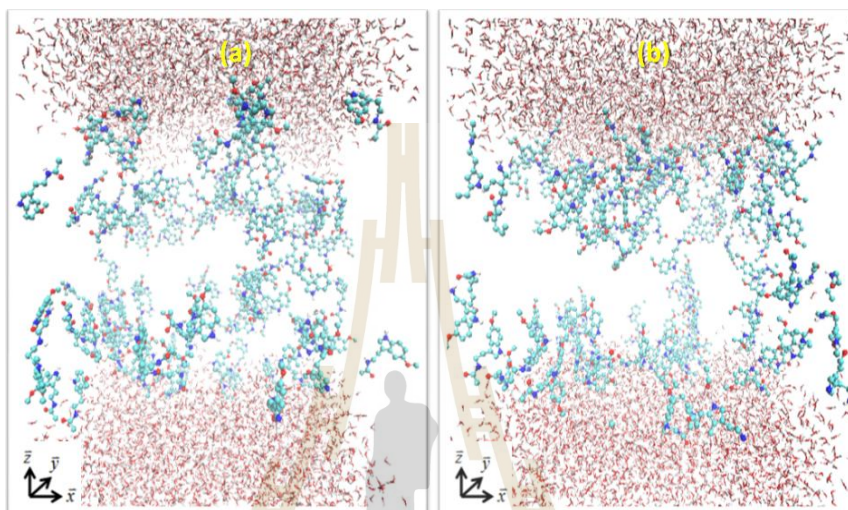


Figure 4.14 Molecular configuration of melatonin molecules (Span60 and cholesterol were not shown) distributed in the Span60 bilayer (a) without cholesterol and (b) with cholesterol inclusion, respectively. Melatonin molecule color scheme: the carbon atom and hydrocarbon group, cyan; oxygen, red; nitrogen, blue; hydrogen, gray.

Figure 4.13b shows the probability distribution of the melatonin tilt angle for the Span60/Mel and the Span60/Chol/Mel bilayers. Definition of the tilt angle, θ , is a vector on melatonin molecule pointing from the first (C) to the last hydrocarbon (CR61) unit (see Figure 3.4c) versus to the bilayer normal vector (the z-axis). Clearly, the melatonin tilt angle distribution for the Span60 bilayer without cholesterol inclusion showed three pronounced peaks with the positions of the first peak $\sim 22.8^\circ$, the second peak $\sim 71.8^\circ$, and the third peak $\sim 138.0^\circ$, respectively. The second peak $\sim 71.8^\circ$ is the highest. This result indicated that melatonin molecules

were rather orderly aligned within the bilayer structure (see Figure 4.14a) versus to the bilayer normal vector (the z -axis). Such a characteristic is similarly observed in the lipid bilayers with melatonin inclusion (Dies *et al.*, 2015; Lu and Martí, 2019). Conversely, the melatonin tilt angle distribution of the Span60 bilayer with cholesterol inclusion was quite broad. It means that the melatonin molecules were rather disorderly aligned within the bilayer structure (see Figure 4.14b) versus to the bilayer normal vector (the z -axis).

4.2.3 Order parameters

It has been widely calculated in a theoretical for the deuterium order parameters (S_{CD}) to characterize the structure of the hydrocarbon chains inside a lipid membrane and can be compared to ^2H NMR measurements (Petrache *et al.*, 1999). Description of the orientational mobility of the C–D bond for such a property and the simulation can be extracted using the following equation

$$S_{CD} = \frac{1}{2} | \langle 3\cos^2\theta - 1 \rangle | \quad (4.7)$$

Here, θ is the angle between the membrane normal (the z -axis) and the C–D bond vector. A time and ensemble average represents by the angular bracket. In this study, a united atom model was employed to describe the hydrocarbon groups (CH_2 or CH_3). Thus, the definition of the C–D bond vector is a vector from C_{n-1} to C_{n+1} site. The C1 site is the carbonyl carbon and the C18 site is the CH_3 group. The CH_2 groups are numbered consecutively from C2 to C17 site (see Figure 3.4a). The order parameters depending on the carbon site of the Span60 molecule obtained from all bilayer systems were presented in Figure 4.15. This result revealed that the Span60 chains for

the pure Span60 bilayer showed the lowest orientational mobility due to the strong interaction between Span60 themselves (Ritwiset *et al.*, 2016).

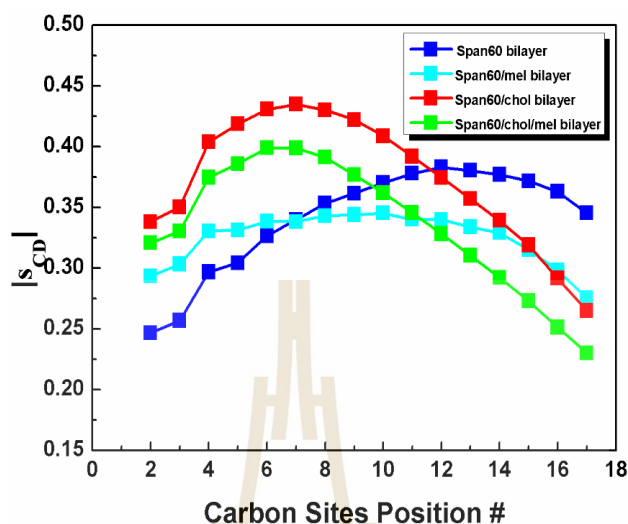


Figure 4.15 Order parameter, S_{CD} , on hydrocarbon chains of the Span60 molecules, as depend on carbon sites position for the pure Span60, the Span60/Mel, the Span60/Chol, and the Span60/Chol/Mel bilayers, respectively.

For the other bilayers, the Span60 chain exhibited more orientational mobility which strongly depends on the concentration of cholesterol or melatonin. However, it is seen that the addition of cholesterol in the Span60 bilayer resulted in the orientational mobility of the Span60 chain significantly rather than melatonin adding. The carbon sites of the Span60 chain (C8-C17) showed more orientational mobility due to those chains being closely packed with the chain–chain interactions (Peltonen *et al.*, 2001). Excluding the pure Span60 bilayer, the S_{CD} increases with carbon positions until to C7 site and after that, it decreases to the minimum site at C17. This suggested that the Span60 tail groups were higher orientational mobility. The carbon segments from C5 to C8 showed high order parameters for the Span60/Chol and the Span60/Chol/Mel bilayers. This means that they were less mobility compared to the other parts of the

Span60 chain. This is because they closely contact the sterol rings of cholesterol which induced the strong interaction with the hydrocarbon chains of the Span60. One can be observed from these simulations that cholesterol molecules not only significantly increase bilayer fluidity but also result to order parameters of the Span60 chain.

4.2.4 Hydrogen bond and energetic interaction analysis

The number of hydrogen bonds between molecules can be defined in different ways, either based on the geometry–donor–hydrogen–acceptor (DHA) angle and the donor-acceptor (DA) or the hydrogen–acceptor (HA) distance or based on the interaction energy and distance (Luzar and Chandler, 1996). For this study, we employed the geometrical criterion with the maximum DA distance of 0.35 nm and the DHA angle of 30°. With this definition, it is useful to describe the stability of melatonin inserted into the Span60 bilayer with and without cholesterol inclusion. The average hydrogen bond number per molecule and the van der Waal interactions were calculated for all bilayer systems and given in Tables 4.5 and 4.6, respectively.

It is seen that the average number of hydrogen bonds and the van der Waal interactions of the pure Span60 and the Span60/Chol bilayers are in good agreement with previous works (Somjid *et al.*, 2018). When melatonin was added to the pure Span60 bilayer and the Span60 bilayer with cholesterol inclusion, the number of hydrogen bonds between the Span60/Span60 decreased from 1.87 ± 0.03 to 1.64 ± 0.03 and 0.97 ± 0.04 to 0.79 ± 0.04 , respectively. However, these decreases were compensated by hydrogen bonds formed between Span60 and melatonin which were 0.40 ± 0.02 and 0.56 ± 0.03 for the Span60/Mel and,

Table 4.5 The calculated average hydrogen bond number per molecule ($\langle n_{HB} \rangle$) for the Span60, the Span60/Mel, the Span60/Chol, and the Span60/Chol/Mel bilayers, respectively. The pair of hydrogen bond formation was represented as the Span60/water (SW), the Span60/Span60 (SS), the Span60/cholesterol (SC), the Span60/melatonin (SM), the cholesterol/water (CW), the cholesterol/melatonin (CM), the melatonin/water (MW), and the melatonin/melatonin (MM), respectively.

Bilayer system	The average number of hydrogen bonds per molecule, $\langle n_{HB} \rangle$							
	SW	SS	SC	SM	CW	CM	MW	MM
Pure Span60	2.35 ± 0.05 (2.17 ± 0.05) ^a	1.87 ± 0.03 (1.89 ± 0.03) ^a	–	–	–	–	–	–
Span60/Mel	2.55 ± 0.06	1.64 ± 0.03	–	0.40 ± 0.02	–	–	0.40 ± 0.04	0.55 ± 0.03
Span60/Chol	3.83 ± 0.10 (3.97 ± 0.10) ^a	0.97 ± 0.04 (0.89 ± 0.05) ^a	0.73 ± 0.04 (0.85 ± 0.04) ^a	–	1.09 ± 0.05 (0.88 ± 0.05) ^a	–	–	–
Span60/Chol/Mel	3.76 ± 0.09	0.79 ± 0.04	0.69 ± 0.03	0.56 ± 0.03	0.82 ± 0.04	0.30 ± 0.02	0.80 ± 0.06	0.46 ± 0.03

^aReference (Somjid *et al.*, 2018)

the Span60/Chol/Mel bilayers, respectively. The average van der Waal interactions obtained from each system exhibited the interactions of the Span60/Span60 system decreased while the interaction of the Span60/melatonin system increased. Furthermore, the number of hydrogen bonds formed by the Span60/water (SW) increased from 2.35 ± 0.05 to 2.55 ± 0.06 when melatonin was added to the Span60 bilayer while they decrease from 3.83 ± 0.10 to 3.76 ± 0.09 when melatonin was added to the Span/Chol bilayer. Additionally, the number of hydrogen bonds for the melatonin/water (MW) increased from 0.40 ± 0.04 to 0.80 ± 0.06 when melatonin was added to the Span60/Chol bilayer. This indicated that melatonin molecules favored interacting with water molecules located at the bilayer interface, leading to making their stability.

The hydrogen bond numbers of the melatonin/melatonin (MM) for the pure Span60 and the Span60/Chol bilayers were 0.55 ± 0.03 and 0.46 ± 0.03 , respectively. This was according to the average van der Waal interactions obtained from our simulation and these results were closely related to melatonin alignment in the bilayers. The hydrogen bond numbers of the cholesterol/water (CW) were 1.09 ± 0.05 and 0.82 ± 0.04 for the Span60/Chol and the Span60/Chol/Mel bilayers, respectively. The reduction of this hydrogen bond number for the Span60/Chol/Mel bilayer was compensated by hydrogen bonds of the cholesterol/melatonin (CM) which was 0.30 ± 0.02 . Furthermore, the hydrogen bond number of the Span60/cholesterol (SC) slightly decreased when melatonin was added to the Span60/Chol bilayer. This was according to the average van der Waal interactions obtained from the two systems. This result indicated that cholesterol can help to improve the bilayer stability via the hydrogen bond interactions.

Table 4.6 The calculated average van der Waals interaction ($\langle E_{vdw} \rangle$) for the Span60, the Span60/Mel, the Span60/Chol, and the Span60/Chol/Mel bilayers, respectively. The van der Waals interactions were represented by the pair of the Span60/Span60(SS), the Span60/cholesterol (SC), the cholesterol/cholesterol (CC), the Span60/melatonin (SM), the cholesterol/melatonin (CM), and the melatonin/melatonin (MM), respectively.

Bilayer system	$\langle E_{vdw} \rangle$ (kJ/mol)					
	SS	SC	CC	SM	CM	MM
Pure Span60	-237.53 ± 0.73 (-234.01 ± 0.16) ^a	–	–	–	–	–
Span60/Mel	-198.97 ± 0.69	–	–	-62.85 ± 0.43	–	-36.49 ± 0.52
Span60/Chol	-137.53 ± 0.85 (-123.14 ± 0.18) ^a	-162.03 ± 1.01 (-190.02 ± 0.11) ^a	-126.57 ± 0.62 (-113.78 ± 0.07) ^a	–	–	–
Span60/Chol/Mel	-113.21 ± 0.83	-142.82 ± 1.00	-111.25 ± 0.61	-67.29 ± 0.68	-49.25 ± 0.55	-36.04 ± 0.51

^aReference (Somjid *et al.*, 2018)



4.2.5 Lateral and transversal diffusion

To quantitatively investigate the motions of the Span60, cholesterol, and melatonin molecules along the membrane (lateral diffusion) and along the bilayer normal (transversal diffusion), the mean square displacements (MSD) and the relevant diffusion coefficients, D , were calculated by using Einstein's equation (Friedman, 1985)

$$D = \lim_{t \rightarrow \infty} \frac{1}{2n} \frac{d}{dt} \langle [r(t + t_0)]^2 \rangle \quad (4.8)$$

where $(r)t$ is the position of the center of mass of a molecule at time t and n is the dimensionality of the motion. The averaging value was done overall molecules and all possible time origins, t_0 . The MSD plots of the Span60 and cholesterol movements in the lateral direction as well as the melatonin movement in the lateral and transversal directions were displayed in Figures 4.16 and 4.17, respectively.

The lateral diffusion coefficients, D_{xy} , and the transversal diffusion coefficients, D_z , were derived from the slopes of the linear regime of the time evolutions of these MSD plots and were summarized in Table 4.7. It is seen from these plots that the movement of the Span60 molecule along the lateral membrane increased when melatonin was added in both the Span60 and the Span60/Chol bilayers. However, it showed the lowest diffusion in the pure Span60 bilayer. Span60 molecules can move easily in the lateral direction when cholesterol and melatonin were added to the Span60 bilayers. According to the average number of hydrogen bonds obtained from each system, the hydrogen bonds of the Span60/Span60 system decreased when melatonin is added to pure Span60 bilayer and Span60 bilayer with cholesterol inclusion.

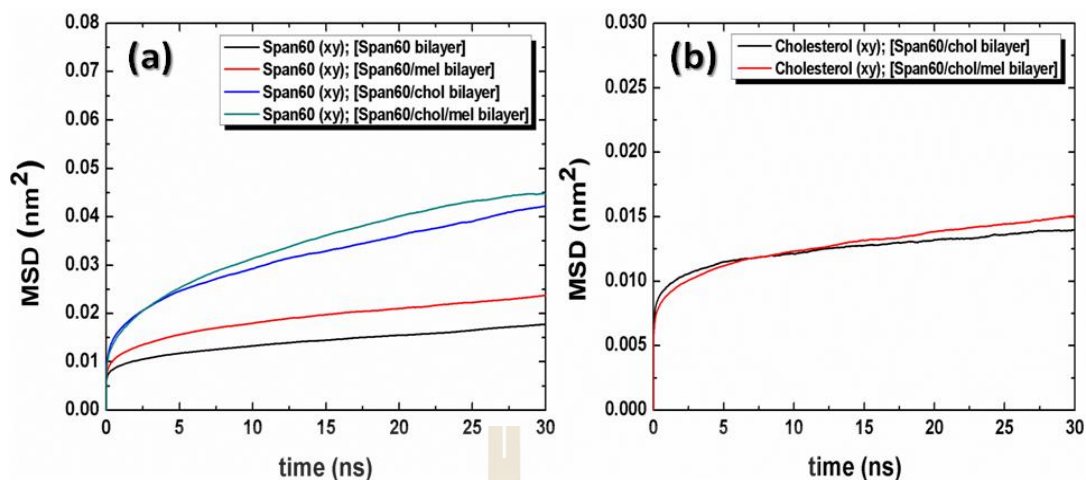


Figure 4.16 Mean squared displacement (MSD) of lateral diffusion (a) for Span60 and (b) for the cholesterol molecules obtained from the simulations of the pure Span60, the Span60/Mel, the Span60/Chol, and the Span60/Chol/Mel bilayers, respectively.

The addition of cholesterol and melatonin in the bilayer membranes caused the Span60 to lose molecular packing. Additionally, it can be observed that the cholesterol showed slightly higher lateral mobility for the Span60/Chol/Mel bilayer than that of the Span60/Chol bilayer. This is according to the stronger van der Waal interactions between cholesterol themselves.

For the movement of melatonin in the Span60 bilayers, it is seen in Figure 4.17 that melatonin favored moving in the lateral surface for the Span60/Mel and the Span60Chol/Mel bilayers. It also showed the highest mobility for the Span60/Chol/Mel bilayer. Cholesterol caused the loose molecular packing of the Span60 bilayer, leading to an increase in the mobility of melatonin molecules in the bilayer. The lateral diffusion coefficient of the melatonin molecule was dramatically increased from 0.42 ± 0.03 to $1.12 \pm 0.03 \mu\text{m}^2/\text{s}$ while its transversal diffusion coefficient was slightly increased from 0.16 ± 0.02 to $0.40 \pm 0.02 \mu\text{m}^2/\text{s}$,

Table 4.7 The diffusion coefficients of Span60, cholesterol, and melatonin molecules, obtained from MD simulations of the Span60 bilayers with and without cholesterol and melatonin inclusion.

Bilayer system	Diffusion coefficient, [$\mu\text{m}^2/\text{s}$]		
	Span60	Cholesterol	Melatonin
Pure Span60	0.22 ± 0.02 (D_{xy}) $(0.33 \pm 0.03)^b$	–	–
Span60/Mel	0.30 ± 0.03 (D_{xy}) 0.16 ± 0.02 (D_z)	–	0.42 ± 0.03 (D_{xy})
Span60/Chol	0.68 ± 0.05 (D_{xy}) $(1.04 \pm 0.04)^b$	0.10 ± 0.01 (D_{xy}) $(0.11 \pm 0.05)^a$	–
Span60/Chol/Mel	0.78 ± 0.12 (D_{xy})	0.14 ± 0.01 (D_{xy})	1.12 ± 0.03 (D_{xy}) 0.40 ± 0.02 (D_z)

^aReference (Somjid *et al.*, 2018)

^bReference (Ritwiset *et al.*, 2016)

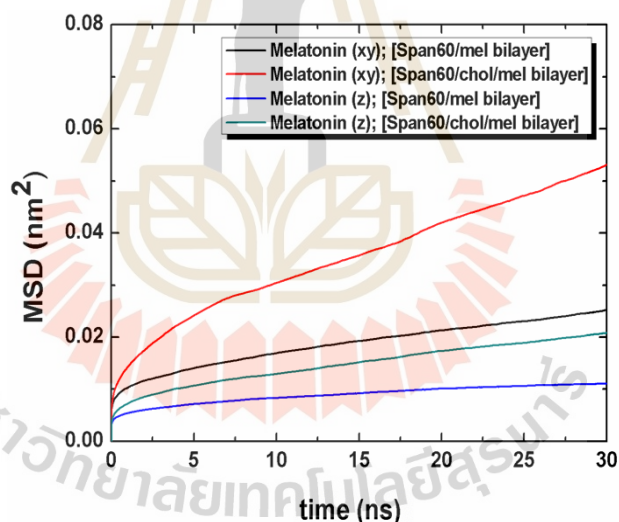


Figure 4.17 Mean squared displacement (MSD) of the lateral and the transversal diffusions of melatonin molecule obtained from the simulations of the Span60/Mel and the Span60/Chol/Mel bilayers, respectively.

as clearly seen in Table 4.7. This slight increase was according to the average number of hydrogen bonds increasing which were obtained from the Span60/Mel bilayer. The lateral diffusion coefficients for the pure Span60 and the Span60/Chol bilayers are in

good agreement with our previous works (Ritwiset *et al.*, 2016; Somjid *et al.*, 2018). Thus, the influence of cholesterols on the niosome membrane not only increases fluidity as seen in the lateral diffusion but also increases melatonin stability by making the hydrogen bonding via the head group of Span60 and cholesterol which will improve the efficiency of melatonin entrapment based on using niosomal drug carriers.



CHAPTER V

CONCLUSIONS & FUTURE DIRECTION OF WORK

5.1 Melatonin in aqueous solution and at the water-air interface

In this study, we employed molecular dynamics (MD) simulations to investigate the structural and dynamical properties of melatonin molecules in the bulk water and at the water-air interface systems. The simulation results revealed that most melatonin molecules in the bulk water system formed self-aggregation due to the stronger melatonin-melatonin interactions, compared with the water-melatonin interaction. However, for the water-air interface system, all melatonin molecules formed a monolayer structure. We found that both head and tail groups of melatonin can be simultaneously interacted with some water molecules at the surface, resulting in the two preferred orientations of melatonin head groups. The stability of melatonin strongly depends on both the melatonin-melatonin and the melatonin-water interactions. The strength of hydrophilic interaction for each function group of melatonin was sequenced as follows: carbonyl O > indole NH > amide NH > methoxy OA, respectively. Additionally, the carbonyl O and the indole NH groups of melatonin are mainly contributed to the hydrogen bonding between the melatonin-melatonin and the melatonin-water interactions for both systems. The hydrogen bond lifetimes of melatonin in the bulk water system exhibit longer than that of melatonin at the water-air interface. This suggests that the formation of self-aggregation of melatonin molecules in an aqueous solution is more stable, leading to the low solubility of

melatonin. Finally, it is seen that this study not only shows a clear picture of the molecular structure and dynamical properties of melatonin in the presence of different water phases but also provides necessary information in terms of drug delivery development for the use of melatonin to resist free radicals and for reduced oxidative stress, where regions having of virus and bacteria adhesion.

5.2 Melatonin in the niosome bilayers

Niosomes are a novel trend of drug delivery that have more advantages than liposomes such as good stability, low cost, ease to be formulated, and scaling-up. Therefore, they have been widely used to encapsulate both lipophilic and hydrophilic drugs. Nowadays, melatonin encapsulated niosomes have been formulated in various applications. However, information at the molecular level of melatonin in niosome bilayers is not well understood. Therefore, in this study, we have focused on the molecular interaction and dynamics of melatonin in the niosome bilayers based on using molecular dynamics simulations. The structural and dynamical properties of niosome bilayers with and without melatonin inclusion have been investigated and compared with the previous studies. The simulation results revealed that the structure of the Span60 bilayer without cholesterol inclusion formed in the gel phase and Span60 molecules were closely packed. Their tail groups were orderly tilted along the bilayer normal direction. For the Span60 bilayer with 30% melatonin inclusion, the bilayer was in gel/expanded phase with the less structured order. This indicates that melatonin has influenced the phase separation of niosome formation. When the 50 mol % cholesterol was added to the pure Span60 bilayer, the bilayer was in the liquid-order phase and fluidity. The tail groups of the Span60 molecules have an

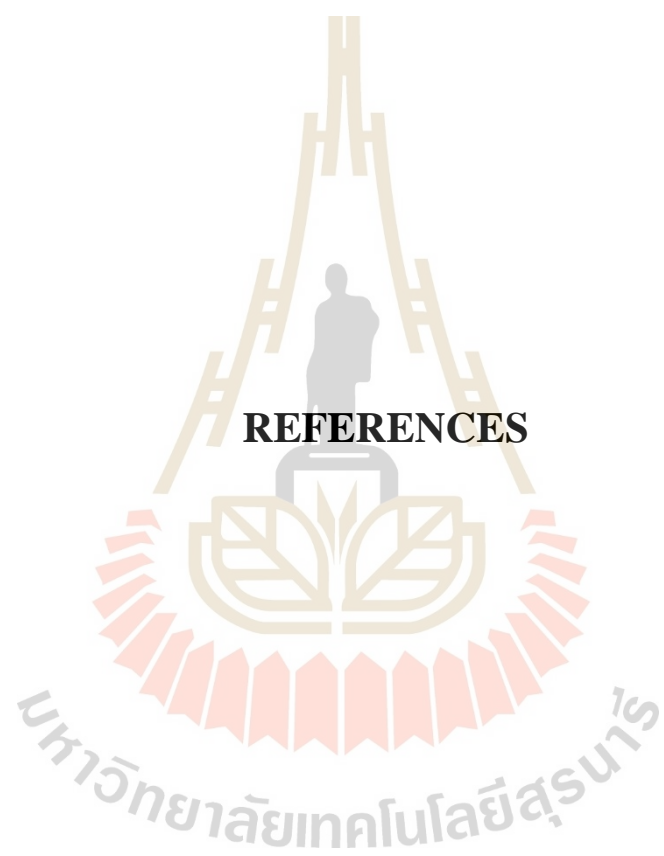
ordered structure. However, the addition of 30% melatonin to the Span60 bilayer with 50% cholesterol inclusion exhibited phase transition of niosome bilayer was in condensed/expanded phase. The bilayer with melatonin and cholesterol inclusion showed less ordered structure and more fluidity when compared to the Span60 bilayers with and with cholesterol incorporation. The effect of cholesterol provided the condensation on bilayer structure, while the influence of melatonin provided the expansion on bilayer structure and local disorder in the cholesterol molecules and Span60 tail groups. The melatonin is preferentially located at the water–Span60 interface for the Span60/Chol bilayer but stayed locally in the region between the head and tail groups for the pure Span60 bilayer. The van der Waals interaction between Span60 and cholesterol exhibits lower than that of Span60 and melatonin, leading to closed packing of Span60 and cholesterol molecules. The addition of cholesterol to the Span60 bilayer causes higher mobility of melatonin molecules in both lateral and transverse directions. Furthermore, our study suggests that the addition of 50% cholesterol in the Span60 bilayers can increase the stability and rigidity of niosomes which can improve the efficacy of melatonin encapsulation, compared with the pure Span60 bilayer. Such information is necessary for the experimental preparation for drug delivery-based niosome materials.

5.3 Future direction of work

This work will be further investigated by MD simulation with varying melatonin concentrations and temperatures to find their influence on the niosome structures such as phase transition, stability of the bilayer, and dynamic behavior of the bilayer structure. Such information provides a clear molecular picture of niosome

formation and understanding of the mechanism of melatonin encapsulation based on using the niosome materials. This leads to novel preparation of drug delivery system, especially, in terms of a variety of applications of melatonin for many disease treatments.





REFERENCES

REFERENCES

- Abraham, M. J., Murtola, T., Schulz, R., Páll, S., Smith, J. C., Hess, B. and Lindahl, E. (2015). GROMACS: High performance molecular simulations through multi-level parallelism from laptops to supercomputers. **SoftwareX**. 1: 19-25.
- Agency, U. F. S. (2011). Current EU approved additives and their E Numbers.
- Akkas, S. B., Inci, S., Zorlu, F. and Severcan, F. (2007). Melatonin affects the order, dynamics and hydration of brain membrane lipids. **Journal of Molecular Structure**. 834: 207-215.
- Allen, M. P. and Tildesley, D. J. (2017). **Computer simulation of liquids**. Oxford university press.
- Armstrong, C. L., Barrett, M. A., Hiess, A., Salditt, T., Katsaras, J., Shi, A.-C. and Rheinstädter, M. C. (2012). Effect of cholesterol on the lateral nanoscale dynamics of fluid membranes. **European Biophysics Journal**. 41(10): 901-913.
- Armstrong, C. L., Häußler, W., Seydel, T., Katsaras, J. and Rheinstädter, M. C. (2014). Nanosecond lipid dynamics in membranes containing cholesterol. **Soft Matter**. 10(15): 2600-2611.
- Armstrong, C. L., Marquardt, D., Dies, H., Kučerka, N., Yamani, Z., Harroun, T. A., Katsaras, J., Shi, A.-C. and Rheinstädter, M. C. (2013). The observation of highly ordered domains in membranes with cholesterol. **PloS One**. 8(6): e66162.

- Auld, F., Maschauer, E. L., Morrison, I., Skene, D. J. and Riha, R. L. (2017). Evidence for the efficacy of melatonin in the treatment of primary adult sleep disorders. **Sleep Medicine Reviews**. 34: 10-22.
- Benloucif, S., Burgess, H. J., Klerman, E. B., Lewy, A. J., Middleton, B., Murphy, P. J., Parry, B. L. and Revell, V. L. (2008). Measuring melatonin in humans. **Journal of Clinical Sleep Medicine**. 4(01): 66-69.
- Berendsen, H., Grigera, J. and Straatsma, T. (1987). The missing term in effective pair potentials. **Journal of Physical Chemistry**. 91(24): 6269-6271.
- Berendsen, H. J., Postma, J. v., van Gunsteren, W. F., DiNola, A. and Haak, J. R. (1984). Molecular dynamics with coupling to an external bath. **The Journal of Chemical Physics**. 81(8): 3684-3690.
- Berendsen, H. J., van der Spoel, D. and van Drunen, R. (1995). GROMACS: a message-passing parallel molecular dynamics implementation. **Computer Physics Communications**. 91(1-3): 43-56.
- Beyer, C. E., Steketee, J. D. and Saphier, D. (1998). Antioxidant properties of melatonin—an emerging mystery. **Biochemical Pharmacology**. 56(10): 1265-1272.
- Bhattacharjee, J., Verma, G., Aswal, V., Date, A. A., Nagarsenker, M. S. and Hassan, P. (2010). Tween 80– sodium deoxycholate mixed micelles: Structural characterization and application in doxorubicin delivery. **The Journal of Physical Chemistry B**. 114(49): 16414-16421.

- Bongiorno, D., Ceraulo, L., Ferrugia, M., Filizzola, F., Giordano, C., Ruggirello, A. and Liveri, V. T. (2004). H-NMR and FT-IR study of the state of melatonin confined in membrane models: location and interactions of melatonin in water free lecithin and AOT reversed micelles. **Arkivoc.** 251: 262.
- Breneman, C. M. and Wiberg, K. B. (1990). Determining atom-centered monopoles from molecular electrostatic potentials. The need for high sampling density in formamide conformational analysis. **Journal of Computational Chemistry.** 11(3): 361-373.
- Bubenik, G. A., Hacker, R. R., Brown, G. M. and Bartos, L. (1999). Melatonin concentrations in the luminal fluid, mucosa, and muscularis of the bovine and porcine gastrointestinal tract. **Journal of Pineal Research.** 26(1): 56-63.
- Bussi, G., Donadio, D. and Parrinello, M. (2007). Canonical sampling through velocity rescaling. **The Journal of Chemical Physics.** 126(1): 014101.
- Cavallo, A. and Hassan, M. (1995). Stability of melatonin in aqueous solution. **Journal of Pineal Research.** 18(2): 90-92.
- Chanda, J. and Bandyopadhyay, S. (2006). Hydrogen bond lifetime dynamics at the interface of a surfactant monolayer. **The Journal of Physical Chemistry B.** 110(46): 23443-23449.
- Chen, C.-Q., Fichna, J., Bashashati, M., Li, Y.-Y. and Storr, M. (2011). Distribution, function and physiological role of melatonin in the lower gut. **World Journal of Gastroenterology: WJG.** 17(34): 3888.

- Chen, X.-J., Liang, Q., Chen, Z., Yu, M., Luo, H., Krasnikov, V., Mayer, A., Karozis, S. N., Bingi, J. and Matham, V. (2015) Studying the lateral chain packing in a ceramide bilayer with molecular dynamics simulations. In **Journal of Physics: Conference Series**, (Vol. 574, pp. 012014).
- Choi, Y., Attwood, S. J., Hoopes, M. I., Drolle, E., Karttunen, M. and Leonenko, Z. (2014). Melatonin directly interacts with cholesterol and alleviates cholesterol effects in dipalmitoylphosphatidylcholine monolayers. **Soft Matter**. 10(1): 206-213.
- Dai, J., Alwarawrah, M. and Huang, J. (2010). Instability of cholesterol clusters in lipid bilayers and the cholesterol's umbrella effect. **The Journal of Physical Chemistry B**. 114(2): 840-848.
- Daya, S., Walker, R., Glass, B. and Anoopkumar-Dukie, S. (2001). The effect of variations in pH and temperature on stability of melatonin in aqueous solution. **Journal of Pineal Research**. 31(2): 155-158.
- De Lima, V. R., Caro, M. S., Munford, M. L., Desbat, B., Dufourc, E., Pasa, A. A. and Creczynski-Pasa, T. B. (2010). Influence of melatonin on the order of phosphatidylcholine-based membranes. **Journal of Pineal Research**. 49(2): 169-175.
- De Lima, V. R., Caro, M. S. B., Tavares, M. I. B. and Creczynski-Pasa, T. B. (2007). Melatonin location in egg phosphatidylcholine liposomes: possible relation to its antioxidant mechanisms. **Journal of Pineal Research**. 43(3): 276-282.
- de Meyer, F. and Smit, B. (2009). Effect of cholesterol on the structure of a phospholipid bilayer. **Proceedings of the National Academy of Sciences**. 106(10): 3654-3658.

- de Meyer, F. d. r. J.-M., Benjamini, A., Rodgers, J. M., Misteli, Y. and Smit, B. (2010). Molecular simulation of the DMPC-cholesterol phase diagram. **The Journal of Physical Chemistry B**. 114(32): 10451-10461.
- Dies, H., Cheung, B., Tang, J. and Rheinstädter, M. C. (2015). The organization of melatonin in lipid membranes. **Biochimica et Biophysica Acta (BBA)-Biomembranes**. 1848(4): 1032-1040.
- Dies, H., Toppozini, L. and Rheinstädter, M. C. (2014). The interaction between amyloid- β peptides and anionic lipid membranes containing cholesterol and melatonin. **PloS One**. 9(6): e99124.
- Drolle, E., Kučerka, N., Hoopes, M., Choi, Y., Katsaras, J., Karttunen, M. and Leonenko, Z. (2013). Effect of melatonin and cholesterol on the structure of DOPC and DPPC membranes. **Biochimica et Biophysica Acta (BBA)-Biomembranes**. 1828(9): 2247-2254.
- Dubey, V., Mishra, D. and Jain, N. (2007). Melatonin loaded ethanolic liposomes: physicochemical characterization and enhanced transdermal delivery. **European Journal of Pharmaceutics and Biopharmaceutics**. 67(2): 398-405.
- El-Mahdy, M., Mohamed, E.-E. M., Saddik, M. S., Ali, M. F. and El-Sayed, A. M. (2020). Formulation and clinical evaluation of niosomal methylene blue for successful treatment of acne. **Journal of Advanced Biomedical and Pharmaceutical Sciences**.
- Faraone, S. V. (2014). **ADHD: Non-Pharmacologic Interventions, An Issue of Child and Adolescent Psychiatric Clinics of North America, E-Book**. Elsevier Health Sciences.

- Filadelfi, A. M. C. and Castrucci, A. M. d. L. (1994). Melatonin desensitizing effects on the in vitro responses to MCH, alpha-MSH, isoproterenol and melatonin in pigment cells of a fish (*S. marmoratus*), a toad (*B. ictericus*), a frog (*R. pipiens*), and a lizard (*A. carolinensis*), exposed to varying photoperiodic regimens. **Comparative Biochemistry and Physiology Part A: Physiology**. 109(4): 1027-1037.
- Florio, G. M. and Zwier, T. S. (2003). Solvation of a flexible biomolecule in the gas phase: the ultraviolet and infrared spectroscopy of melatonin– water clusters. **The Journal of Physical Chemistry A**. 107(7): 974-983.
- Friedman, H. L. (1985). **A course in statistical mechanics**. Prentice-Hall Englewood Cliffs, NJ.
- Frisch, M., Trucks, G., Schlegel, H., Scuseria, G., Robb, M., Cheeseman, J., Scalmani, G., Barone, V., Mennucci, B. and Petersson, G. (2009). Gaussian, Inc., Wallingford CT. **Gaussian 09**.
- García, I. G., Rodríguez-Rubio, M., Mariblanca, A. R., de Soto, L. M., García, L. D., Villatoro, J. M., Parada, J. Q., Meseguer, E. S., Rosales, M. J. and González, J. (2020). A randomized multicenter clinical trial to evaluate the efficacy of melatonin in the prophylaxis of SARS-CoV-2 infection in high-risk contacts (MeCOVID Trial): A structured summary of a study protocol for a randomised controlled trial. **Trials**. 21(1): 1-4.
- García, J. n. J., Reiter, R. J., Guerrero, J. M., Escames, G., Yu, B. P., Oh, C. S. and Muñoz-Hoyos, A. (1997). Melatonin prevents changes in microsomal membrane fluidity during induced lipid peroxidation. **FEBS Letters**. 408(3): 297-300.

- Giddi, H., Adhimoolam, A. and Bellare, J. (2007). Self-assembled surfactant nano-structures important in drug delivery: A review. **Indian Journal of Experimental Biology**. 45: 133-159.
- Gunsteren, W. v. and Berendsen, H. (1987). Groningen molecular simulation (GROMOS) library manual. **Netherlands: Biomos**.
- Han, S. (2013). Molecular dynamics simulation of sorbitan monooleate bilayers. **Bulletin of the Korean Chemical Society**. 34(3): 946-948.
- Heneweer, C., Gendy, S. E. and Peñate-Medina, O. (2012). Liposomes and inorganic nanoparticles for drug delivery and cancer imaging. **Therapeutic Delivery**. 3(5): 645-656.
- Hess, B., Bekker, H., Berendsen, H. J. and Fraaije, J. G. (1997). LINCS: a linear constraint solver for molecular simulations. **Journal of Computational Chemistry**. 18(12): 1463-1472.
- Höltje, M., Förster, T., Brandt, B., Engels, T., von Rybinski, W. and Höltje, H.-D. (2001). Molecular dynamics simulations of stratum corneum lipid models: fatty acids and cholesterol. **Biochimica et Biophysica Acta (BBA)-Biomembranes**. 1511(1):156-167.
- Huang, J. and Feigenson, G. W. (1999). A microscopic interaction model of maximum solubility of cholesterol in lipid bilayers. **Biophysical Journal**. 76(4): 2142-2157.
- Humphrey, W., Dalke, A. and Schulten, K. (1996). VMD: visual molecular dynamics. **Journal of Molecular Graphics**. 14(1): 33-38.

- Katsaras, J., Yang, D. and Epand, R. M. (1992). Fatty-acid chain tilt angles and directions in dipalmitoyl phosphatidylcholine bilayers. **Biophysical Journal**. 63(4): 1170-1175.
- Khan, R. and Irchhaiya, R. (2016). Niosomes: a potential tool for novel drug delivery. **Journal of Pharmaceutical Investigation**. 46(3): 195-204.
- Krynicky, K., Green, C. D. and Sawyer, D. W. (1978). Pressure and temperature dependence of self-diffusion in water. **Faraday Discussions of the Chemical Society**. 66: 199-208.
- Lee, B.-J., Choi, H.-G., Kim, C.-K., Parrott, K. A., Ayres, J. W. and Sack, R. L. (1997). Solubility and stability of melatonin in propylene glycol and 2-hydroxypropyl- β -cyclodextrin vehicles. **Archives of Pharmacal Research**. 20(6): 560-565.
- Lu, H. and Marti, J. (2020). Cellular absorption of small molecules: free energy landscapes of melatonin binding at phospholipid membranes. **Scientific Reports**. 10(1): 1-12.
- Lu, H. and Marti, J. (2019). Binding and dynamics of melatonin at the interface of phosphatidylcholine-cholesterol membranes. **PloS One**. 14(11): e0224624.
- Luzar, A. and Chandler, D. (1996). Effect of environment on hydrogen bond dynamics in liquid water. **Physical Review Letters**. 76(6): 928.
- Mahale, N., Thakkar, P., Mali, R., Walunj, D. and Chaudhari, S. (2012). Niosomes: novel sustained release nonionic stable vesicular systems—an overview. **Advances in Colloid and Interface Science**. 183: 46-54.

- Manosroi, A., Khanrin, P., Lohcharoenkal, W., Werner, R. G., Götz, F., Manosroi, W. and Manosroi, J. (2010). Transdermal absorption enhancement through rat skin of gallidermin loaded in niosomes. **International Journal of Pharmaceutics**. 392(1-2): 304-310.
- Mark, P. and Nilsson, L. (2001). Structure and dynamics of the TIP3P, SPC, and SPC/E water models at 298 K. **The Journal of Physical Chemistry A**. 105(43): 9954-9960.
- Mark, P. and Nilsson, L. (2002). A molecular dynamics study of tryptophan in water. **The Journal of Physical Chemistry B**. 106(36): 9440-9445.
- Meinhardt, S., Vink, R. L. and Schmid, F. (2013). Monolayer curvature stabilizes nanoscale raft domains in mixed lipid bilayers. **Proceedings of the National Academy of Sciences**. 110(12): 4476-4481.
- Milani, M. and Sparavigna, A. (2018). Antiaging efficacy of melatonin-based day and night creams: A randomized, split-face, assessor-blinded proof-of-concept trial. **Clinical, Cosmetic and Investigational Dermatology**. 11: 51.
- Miyamoto, S. and Kollman, P. A. (1992). Settle: An analytical version of the SHAKE and RATTLE algorithm for rigid water models. **Journal of Computational Chemistry**. 13(8): 952-962.
- Moghassemi, S. and Hadjizadeh, A. (2014). Nano-niosomes as nanoscale drug delivery systems: an illustrated review. **Journal of Controlled Release**. 185: 22-36.
- Mouritsen, O. G. (2010). The liquid-ordered state comes of age. **Biochimica et Biophysica Acta (BBA)-Biomembranes**. 1798(7): 1286-1288.

- Muzzalupo, R., Tavano, L., Cassano, R., Trombino, S., Ferrarelli, T. and Picci, N. (2011). A new approach for the evaluation of niosomes as effective transdermal drug delivery systems. **European Journal of Pharmaceutics and Biopharmaceutics**. 79(1): 28-35.
- Myung, Y., Yeom, S. and Han, S. (2016). A niosomal bilayer of sorbitan monostearate in complex with flavones: a molecular dynamics simulation study. **Journal of Liposome Research**. 26(4): 336-344.
- Nasr, M., Mansour, S., Mortada, N. D. and Elshamy, A. (2008). Vesicular aceclofenac systems: a comparative study between liposomes and niosomes. **Journal of Microencapsulation**. 25(7): 499-512.
- Nasseri, B. (2005). Effect of cholesterol and temperature on the elastic properties of niosomal membranes. **International Journal of Pharmaceutics**. 300(1-2): 95-101.
- Pabst, G., Kučerka, N., Nieh, M.-P., Rheinstädter, M. and Katsaras, J. (2010). Applications of neutron and X-ray scattering to the study of biologically relevant model membranes. **Chemistry and Physics of Lipids**. 163(6): 460-479.
- Pala, D., Lodola, A., Bedini, A., Spadoni, G. and Rivara, S. (2013). Homology models of melatonin receptors: challenges and recent advances. **International Journal of Molecular Sciences**. 14(4): 8093-8121.
- Páll, S. and Hess, B. (2013). A flexible algorithm for calculating pair interactions on SIMD architectures. **Computer Physics Communications**. 184(12): 2641-2650.

- Pandey, P. R. and Roy, S. (2011). Headgroup mediated water insertion into the DPPC bilayer: a molecular dynamics study. **The Journal of Physical Chemistry B.** 115(12): 3155-3163.
- Parrinello, M. and Rahman, A. (1981). Polymorphic transitions in single crystals: A new molecular dynamics method. **Journal of Applied Physics.** 52(12): 7182-7190.
- Peltonen, L., Hirvonen, J. and Yliruusi, J. (2001). The effect of temperature on sorbitan surfactant monolayers. **Journal of Colloid and Interface Science.** 239(1): 134-138.
- Petersen, H. G. (1995). Accuracy and efficiency of the particle mesh Ewald method. **The Journal of Chemical Physics.** 103(9): 3668-3679.
- Petrache, H. I., Tu, K. and Nagle, J. F. (1999). Analysis of simulated NMR order parameters for lipid bilayer structure determination. **Biophysical Journal.** 76(5): 2479-2487.
- Pirvu, C. D., Hlevca, C., Ortan, A. and Prisada, R. (2010). Elastic vesicles as drugs carriers through the skin. **Farmacia.** 58(2): 128-135.
- Poger, D. and Mark, A. E. (2010). On the validation of molecular dynamics simulations of saturated and cis-monounsaturated phosphatidylcholine lipid bilayers: a comparison with experiment. **Journal of Chemical Theory and Computation.** 6(1): 325-336.
- Pripem, A., Netweera, V., Mahakunakorn, P., Johns, N. P. and Johns, J. R. (2014) Prolonged Anti-inflammatory Activity of Topical Melatonin by Niosomal Encapsulation. In **Advanced Materials Research**, (Vol. 902, pp. 70-75) Trans Tech Publ.

- Priprem, A., Nukulkit, C., Johns, N. P., Laohasiriwong, S., Yimtae, K. and Soontornpas, C. (2018). Transmucosal delivery of melatonin-encapsulated niosomes in a mucoadhesive gel. **Therapeutic Delivery**. 9(5): 343-357.
- Pshenichnyuk, S. A., Modelli, A., Jones, D., Lazneva, E. F. and Komolov, A. S. (2017). Low-energy electron interaction with melatonin and related compounds. **The Journal of Physical Chemistry B**. 121(16): 3965-3974.
- Reiter, R., Tan, D.-X., Cabrera, J., D'Arpa, D., Sainz, R., Mayo, J. and Ramos, S. (1999). The oxidant/antioxidant network: role of melatonin. **Neurosignals**. 8(1-2): 56-63.
- Reiter, R. J., Sharma, R., Ma, Q., Dominquez-Rodriguez, A., Marik, P. E. and Abreu-Gonzalez, P. (2020). Melatonin Inhibits COVID-19-induced Cytokine Storm by Reversing Aerobic Glycolysis in Immune Cells: A Mechanistic Analysis. **Medicine in Drug Discovery**. 6: 100044.
- Reiter, R. J., Tan, D. X. and Qi, W. B. (1998). Suppression of oxygen toxicity by melatonin. **Zhongguo yao li xue bao= Acta pharmacologica Sinica**. 19(6): 575-581.
- Rheinstädter, M. C. and Mouritsen, O. G. (2013). Small-scale structure in fluid cholesterol–lipid bilayers. **Current Opinion in Colloid & Interface Science**. 18(5): 440-447.
- Ritwiset, A., Kongsuk, S. and Johns, J. (2014). Molecular structure and stability of the sorbitan monostearate (Span60) monolayers film at the water–air interface: A molecular dynamics simulation study. **Journal of Molecular Liquids**. 195: 157-164.

- Ritwiset, A., Krongsuk, S. and Johns, J. R. (2016). Molecular structure and dynamical properties of niosome bilayers with and without cholesterol incorporation: A molecular dynamics simulation study. **Applied Surface Science**. 380: 23-31.
- Romano, B., Pagano, E., Montanaro, V., Fortunato, A. L., Milic, N. and Borrelli, F. (2013). Novel insights into the pharmacology of flavonoids. **Phytotherapy Research**. 27(11): 1588-1596.
- Rosales-Corral, S. A., Acuña-Castroviejo, D., Coto-Montes, A., Boga, J. A., Manchester, L. C., Fuentes-Broto, L., Korkmaz, A., Ma, S., Tan, D. X. and Reiter, R. J. (2012). Alzheimer's disease: pathological mechanisms and the beneficial role of melatonin. **Journal of Pineal Research**. 52(2): 167-202.
- Ryckaert, J.-P. and Bellemans, A. (1978). Molecular dynamics of liquid alkanes. **Faraday Discussions of the Chemical Society**. 66: 95-106.
- Saija, A., Tomaino, A., Trombetta, D., Pellegrino, M. L., Tita, B., Caruso, S. and Castelli, F. (2002). Interaction of melatonin with model membranes and possible implications in its photoprotective activity. **European Journal of Pharmaceutics and Biopharmaceutics**. 53(2): 209-215.
- Sajid, M., Khan, M. S. A., Cameotra, S. S. and Ahmad, I. (2014) **Drug delivery systems that eradicate and/or prevent biofilm formation**. In *Antibiofilm Agents* Springer, pp. 407-424.
- Sankhyan, A. and Pawar, P. (2012). Recent trends in niosome as vesicular drug delivery system. **Journal of Applied Pharmaceutical Science**. 2(6): 20-32.

- Schüttelkopf, A. W. and Van Aalten, D. M. (2004). PRODRG: a tool for high-throughput crystallography of protein–ligand complexes. **Acta Crystallographica Section D: Biological Crystallography**. 60(8): 1355-1363.
- Severcan, F., Sahin, I. and Kazancı, N. (2005). Melatonin strongly interacts with zwitterionic model membranes—evidence from Fourier transform infrared spectroscopy and differential scanning calorimetry. **Biochimica et Biophysica Acta (BBA)-Biomembranes**. 1668(2): 215-222.
- Shida, C., Castrucci, A. M. d. L. and Lamy-Freund, M. (1994). High melatonin solubility in aqueous medium. **Journal of Pineal Research**. 16(4): 198-201.
- Shilakari Asthana, G., Sharma, P. K. and Asthana, A. (2016). In vitro and in vivo evaluation of niosomal formulation for controlled delivery of clarithromycin. **Scientifica**. 2016.
- Shillady, D. D., Castevens IV, C. M., Trindle, C., Sulik, J. and Klonowski, P. (2003). Conformational complexity of melatonin in water and methanol. **Biophysical Chemistry**. 105(2-3): 471-494.
- Shirts, M. R., Mobley, D. L., Chodera, J. D. and Pande, V. S. (2007). Accurate and efficient corrections for missing dispersion interactions in molecular simulations. **The Journal of Physical Chemistry B**. 111(45): 13052-13063.
- Shneider, A., Kudriavtsev, A. and Vakhrusheva, A. (2020). Can melatonin reduce the severity of COVID-19 pandemic? **International Reviews of Immunology**. 1-10.

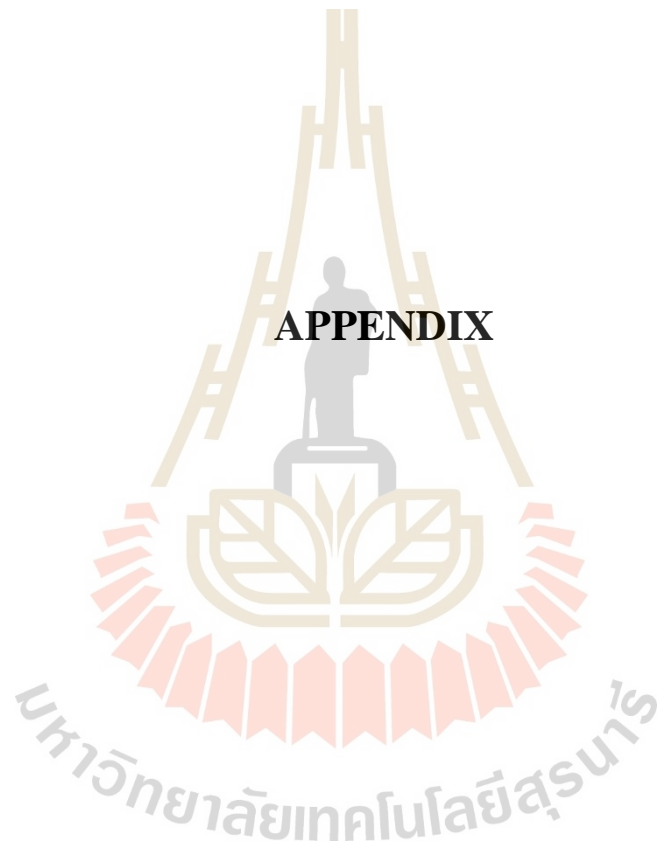
- Siwko, M. E., de Vries, A. H., Mark, A. E., Kozubek, A. and Marrink, S. J. (2009). Disturb or stabilize? A molecular dynamics study of the effects of resorcinolic lipids on phospholipid bilayers. **Biophysical Journal**. 96(8): 3140-3153.
- Sodt, A. J., Sandar, M. L., Gawrisch, K., Pastor, R. W. and Lyman, E. (2014). The molecular structure of the liquid-ordered phase of lipid bilayers. **Journal of the American Chemical Society**. 136(2): 725-732.
- Somjid, S., Kongsuk, S. and Johns, J. R. (2018). Cholesterol concentration effect on the bilayer properties and phase formation of niosome bilayers: A molecular dynamics simulation study. **Journal of Molecular Liquids**. 256: 591-598.
- Sommer, B. r., Dingersen, T., Gamroth, C., Schneider, S. E., Rubert, S., Krüger, J. and Dietz, K.-J. (2011). CELLmicrocosmos 2.2 MembraneEditor: a modular interactive shape-based software approach to solve heterogeneous membrane packing problems. **Journal of Chemical Information and Modeling**. 51(5): 1165-1182.
- Spaar, A. and Salditt, T. (2003). Short range order of hydrocarbon chains in fluid phospholipid bilayers studied by x-ray diffraction from highly oriented membranes. **Biophysical Journal**. 85(3): 1576-1584.
- Starr, F. W., Nielsen, J. K. and Stanley, H. E. (2000). Hydrogen-bond dynamics for the extended simple point-charge model of water. **Physical Review E**. 62(1): 579.
- Tengattini, S., Reiter, R. J., Tan, D. X., Terron, M. P., Rodella, L. F. and Rezzani, R. (2008). Cardiovascular diseases: protective effects of melatonin. **Journal of Pineal Research**. 44(1): 16-25.

- Uchegbu, I. F. and Vyas, S. P. (1998). Non-ionic surfactant based vesicles (niosomes) in drug delivery. **International Journal of Pharmaceutics**. 172(1-2): 33-70.
- Van Der Spoel, D., Lindahl, E., Hess, B., Groenhof, G., Mark, A. E. and Berendsen, H. J. (2005). GROMACS: fast, flexible, and free. **Journal of Computational Chemistry**. 26(16): 1701-1718.
- Vance, D. E. and Van den Bosch, H. (2000). Cholesterol in the year 2000. **Biochimica et Biophysica Acta (BBA)-Molecular and Cell Biology of Lipids**. 1529(1-3): 1-8.
- Vijayalaxmi, Thomas Jr, C. R., Reiter, R. J. and Herman, T. S. (2002). Melatonin: from basic research to cancer treatment clinics. **Journal of Clinical Oncology**. 20(10): 2575-2601.
- Vöhringer-Martinez, E. and Toro-Labbé, A. (2010). Amino acids at water– vapor interfaces: surface activity and orientational ordering. **The Journal of Physical Chemistry B**. 114(40): 13005-13010.
- Xiang, T.-X. and Anderson, B. D. (2006). Liposomal drug transport: a molecular perspective from molecular dynamics simulations in lipid bilayers. **Advanced Drug Delivery Reviews**. 58(12-13): 1357-1378.
- Yamamoto, A., Uchiyama, T., Nishikawa, R., Fujita, T. and Muranishi, S. (1996). Effectiveness and toxicity screening of various absorption enhancers in the rat small intestine: effects of absorption enhancers on the intestinal absorption of phenol red and the release of protein and phospholipids from the intestinal membrane. **Journal of Pharmacy and Pharmacology**. 48(12): 1285-1289.

- Yeom, S., Shin, B. S. and Han, S. (2014). An electron spin resonance study of non-ionic surfactant vesicles (niosomes). **Chemistry and Physics of Lipids**. 181: 83-89.
- Yu, H., Dickson, E. J., Jung, S.-R., Koh, D.-S. and Hille, B. (2016). High membrane permeability for melatonin. **Journal of General Physiology**. 147(1): 63-76.



APPENDIX



APPENDIX

PUBLICATION AND PRESENTATION

A.1 Publication

Ritwiset, A., Khajonrit, J., Kongsuk, S., and Maensiri, S. (2021). Molecular insight on the formation structure and dynamics of melatonin in an aqueous solution and at the Water–Air interface: A molecular dynamics study. **Journal of Molecular Graphics and Modelling**. 108: 107983.

A.2 Oral presentation

Ritwiset A., Kongsuk S., and Maensiri S., Molecular Structure and Formation of Melatonin in the Bulk Water and at the Water–Air Interface: A Molecular Dynamics Simulation Study. Oral presenter at International Conference Nano Thailand, Khao Yai, Thailand.

A.3 Poster presentation

Ritwiset A., Kongsuk S., and Maensiri S., Molecular Dynamics Simulations of Gel Phase Sorbitan Monostearate (Span60) Bilayer Niosome. Poster presenter at The First Materials Research Society of Thailand International Conference, Chiang Mai, Thailand.

Ritwiset A., Kongsuk S., and Maensiri S., Structural and Dynamic Properties of Melatonin Molecule in Aqueous Solution using Molecular Dynamics Simulation Study. Poster presenter at International Conference the Union of Materials Research Societies-on Electronic Materials, Daejeon, Korea.

Ritwiset A., Kongsuk S., and Maensiri S., Molecular Structure and Dynamical Properties of the Melatonin Effect Inserted into the Niosome Bilayers with and without Cholesterol Incorporation: A Molecular Dynamics Simulation Study. Poster presenter at International Conference on the 4th Industrial Revolution and Its Impacts, Walailak University, Nakhon Si Thammarat, Thailand.



CURRICULUM VITAE

Name Aksornnarong Ritwiset

Date of Birth August 7, 1987

Place of Birth Udon Thani, Thailand

Education

2015 – 2020. Ph.D. in Physics

School of Physics, Suranaree University of Technology, Nakhon Ratchasima, Thailand.

Thesis supervisor: Prof. Dr. Santi Maensiri

Thesis Co-supervisor: Assoc. Prof. Dr. Sriprajak Krongsuk

2010 – 2015. MSc in Material Science

School of Physics, Khon Kaen University, Khon Kaen, Thailand.

Thesis supervisor: Asst. Prof. Dr. Sriprajak Krongsuk

2006 – 2010. BSc in Physics

School of Physics, Khon Kaen University, Khon Kaen, Thailand.

2004 - 2006. High school Namsomphitthayakhom, Udon Thani, Thailand.

Grants and Fellowships

2015 – 2020. The SUT Center of Excellence on Advanced Functional Materials, Suranaree University of Technology, Nakhon Ratchasima, Thailand.